

**INVESTIGATION OF METHODS
USED TO PREDICT THE HEAT
RELEASE RATE AND ENCLOSURE
TEMPERATURES DURING
MATTRESS FIRES**

A Thesis Submitted to the College of
Graduate Studies and Research
in Partial Fulfillment of the Requirements
for the Master of Science Degree
in the Department of Mechanical Engineering
in the College of Engineering at the
University of Saskatchewan
Saskatoon

By

Todd Threlfall

PERMISSION TO USE

In presenting this thesis in partial fulfilment of the requirements for a Postgraduate degree from the University of Saskatchewan, I agree that the Libraries of this University may make it freely available for inspection. I further agree that permission for copying of this thesis in any manner, in whole or in part, for scholarly purposes may be granted by the professor or professors who supervised my thesis work or, in their absence, by the Head of the Department or the Dean of the College in which my thesis work was done. It is understood that any copying or publication or use of this thesis or parts thereof for financial gain shall not be allowed without my written permission. It is also understood that due recognition shall be given to me and to the University of Saskatchewan in any scholarly use which may be made of any material in my thesis.

Requests for permission to copy or to make other use of material in this thesis in whole or part should be addressed to:

Head of the Department of Mechanical Engineering

University of Saskatchewan

Saskatoon, Saskatchewan S7N 5A9

ABSTRACT

Fires in buildings ranging in size from small residential houses to large office buildings and sports stadiums pose significant threats to human safety. Many advances have been made in the area of fire behaviour modeling and have led to much safer, and more efficient fire protection engineering designs, saving countless lives. Fire, however, is still a difficult phenomenon to accurately model and the most important quantity used to describe a fire is the heat (energy) release rate (HRR).

Predictions of the fire hazard posed by mattresses, using relatively simple modeling techniques, were investigated in this research work and compared to full-scale experimental results. Specifically, several common methods of predicting the HRR from a mattress fire were examined. Current spatial separation guidelines, which exist in order to mitigate fire spread between buildings, were used to predict radiation heat flux levels emitted by a burning building and compared to experimental results measured in the field. Enclosure ceiling temperatures, predicted using the Alpert temperature correlation, and average hot gas layer temperature predictions were also compared to experimental results.

Results from this work indicate that the t-squared fire heat release rate modeling technique combined with the common Alpert ceiling temperature correlation, provide a reasonable prediction of real-life fire temperatures as results within 30% were obtained. The cone calorimeter was also found to be a useful tool in the prediction of full-scale fire behaviour and the guidelines used for spatial separation calculations were found to predict the radiant heat flux emitted by a burning building reasonably well.

ACKNOWLEDGEMENTS

The author wishes to acknowledge the following for their assistance with this research project:

- Dr. D.A. Torvi for his supervision of this research and with assistance in preparing this thesis.
- Dr. C.J. Simonson and Dr. D.J. Bergstrom for their help as members of the supervisory committee.
- The Department of Mechanical Engineering and the College of Graduate Studies and Research at the University of Saskatchewan in addition to the Natural Sciences and Engineering Research Council of Canada (NSERC) for additional support and funding.
- Departmental assistants Dave Deutscher and Chris James provided valuable technical assistance.
- Dr. Doug Dale and Mark Ackerman of the Department of Mechanical Engineering, University of Alberta are also gratefully acknowledged for their assistance and technical support during the house burns.
- The Edmonton Fire Department is acknowledged for technical support and assistance during both full-scale fire tests in July 2003 and September 2004. Members of the Fire Department made the full-scale fire tests a very enjoyable experience.
- Crystal Samborski for her work in organizing the full-scale fire tests in Edmonton, AB.
- Sleepers Mattress Factory is gratefully acknowledged for providing mattress samples for laboratory burning.
- Dr. Vyto Babrauskas, Dr. Gary Loughheed, Gordon Damant and Dr. David Yung for technical assistance.

TABLE OF CONTENTS

PERMISSION TO USE.....	ii
ABSTRACT.....	iii
ACKNOWLEDGEMENTS	iv
LIST OF TABLES	vii
LIST OF FIGURES	viii
LIST OF FIGURES	viii
NOMENCLATURE.....	xiv
Chapter 1: Introduction	1
1.1 Fire Statistics	1
1.2 Introduction to Fire Protection Engineering	2
1.2.1 History	3
1.2.2 Important Quantities in Fire Protection Engineering	4
1.3 Challenges Facing Fire Protection Engineers.....	5
1.3.1 Fire Codes	7
1.4 Experimental Fire Research.....	9
1.4.1 Full-Scale Fire Tests.....	10
1.4.2 Field Fire Tests.....	11
1.4.3 Small-Scale Fire Tests.....	12
1.5 Enclosure Fires	13
1.5.1 Fire Plume in an Enclosure	14
1.5.2 Flashover	15
1.5.3 Fuel and Ventilation Controlled Fires.....	16
1.6 Fire Protection Engineering Analyses	16
1.6.1 Numerical/Computational Methods	17
1.6.2 Engineering Correlations.....	19
1.7 Other Major Upholstered Furniture Fire Modeling Studies	19
1.8 Research Objectives	21
1.9 Overview of Thesis.....	22
Chapter 2: Fire Growth Modeling Techniques and Engineering Correlations.....	24
2.1 Spatial Separation	25
2.2 Heat Release Rate Modeling	28
2.3 HRR Growth Phase Modeling.....	29
2.3.1 Combustion Science Theoretical Rate of Heat Release	30
2.3.2 Semi-Universal Heat Release Model	31
2.3.3 Generic Upholstered Furniture Fire Growth Model.....	32
2.3.4 Time-Squared (t-Squared) HRR Fire Models	34
2.3.5 Ventilation vs. Fuel Controlled Fires During Fire Growth Phase.....	36
2.4 Maximum HRR (Post-Flashover Fire Region).....	37
2.4.1 McCaffrey Prediction of Flashover.....	38
2.4.2 NIST/CBHF Upholstered Furniture and Mattress Peak HRR Correlation	39

2.5 FPE Empirical Temperature Correlations	42
2.5.1 Alpert Ceiling Temperature Correlation	42
2.5.2 Average Hot Upper Gas Layer Temperature Correlation	45
2.6 Flame Height Correlation	46
2.7 Summary.....	47
Chapter 3: Small-Scale Fire Testing	48
3.1 Introduction to the Cone Calorimeter	49
3.1.1 Description of Cone Calorimeter Equipment.....	51
3.1.2 Oxygen Consumption Calorimetry	54
3.2 Edmonton II Mattress Sample Cone Calorimeter Testing.....	56
3.2.1 Mattress Sample Preparation.....	59
3.2.2 Cone Calorimeter Heat Release Rate and Total Heat Release Results	64
3.2.3 Cone Calorimeter Smoke Production Results	67
3.2.4 Effect of Moisture Content on Cone Calorimeter Heat Release Results	68
3.2.5 Effect of Incident Heat Flux on Cone Calorimeter Heat Release Results	70
3.2.6 Investigation of Individual Mattress Layer Component Heat Release Rates...	71
3.3 Summary.....	76
Chapter 4: Full-Scale Fire Testing	77
4.1 Standardized Full-scale Tests	77
4.2 Building Field Fire Tests	80
4.3 Small-Scale and Full-Scale Heat Flux Test Instrumentation.....	81
4.3.1 Heat Flux Sensors	82
4.3.2 Skin Simulant Sensor (Thin Film)	83
4.3.3 Schmidt-Boelter Gauge.....	85
4.3.4 Gardon Gauge	87
4.4 Edmonton I	88
4.4.1 Edmonton I Instrumentation	90
4.4.2 Edmonton I Results	93
4.5 Edmonton I Heat Flux Sensor Response	98
4.5.1 Heat Flux Exposure Level of 5 kW/m ²	99
4.5.2 Exposure level of 20 kW/m ²	101
4.5.3 Exposure level of 40 kW/m ²	102
4.5.4 Exposure level of 80 kW/m ²	103
4.5.5 Discussion of Cone Calorimeter Heat Flux Sensor Test Results	104
4.6 Edmonton II.....	106
4.6.1 Edmonton II Instrumentation	108
4.6.2 Edmonton II Results.....	109
4.7 Summary.....	118
Chapter 5: Fire Growth Model and Temperature Predictions Compared to Experimental Results.....	119
5.1 Edmonton I Spatial Separation Calculations	119
5.1.1 Minimum Separation Distance.....	120
5.1.2 Spatial Separation Correlations Compared to Experimental Measurements ..	121
5.1.3 Discussion	123
5.2 Edmonton II Heat Release Modeling	124

5.3	Edmonton II Incubation Time	126
5.4	Edmonton II Fire Growth Phase HRR Modeling	128
5.4.1	Combustion Science Theoretical Rate of Heat Release	128
5.4.2	Semi-Universal Heat Release Model	131
5.4.3	Generic Upholstered Furniture Fire Growth Model.....	133
5.4.4	t-Squared Heat Release Rate Model.....	136
5.4.5	Fuel/Ventilation-Controlled Fire.....	142
5.5	Edmonton II Maximum HRR Modeling	143
5.5.1	Edmonton II McCaffrey Prediction of Flashover	143
5.5.2	NIST/CBHF Upholstered Furniture and Mattress HRR Correlation	144
5.6	Summary of Edmonton II Mattress HRR Model.....	149
5.7	Edmonton II Temperature Predictions.....	151
5.7.1	Comparison of Predicted Ceiling Temperatures and Experimental Results ...	152
5.7.2	Edmonton II Average Hot Gas Layer Temperature Predictions	161
5.8	Summary.....	164
Chapter 6: Conclusions & Future Work		166
6.1	Conclusions	166
6.2	Recommendations for Future Work	168
REFERENCES.....		171

APPENDICES:

Appendix A: Edmonton I Spatial Separation Calculations and Additional Information.....		177
A.1	Spatial Separation Sample Calculations	177
A.2	Theoretical Heat Flux At Sensor Location	181
A.3	Edmonton I House Floor Plan Drawings.....	184
A.4	Additional Edmonton I Temperature Results	189
Appendix B: HRR Calculations.....		193
B.1	Sample Flame Height Calculation	193
B.2	Combustion Science Theoretical HRR Sample Calculation.....	195
B.2.1	Combustion Science Theoretical HRR Sample Calculations.....	196
B.3	Semi-Universal HRR Model.....	198
B.3.1	Semi-Universal HRR Model Sample Calculations	198
B.4	Generic Upholstered Furniture Fire Growth Model	200
B.4.1	Generic Upholstered Furniture Fire Growth Model Sample Calculations	200
B.5	t-Squared HRR Model	203
B.6	Fuel/Ventilation-Controlled Fire	204
B.7	McCaffrey Prediction of Flashover	205
B.8	NIST/CBHF Upholstered Furniture and Mattress Peak HRR Correlation.....	208
Appendix C: Temperature Calculations.....		210
C.1	Alpert Ceiling Temperature Correlation Predictions	210
C.2	Average Hot Upper Gas Layer Temperature Correlation.....	213

LIST OF TABLES

Table 1 - 1: United States Fire Deaths and Reported Incidents by Occupancy (1994-1998 Average).....	2
Table 2 - 1: Suggested Input Values for Generic Upholstered Furniture Fire Growth Model	34
Table 2 - 2: Typical Materials Associated With t-Squared Fires.....	35
Table 3 - 1: Mattress Description.....	57
Table 3 - 2: Summary of Edmonton II Mattress Cone Calorimeter Mattress Results	66
Table 4 - 1: Summary of Edmonton I Experiments	88
Table 5 - 1: Suggested Factors for Upholstered Furniture Fire Growth Model.....	134
Table 5 - 2: Average Cone Calorimeter Mattress Sample Results	138
Table 5 - 3: Typical Cone Calorimeter Mattress & Polyurethane Foam Results	139
Table 5 - 4: t-Squared Fire Mattress Classification Based on the Literature.....	139
Table 5 - 5: NIST/CBHF Peak HRR Predictions.....	147
Table A - 1: Summary of Edmonton I Set of Experiments.....	189
Table B - 1: Combustion Science Theoretical HRR.....	195
Table B - 2: Semi-Universal HRR Model Prediction Shown for Mattress One	199
Table B - 3: Suggested Values for Factors	201
Table B - 4: Generic Upholstered Furniture Fire Growth Model Prediction.....	202
Table B - 5: Average Cone Calorimeter Results for the Three Mattress Samples	209
Table C - 1: Radial Distances for Edmonton II Thermocouple Locations	212

LIST OF FIGURES

Figure 1 - 1: Fire Plume in an Enclosure	14
Figure 1 - 2: CBUF Project Structure	20
Figure 2 - 1: Schematic Describing Spatial Separation Variables	27
Figure 2 - 2: Theoretical Fire Heat Release Behaviour	29
Figure 2 - 3: Generic Upholstered Furniture Fire Growth Model	32
Figure 2 - 4: NIST/CBHF Upholstered Furniture and Mattress HRR Correlation.....	40
Figure 3 - 1: University of Saskatchewan Cone Calorimeter	50
Figure 3 - 2: Cone Calorimeter Specimen Test Area.....	52
Figure 3 - 3: Cone Calorimeter Specimen Holder	53
Figure 3 - 4: Mattress 1 Cone Calorimeter Composite Sample Showing Different Components.....	58
Figure 3 - 5: Mattress 2 Cone Calorimeter Composite Sample Showing Different Components.....	58
Figure 3 - 6: Mattress 3 Cone Calorimeter Composite Sample Showing Different Components.....	59
Figure 3 - 7: Specimen Holder With Wire Grid	61
Figure 3 - 8: Individual Mattress Test Results (Mattress 1 Tests Shown).....	62
Figure 3 - 9: Individual PMMA Calibration Sample Test Results	63
Figure 3 - 10: Mattress 1 Sample Wrapped in Aluminum Foil	64
Figure 3 - 11: Average Cone Calorimeter HRR Results)	65
Figure 3 - 12: Average Cone Calorimeter THR Results.....	67
Figure 3 - 13: Average Cone Calorimeter Smoke Production Results	68

Figure 3 - 14: Effect of Relative Humidity on Cone Calorimeter Results.....	69
Figure 3 - 15: Effect of Heat Flux on Cone Calorimeter Results	70
Figure 3 - 16: Mattress 1 Comparison of Individual Mattress Layer Tests versus the Entire Ensemble	72
Figure 3 - 17: Mattress 2 Comparison of Individual Mattress Layer Tests versus the Entire Ensemble	73
Figure 3 - 18: Comparison of Backing Material Heat Release	74
Figure 3 - 19: Comparison of Polyurethane Foam Heat Release.....	75
Figure 4 - 1: ISO 9705 Standard Test Apparatus.....	79
Figure 4 - 2: Front View of ISO 9705 Standard Test Room During Flashover Fire	79
Figure 4 - 3: Skin Simulant Sensor	83
Figure 4 - 4: Schmidt-Boelter Gauge.....	86
Figure 4 - 5: Gardon Gauge in Insulating Block.....	87
Figure 4 - 6: House Used In Full-scale Tests.....	89
Figure 4 - 7: Edmonton I House Floor Plan.....	90
Figure 4 - 8: Thermocouple Tree Located in North Bedroom.....	91
Figure 4 - 9: Thermal Insulating Board with Heat Flux Gauges	92
Figure 4 - 10: Support Structure for Heat Flux Gauges.....	92
Figure 4 - 11: Data Acquisition System.....	93
Figure 4 - 12: Sequence Showing Single Room Fire Growth and Location of Sensors..	94
Figure 4 - 13: Exterior Heat Flux Measured During Single Room Fire	95
Figure 4 - 14: Sequence Showing Entire House Fire Growth and Location of Sensors..	96
Figure 4 - 15: Exterior Heat Flux During Initial Portion of Full House Burn.....	97

Figure 4 - 16: Comparison of Sensor Response at 5 kW/m ²	100
Figure 4 - 17: Comparison of Sensor Response at 20 kW/m ²	101
Figure 4 - 18: Comparison of Sensor Response at 40 kW/m ²	102
Figure 4 - 19: Comparison of Sensor Response at 80 kW/m ²	103
Figure 4 - 20: Abandoned Office Building Used for Edmonton II Fire Tests.....	106
Figure 4 - 21: Plan View of Test Room Showing Location of Sensors.....	108
Figure 4 - 22: Example of Mattress (a) Before and (b) After Test	110
Figure 4 - 23: Test 1 Thermocouple Tree Temperature Measurements	110
Figure 4 - 24: Test 1 Ceiling Temperature Measurements	111
Figure 4 - 25: Test 2 Thermocouple Tree Temperature Measurements	112
Figure 4 - 26: Test 2 Ceiling Temperature Measurements	112
Figure 4 - 27: Comparison of h = 0.6 m Thermocouple Tree Results	113
Figure 4 - 28: Comparison of h = 1.2 m Thermocouple Tree Results.....	114
Figure 4 - 29: Comparison of h = 1.8 m Thermocouple Tree Results.....	114
Figure 4 - 30: Comparison of h = 2.4 m Thermocouple Tree Results.....	115
Figure 4 - 31: Comparison of Ceiling Thermocouple Location 1 Results.....	116
Figure 4 - 32: Comparison of Ceiling Thermocouple Location 2 Results.....	116
Figure 4 - 33: Comparison of Ceiling Thermocouple Location 3 Results.....	117
Figure 4 - 34: Comparison of Ceiling Thermocouple Location 4 Results.....	117
Figure 4 - 35: Comparison of Ceiling Thermocouple Location 5 Results.....	118
Figure 5 - 1: Edmonton I House Used for Test Burns	120
Figure 5 - 2: Schematic of House Used for Spatial Separation Calculations	121
Figure 5 - 3: Edmonton I Radiation Heat Flux Results	122

Figure 5 - 4: Theoretical Fire Heat Release Behaviour	125
Figure 5 - 5: Idealized Fire Heat Release Rate Curve	126
Figure 5 - 6: Comparison of Ceiling Thermocouple Location 5 Results.....	127
Figure 5 - 7: HRR Predicted Using Combustion Science Theoretical HRR	130
Figure 5 - 8: HRR Predicted Using Semi-Universal Fire	131
Figure 5 - 9: HRR Predicted Using Generic Upholstered Furniture Fire	138
Figure 5 - 10: NIST Full-Scale Mattress Burns	140
Figure 5 - 11: Comparison of Mattress HRR Modeling Techniques.....	142
Figure 5 - 12: NIST/CBHF Upholstered Furniture and Mattress HRR Correlation.....	145
Figure 5 - 13: Mattress 1 Predicted HRR Showing Point of Ceiling Flame Impingement and Temperature Correlations Used in Analysis.....	150
Figure 5 - 14: Mattress 2 Predicted HRR Showing Point of Ceiling Flame Impingement and Temperature Correlations Used in Analysis.....	151
Figure 5 - 15: Schematic of Enclosure Showing Thermocouple Locations 1 to 5 Relative to Mattress	154
Figure 5 - 16: Thermocouple 1 Location Predicted and Measured Temperatures	154
Figure 5 - 17: Thermocouple 2 Location Predicted and Measured Temperatures	155
Figure 5 - 18: Thermocouple 3 Location Predicted and Measured Temperatures	155
Figure 5 - 19: Thermocouple 4 Location Predicted and Measured Temperatures	156
Figure 5 - 20: Thermocouple 5 Location Predicted and Measured Temperatures	156
Figure 5 - 21: Model Sensitivity to Radial Distance, R, During Fire Growth to Flame Impingement.....	158

Figure 5 - 22: Model Sensitivity to Fire HRR, Q, During Fire Growth to Flame	
Impingement.....	159
Figure 5 - 23: Comparison of Other HRR Models Combined With the Alpert Ceiling	
Temperature Correlation to Experimental Results for Thermocouple 1	160
Figure 5 - 24: Average Hot Gas Layer Temperature Compared to Edmonton II	
Experimental Thermocouple Tree Results for Mattress 1	162
Figure 5 - 25: Average Hot Gas Layer Temperature Compared to Edmonton II	
Experimental Thermocouple Tree Results for Mattress 2	165
Figure A - 1: Schematic Diagram of Edmonton I House for Spatial Separation	
Calculations	177
Figure A - 2: Schematic of Bay Window and Sensor Tripod Location.....	181
Figure A - 3: Schematic Diagram Used to Determine View Factor	182
Figure A - 4: General Floor-Level Schematic of Edmonton I House.....	185
Figure A - 5: Living Room Floor Plan of Edmonton I House Showing Location of	
Sensors Used for Measuring Radiant Heat Flux Outside Window	186
Figure A - 6: North Bedroom Floor Plan of Edmonton I House	187
Figure A - 7: South Bedroom Floor Plan of Edmonton I House Showing Location of	
Sensors Used for Measuring Radiant Heat Flux Outside Window	188
Figure A - 8: Burn Test 1–South Bedroom Thermocouple Tree Temperature Results..	189
Figure A - 9: Burn Test 1 – Living Room Thermocouple Tree Temperature Results....	190
Figure A - 10: Burn Test 1–North Bedroom Thermocouple Tree Temperature Results	190
Figure A - 11: Burn Test 2 – Living Room Thermocouple Tree Temperature Results.	191
Figure A - 12: Burn Test 3 – Basement Thermocouple Tree Temperature Results	191

Figure A - 13: Burn Test 4–Living Room Thermocouple Tree Temperature Results.... 192

Figure A - 14: Burn Test 4–North Bedroom Thermocouple Tree Temperature Results 192

Figure B - 1: NIST/CBHF Upholstered Furniture and Mattress Correlation 208

Figure C - 1: Schematic of Enclosure Showing Thermocouple Locations 1 to 5 Relative
to Mattress 211

NOMENCLATURE

Notation

A	Area [m ²]
c	Thermal Capacity [kJ/kg·K]
C	Orifice Flow Constant
CM	Combustion Mass [kg]
d	Distance [m]
F	View Factor
FC	Frame Combustibility Factor
FF	Fabric Factor
FM	Frame Material Factor
H	Height [m]
h	Thermocouple Height [m]
h_k	Enclosure Conductance [kW/m ² /K]
k	Configuration Factor
$k_{thermal}$	Thermal Conductivity [kW/m·K]
L	Length [m]
\dot{m}	Mass Loss Rate [g/s]
\dot{m}_a	Mass Flow Rate of Air [kg/s]
PF	Padding Factor
\dot{Q}	Heat Release Rate [kW]
q''	Heat Flux [kW/m ²]
q''_o	Effective Peak Heat Flux Emitted by Fire [kW/m ²]
r	Radial Distance [m]
SF	Style Factor
t	Time [s]
t_o	Incubation Time [s]
u	Fraction of Unprotected Openings
x	Combustion Efficiency Factor
X_{CO}	Mole Fraction of Carbon Monoxide
X_{O_2}	Mole Fraction of Oxygen
X_{CO_2}	Mole Fraction of Carbon Dioxide
$X_{H_2O}^o$	Initial Mole Fraction of Water Vapour
$X_{O_2}^o$	Initial Mole Fraction of Oxygen
Z	Flame Height [m]

Greek Symbols

α	Fire Growth Coefficient [kW/s ²]
α_{th}	Thermal Diffusivity [m ² /s]
τ	Dummy Variable of Integration
ΔH_c	Heat of Combustion [kJ/kg]
ΔP	Pressure Drop [Pa]
ΔT	Change in Temperature [°C]
δ	Wall Thickness [m]
ρ	Density [kg/m ³]

Subscripts

1	Larger of Width or Height [m]
2	Smaller of Width or Height [m]
<i>a</i>	Actual
<i>b</i>	Burn
<i>e</i>	Exhaust
<i>f</i>	Flame Projection
<i>g</i>	Gas
<i>i</i>	Initial
<i>o</i>	Openings
<i>p</i>	Penetration
<i>s</i>	Surface
<i>u</i>	Unprotected Openings to Adjacent Building
max	Maximum
<i>vc</i>	Ventilation Controlled
<i>FO</i>	Flashover
<i>T</i>	Enclosure Interior
∞	Ambient
<i>cr</i>	Critical

Abbreviations

CFAST	Consolidated Model of Fire and Smoke Transport
CFD	Computational Fluid Dynamics
FDS	Fire Dynamics Simulator
HRR	Heat Release Rate
NIST	National Institute of Standards and Technology
NRC	National Research Council of Canada
NBC	National Building Code of Canada

CHAPTER 1: INTRODUCTION

There is a constant threat to life and property loss as a result of fires occurring in buildings ranging in size from houses to large office buildings and sports stadiums. There has been much attention to the threat of fire, especially in the last century, as evidenced by the many codes and standards developed by organizations such as the International Organization of Standards (ISO), American Society for Testing and Materials (ASTM) and the National Fire Protection Association (NFPA.) Many countries throughout the world have implemented National Building and Fire Codes, aimed at reducing the likelihood of fire, and reducing the property and life loss when fires do occur.

1.1 Fire Statistics

The Council of Canadian Fire Marshals and Fire Commissioners [1] indicate that there were 53,720 fires reported, 327 deaths and 2490 injuries due to fire in Canada in the year 2000 alone. Table 1-1, which follows, shows a relative listing of the average number of fire deaths and reported fire incidents based on occupancies for the time period 1994 to 1998, in the United States.

Table 1 - 1: United States Fire Deaths and Reported Incidents by Occupancy (1994-1998 Average) [2]

Property Description	Civilian Deaths (% of Total Fire Deaths)	Reported Fire Incidents (% of Total Fires Reported)
Homes and Garages	80.1	22.0
Transportation (e.g. vehicles)	13.4	21.2
All Public Buildings (e.g. hotels)	2.8	3.7
Other Structures (e.g. bridges)	1.7	1.8
Outdoor and Other (e.g. forests)	1.3	41.4
Industrial Environment	0.8	2.1

The data in the above table illustrates the serious problem of fire occurring in individuals' homes and also highlights the importance of public fire education and fire prevention in the home. The data contained in Table 1-1 also highlights the importance of this work, which will focus on analysis methods used to predict fire behaviour in single enclosures, and ultimately lead to more efficient and safe building designs.

1.2 Introduction to Fire Protection Engineering

There are different approaches that the fire industry currently takes in order to combat fire in buildings [2]. One of the methods, usually referred to as fire prevention, attempts to prevent fires from occurring in the first place, an example of which would be public fire safety education and the application of so-called 'fire-proof' or 'flame-resistant' materials. Another method that is used, usually referred to as fire protection, realizes that not all fires can be prevented and aims to limit the destruction when fires do occur. Examples of fire protection systems in buildings are: fire-resistant construction methods such as using drywall and concrete building materials, automatic fire detection and suppression systems as well as efficient occupant evacuation methods. Fire protection engineering, therefore, is the term that describes the application of engineering

principles to prevent fires from occurring and to limit the damage caused when fires do occur.

1.2.1 History

The specific discipline called fire protection engineering is a relatively new area of research and practice; however, engineers and building designers have been aware of the fire problem and have used different fire protection techniques in some form for hundreds of years, dating back to ancient civilizations [3]. The modern discipline of fire protection engineering involves fire protection design in buildings and other structures, in outdoor environments, in protective clothing research for industrial workers and firefighters and other materials research. Fire protection engineers often use experimental methods as well as empirical correlations and computer modelling techniques when analyzing problems, as will be discussed in more detail in the following sections.

Fire protection engineering research has been growing in popularity in the last 20 to 30 years. In his article for the 1986 Society of Fire Protection Engineers symposium titled “Techniques for Quantitative Fire Hazard Analysis”, Budnick proposes that historically, the approach to fire protection has little, if any, scientific basis [4]. He goes on to say that “beyond the simple concept that fire requires heat, oxygen and fuel, lies complex phenomena involving kinetics, fluid mechanics, thermodynamics and heat transfer. The development of a quantitative understanding of these processes, and the interaction with the environment and people has been slow.” [4]

Budnick highlights the need for more advanced quantitative analysis techniques that should be used in conjunction, and not to replace, existing methods based on prescriptive fire and building codes (which will be discussed in more detail in Section 1.3.1) and experience [4]. Since this article was published in 1986, fire research has increased and advancements in this field continue to occur.

1.2.2 Important Quantities in Fire Protection Engineering

Fire protection engineering is a broad, multi-disciplinary field of study as it incorporates many disciplines including chemistry, heat transfer, thermodynamics and fluid dynamics. There are many physical and chemical processes that occur within a fire, such as the combustion chemistry reactions and smoke and flame spread within a building, requiring researchers to have a broad understanding of different scientific and engineering disciplines.

In general, the combustion process involves a fuel (solid, liquid or gas) combining with oxygen and a heat source under the right atmospheric conditions to release energy to the surroundings by means of chemical reactions [5]. The heat or energy released from a fire is quantified by the term heat release rate (HRR), usually expressed in SI units of kW, and is the most important quantity to fire protection engineers and researchers [6,7]. The HRR describes the effective fire size or intensity, and is often quoted by fire protection engineers and researchers to describe a particular fire. In addition, the HRR is often the most important input variable for computer fire models [8] and fire protection engineering correlations [9]. It will be shown that the fire HRR, in addition to

other factors including geometry, can be used to estimate enclosure fire temperature, radiation heat transfer, flame height and other parameters [9].

It is commonly known that the inhalation of combustion products, commonly referred to as “smoke,” is the cause of the majority of fire deaths [10]. In general, the products of combustion can be toxic, obscuring and corrosive. As a result of the importance of the smoke production, during fire with respect to life safety, it is another one of the important quantities of interest to fire protection engineers [11]. In addition to HRR and smoke production fire protection engineers and researchers are concerned with the ignitability and rates of flame spread over materials [6,12], as these properties both help to describe the hazard of a fire and the propensity for materials to burn. An example of a common, standard flame spread and ignitability test method that is commonly performed is the ASTM E 1321: Standard Test Method for Determining Material Ignition and Flame Spread Rates Properties [13]. Other important standard fire tests will be discussed in Section 1.4.

1.3 Challenges Facing Fire Protection Engineers

There has been a significant campaign in many countries to increase the public knowledge and awareness of fire safety concerns. Recent events such as several devastating nightclub fires in the United States [14] and the World Trade Centre fires and subsequent building collapses in New York in 2001 [15] have thrust engineers, and specifically fire protection engineers into the public spotlight. Before events such as

these, many people did not know that engineers specialize in the area of fire protection engineering.

There are many challenges facing engineers that specialize in fire protection. These challenges range from the increased complexity and size of new buildings to the increased use of polymers in the manufacturing industry, which are known to release large amounts of energy and smoke, when burned, in comparison to more traditional building materials such as wood, concrete and metal [5]. One simply has to look around the home and notice how many products are manufactured from some kind of plastic or foam. Compared to fifty years ago, the amount of these products in everyday use has grown enormously. This has presented a unique problem to engineers tasked with protecting the public, both in homes and in public buildings.

One feature of building design and architecture that has become more common in large, public buildings is the atrium [11]. Atriums pose a challenge because they are typically a large, open space with very high ceilings, and yet many have combustible materials on the ground level [11]. Fire and smoke in an open space such as this, could spread quite quickly. Another example of the challenges facing fire protection engineers is the design of fire protection systems for larger, open floor-plan buildings such as those used in large retail stores or open-plan offices (e.g. cubicles.) These buildings pose challenges over more traditional smaller buildings, which are compartmentalized, reducing the rate of fire and smoke spread.

1.3.1 Fire Codes

There have been many devastating fires that have been documented throughout history that have virtually burned entire towns and cities to the ground. Historians believe that the first fire codes date back to the ancient Roman Empire [3], when fires would burn for days and ravage entire cities. At the same time, the first firefighters are thought to be soldiers and slaves attempting to extinguish fires with small buckets of water, handheld water syringes and short ladders.

In more recent times, modern-day engineers, contractors and builders have relied on codes, standards and guidelines such as the National Building Code of Canada [16], that prescribe fire protection techniques and construction methods in buildings. The existing National Building Code of Canada is very prescriptive as it outlines exact methods that must be used during construction and leaves little room for interpretation. The building code covers such items as wall and floor construction, smoke detector spacing and occupant egress.

As the NFPA Fire Protection Handbook indicates, the problem with the prescriptive-based fire code is that it may have limited scientific basis and relies quite heavily on past experience. Many of the details of the prescriptive code originated in reaction to major fire disasters in the last hundred years [17]. As a result, by today's scientific standards, the building code is a poor example of the application of solid engineering principles such as efficiency and innovation. Puchovsky [17] states that:

Many advances in fire safety have been made in recent time, but they are not being incorporated into everyday fire safety practice partly because of the prescriptive nature of our current codes...some believe that this lack of

technology transfer has allowed fire safety to fall behind other engineering disciplines, such as structural design, which is thought of as relying more heavily on scientific and engineering principles.

With fairly recent advances in fire protection engineering methods and analysis techniques, Canada, along with several other countries, is moving towards a new fire code approach, known as objective-based [18]. An objective-based fire code differs from the current prescriptive fire code in that it allows for more fire protection engineering design. The concept behind objective-based codes is that they will set the overall objective of a specific aspect of building construction. An engineer can then select how they will meet the objective, therefore allowing the most flexibility and opportunity for innovative design. The new objective-based approach, however, will still allow designers to adopt the old, prescriptive-based approach as well. Performance-based codes are another type of code, in which the code outlines a minimum performance level and an engineer must prove that their design meets this certain, minimum performance level. Many, especially fire protection engineers, are excited about the new codes in Canada, as they anticipate that it will allow for much more innovation, and also has the potential to reduce the cost associated with fire protection systems in buildings [18].

In the 2003 version of the NFPA Fire Protection Handbook, Puchovsky [17] says about performance-based codes “The principal argument [against prescriptive codes] is that fire safety can be accomplished more effectively by quantifying the level of safety required, and verifying that the entire fire safety package delivers that level of safety.”

He goes on to say about the challenges of performance-base codes: “The lack of

quantifiable fire safety goals, as well as a tangible interface between regulations and the relevant tools and data needed to conduct performance-based design, present such barriers.”

One source of concern that is associated with the move towards objective-based codes, is the requirement for accurate, reliable analysis techniques that engineers can use when assessing the performance and feasibility of new fire protection designs [18]. The engineering industry, combined with the appropriate government agencies, must establish acceptable analysis techniques and methods for approving the new designs. The challenge of acceptable analysis techniques forms the basis for this research work, as will be discussed in Section 1.5.

1.4 Experimental Fire Research

Experimental fire research is commonly performed in government research facilities such as the National Research Council of Canada (NRC) as well as in university and private industrial laboratory settings. Fire researchers perform both full-scale and small-scale fire tests. Full-scale fire tests typically refer to full-size building, room (enclosure) mock-ups or full-size product tests representing a real-life fire scenario. Small-scale fire tests, on the other hand, typically refer to tests performed on a small representative sample of a larger product or assembly. Full-scale and small-scale fire tests will be discussed in more detail in the following sections.

Even with the recent advances in computers and successes in numerical modelling, fire protection engineering research still relies quite heavily on experimental research, due to challenges in accurately modeling the fire combustion and physical processes that occur. In general, full-scale fire tests can be broken down into two types: standardized tests performed in a laboratory setting and field fire tests, typically performed in real-life scenarios as will be discussed in more detail in Chapter 4.

1.4.1 Full-Scale Fire Tests

A common laboratory-based full-scale experimental test that is performed is described by the ASTM E 2067: Standard Practice for Full-Scale Oxygen Consumption Calorimetry Fire Tests [19] as will be discussed in more detail in Chapter Four. The test apparatus described in ASTM E 2067 [19] is commonly used to determine the burning behaviour of surface lining materials (as described in the ISO 9705 test standard [20]) and products such as mattresses. Another type of full-scale fire test that is commonly performed is the furniture calorimeter test, which was developed in the early 1980s [21]. The furniture calorimeter apparatus was designed for full-scale tests of furniture products such as upholstered furniture, however, it has been used to test many other products such as warehouse-style stacked commodities [21]. The furniture calorimeter differs from the ASTM E 2067 full-scale enclosure test in that objects are burned in an open space, directly under a large hood which collects the products of combustion for analysis.

Full-scale fire tests are typically expensive and time-consuming to perform, however, they provide a good means for determining real-life burning behaviour of products and

surface linings. Laboratory-based full-scale fire tests such as the ASTM E 2067 [19] and ISO 9705 [20] fire tests use the oxygen consumption calorimetry technique to determine the heat or energy released by the fire, as will be discussed further in Chapter 3. Laboratory-based full-scale fire tests typically measure the heat or energy release rate and smoke production, however, they can be also be instrumented to measure other quantities of interest such as heat flux, temperature and combustion product gas species analysis depending on the specific type of test being conducted.

1.4.2 Field Fire Tests

Field fire tests, which are carried out in actual buildings, are typically not as controlled as laboratory-based full-scale fire tests. There is often a lack of control over environmental variables such as ambient temperature, relative humidity and wind conditions during field fire tests. In addition, field-fire tests typically do not measure the heat release rate or smoke production rates, as relatively complicated and specialized equipment is necessary for these measurements, and instead measure quantities such as temperature and heat flux. Field fire tests, however, often give researchers the opportunity to conduct full-scale fire testing that otherwise could not have been accomplished, as very few facilities exist in Canada which have a dedicated full-scale fire testing apparatus.

Perhaps the most famous set of field fire tests that have been performed in Canada were done by the NRC in the late 1950's, commonly known as the St Lawrence Burns [22]. The NRC collected data from eight different building fires in the abandoned village of Aultsville, Ontario, which was to be flooded as a result of the St. Lawrence Seaway

construction. Researchers from the NRC measured heat fluxes at various distances as well as the horizontal flame projection from the burning buildings in order to investigate the radiation heat transfer from the buildings, and the propensity for fire spread fire between the buildings. It has been found and well documented (e.g. [5,23]) that cellulosic materials (wood-based), will ignite in the presence of a pilot flame or heat source at a critical incident heat flux of 12.5 kW/m^2 . These results were used to determine the minimum separation distance between buildings, termed spatial separation, in order to prevent fire spread. The research performed by the NRC in the 1950's and 1960's forms the basis for current spatial separation requirements in many countries including Canada and is expressed in terms of tabulated results allowing designers to estimate the required distances between buildings for a particular building design [18].

1.4.3 Small-Scale Fire Tests

Small-scale fire testing is another type of experimental fire testing that is commonly performed. Often, the main goal of small-scale testing is to understand how a material or assembly will perform during a real-life fire scenario or a full-scale fire test, based on results from burning a small sample. Small-scale experiments are also run in a laboratory setting, allowing conditions such as temperature and humidity to be controlled. Small-scale tests also allow researchers to more easily measure certain fire parameters, such as flame spread and temperature variation, versus full-scale tests. Perhaps the greatest advantage of small-scale testing, however, is that it is much more economical than full-scale tests. Small-scale tests can be performed at a fraction of the cost of full-scale tests.

Within the area of building materials research, one of the more common small-scale tests performed uses the cone calorimeter as described in ASTM E 1354: Standard Test Method for Heat and Visible Smoke Release Rates for Materials and Products Using an Oxygen Consumption Calorimeter [24]. The cone calorimeter has become one of the most important small-scale fire research tools in recent years [21,25] and will be discussed in more detail in Chapter 3.

Perhaps the greatest disadvantage of small-scale testing is that it is often difficult to predict full-scale or real-life behaviour from the small-scale results. There has been much work by researchers (e.g. [12,26-28]) to try and correlate small-scale and full-scale results, with varying degrees of success, as will be discussed in Section 2.4.2. Another disadvantage of small-scale testing is that often it does not represent the ‘real-life’ or full-scale situation exactly. An example of this is that small-scale testing is often done only in two-dimensions, such as the cone calorimeter standard test method, however, fire spread in full-scale tests often has three-dimensional effects as fires burn in both the horizontal and vertical directions.

1.5 Enclosure Fires

The emphasis of this research was to examine building fire research and analysis methods. More specifically, it dealt with fires in single, relatively small scale enclosures (e.g. bedrooms.) This is different than the work of other researchers who have investigated larger, multi-room and multi-storey buildings both through experimental

methods and computer simulations (e.g. [29,30].) This section will describe some of the terminology and background information associated with enclosure fires.

1.5.1 Fire Plume in an Enclosure

Figure 1 - 1, following, shows a schematic of a fire plume inside an enclosure. The term fire plume refers to three distinct portions of the fire; the persistent flame located immediately above the fuel, the intermittent flame region characterized by intermittent flames in time and space and the buoyant fire plume characterized by decreasing temperature and velocity with increasing height above the fuel [5]. The buoyant fire plume is comprised of the hot gases and smoke products released by the fire, and if unbounded, will continue to grow in radius, r , and height, z , until buoyancy forces are overcome by frictional drag forces acting between the buoyant plume and ambient air.

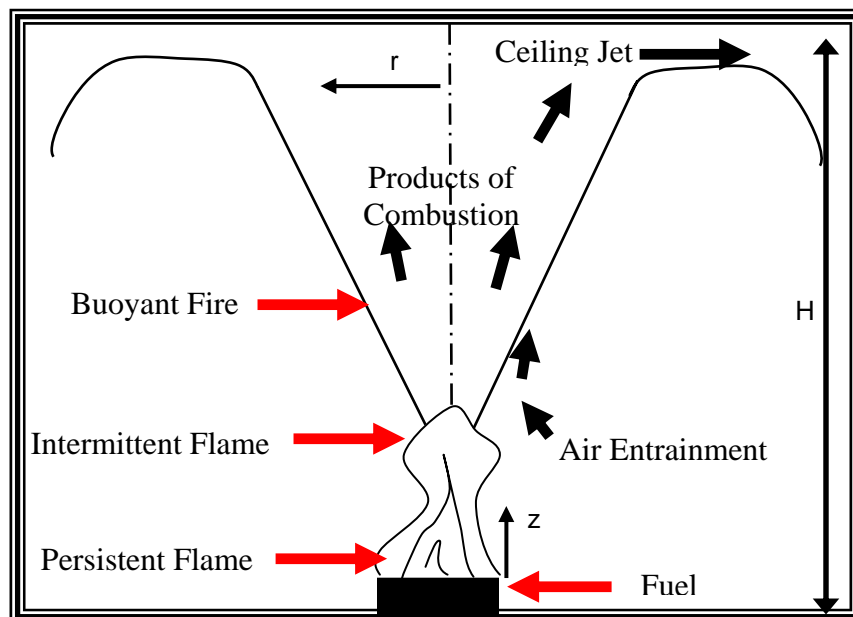


Figure 1 - 1: Fire Plume in an Enclosure

As demonstrated in Figure 1 - 1, ambient air will be entrained in the buoyant fire plume due to viscous forces acting between the buoyant plume and ambient air. The entrained air will serve to effectively cool the buoyant plume. If the fire is bounded by an enclosure, such as in the above schematic, the rising buoyant plume will impact the ceiling and form a ceiling jet. The ceiling jet will move horizontally across the ceiling until it sufficiently cools and begins to fall, or until it impacts an obstacle (such as a wall.) If the fire has sufficient conditions to continue growing, in an enclosure (room), a layer of hot combustion gases or products of combustion will eventually form at the ceiling and will grow until the fire is extinguished or until the hot combustion gas layer escapes the room (possibly through a door or window.)

1.5.2 Flashover

Flashover is a term which describes a transition in an enclosure fire from localized burning to a full-developed enclosure fire where all combustible items are involved. Flashover is a very dangerous in terms of occupant and fire service personnel life safety, as extremely intense fire conditions are present [5]. Drydale [5] indicates that flashover is also defined as the transition from a fuel to ventilation controlled fire and the point where the heat flux measured on the enclosure floor reaches 20 kW/m^2 . Several methods of predicting the fire size or HRR required for flashover have been developed [29] and one of these methods will be presented in Section 2.4

In order for flashover to occur, a fire must produce a significant build-up of hot products of combustion at the ceiling of an enclosure. Flashover occurs when the effective temperature of the hot gas layer becomes sufficient enough to radiate a heat flux

exceeding that required for the piloted ignition of the other combustible products in the enclosure, causing them to ignite. As a consequence of the rapid fire spread in the enclosure, very dangerous thermal conditions are present likely resulting in very serious injury or death of any occupants, including fire service personnel wearing protective clothing. Flashover in one room can also cause rapid fire spread throughout the rest of a building.

1.5.3 Fuel and Ventilation Controlled Fires

The transition from fuel to ventilation controlled fire is one of the definitions proposed for the onset of flashover. The two major factors affecting the ability for a fire to grow are the amount of fuel and the amount of oxygen present in the enclosure, corresponding to either a fuel controlled or ventilation controlled fire respectively. In simple terms, a fuel controlled fire is limited only by the amount of fuel present, whereas a ventilation controlled fire is limited only by the amount of oxygen available for the combustion reactions. Ventilation and fuel-controlled fires will be discussed in more detail in Section 2.3.5.

1.6 Fire Protection Engineering Analyses

As discussed in Section 1.3.1, with respect to objective-based building codes, it is becoming increasingly important to have reliable and accurate methods of predicting fire behaviour for purposes of building and fire protection system design. The methods commonly used for engineering analyses are numerical methods involving computer programs, ranging from zone to computational fluid dynamics programs, and empirical

correlations. The following sections will discuss several of the common approaches of both computational and correlative methods.

1.6.1 Numerical/Computational Methods

In recent years, with great advances in computer technology, numerical and computational tools to model fire scenarios have been increasing in popularity. Several tools exist which model fire scenarios with varying degrees of success (e.g. [30-32]).

Two of the most common types of computer fire modeling approaches are zone models and computational fluid dynamics (CFD) or field models [33]. A few examples of widely used, and well-supported numerical modelling programs include the Consolidated Fire and Smoke Transport model (CFAST) [34], developed by the United States National Institute of Science and Technology (NIST), which is a two-zone model and Fire Dynamics Simulator (FDS) [34] also developed by NIST, which is a CFD or field model.

Observations of distinct, stratified regions of smoke made during experimental building fires led to the development of the zone modeling approach. A zone model divides the compartment into a small number (usually two) of separate regions (zones), and then the interaction between the zones is determined. Zone models most commonly divide the enclosure into two zones: a hot upper gas layer and a cool, lower layer [30,35,36]. The zone models assume the temperature, smoke and gas concentrations are constant within a specific zone and use simplified versions of conservation equations of energy, mass and momentum in addition to the ideal gas law [37] to determine the heat transfer and smoke movement between the zones [35]. Zone models have been used very

successfully for a number of fire scenarios and are typically less computationally intensive than CFD models due to their simplifying assumptions [33].

Field computer models or CFD fire models are more sophisticated than zone models in that they discretize the enclosure into a large number of cells and then calculate the temperature, velocity and gas concentrations for each cell based on solving the mass, energy and momentum conservation equations and chemical species equations at each cell [33]. The CFD models are not subject to as many simplifying assumptions as zone models, and as a result, should be more accurate [35,37]. The application of CFD models to solve real-life fire scenarios is ever-increasing [30,33], however, challenges such as modeling the heat release rate of the fire still exist.

Current CFD models cannot generally model the fire heat release rate and require the user to input the fire growth characteristics such as a heat release rate – time history [8]. Difficulties such as these limit the use of CFD models in solving real-life fire problems as evidenced by Bounagui et al. [32] during an investigation by NRC to model the heat release rate of upholstered furniture fires by FDS. Presently, CFD models still have many problems that must be addressed including the modeling of flame spread, turbulence in the buoyant fire plume and radiation exchange between soot, gases and solid surfaces, combustion, fire growth and the resulting heat fluxes [33], however, they do represent the state-of-the-art in computer fire modeling and will undoubtedly overcome these challenges in the future.

1.6.2 Engineering Correlations

In addition to the many computer fire modeling codes available, fire protection engineers continue to rely on simplified fire growth and fire hazard calculation techniques that have largely been developed using empirical results, obtained from relatively small spaces [38]. The chemistry and physics of fire combined with considerable experimental research has lead to the development of reasonably accurate approximations for quantities such as heat release rate, flame height, fire temperature, prediction of flashover, smoke growth and fire detector response times. With respect to practicing fire protection engineering consultants, simplified engineering correlations which can be hand-solved without the use of a sophisticated computer program, while still providing reasonable estimates of fire behaviour are obviously preferred due to time constraints and specific software costs and training. Complex fire problems require the use of a computer modeling technique, although simplified engineering correlations often produce acceptable results [32,39]. Relatively simple engineering correlations are the focus of this research work and will be discussed in more detail in Chapter 2 and throughout the thesis.

1.7 Other Major Upholstered Furniture Fire Modeling Studies

There have been several initiatives by large research organizations such as the National Institute of Standards and Technology (NIST) in the United States, the California Bureau of Home Furnishings (CBHF) and the Combustion Behaviour of Upholstered Furniture (CBUF) group [34] to investigate methods of using small-scale fire test results to predict full-scale fire behaviour. Methods of predicting full-scale fire behaviour

based on small-scale results presents unique challenges to researchers [40,41], such as the choice of representative small-scale test samples and preparation procedures.

The CBUF study, undertaken as a collaboration of 11 participants from eight European countries, costing approximately 2.5 to 3.0 Million ECU and taking approximately two years to complete, is the most comprehensive research into the combustion of upholstered furniture that has ever been undertaken [41]. The purpose of the CBUF project was to develop both small and full-scale fire test methods to assess the burning behaviour of upholstered furniture leading to European standards aimed at improving fire safety of upholstered furniture [42]. The general approach taken by the CBUF project is outlined below.

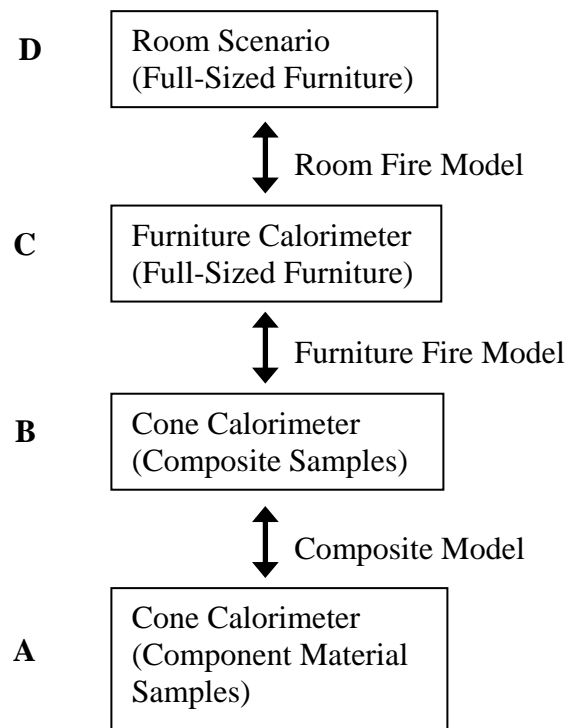


Figure 1 - 2: CBUF Project Structure [42]

With reference to Figure 1 - 2, the goal of the CBUF project was to be able to take cone calorimeter results of individual upholstered furniture materials and accurately predict cone calorimeter composite sample results (a combination of upholstered furniture material layers), predict furniture calorimeter full-scale results and ultimately predict real-life room scenario results. Considering the immense investment in the CBUF project, several researchers (e.g. [43]) have found that the models presented do not necessarily provide acceptable predictions of fire growth characteristics, highlighting the challenges of this area of fire research. While the CBUF project represents the most sophisticated and comprehensive investigation of upholstered furniture, it was the intent of this thesis work to investigate a simpler, more direct approach to fire modeling mattresses. With respect to this thesis project, the objective was to go directly from cone calorimeter component material and composite sample results (shown in boxes A & B in Figure 1 – 2) to predicting full-sized furniture behaviour in an enclosure, (shown in box D in Figure 1 - 2) without performing furniture calorimeter experiments or modeling.

1.8 Research Objectives

The research conducted for this thesis project had the following objectives:

- The primary objective of this research work was to examine methods of predicting enclosure fire behaviour. Various methods commonly used to predict heat release rates in fires were evaluated, based on practicality (ease-of-use), and by comparisons with results from fire tests of mattresses conducted in a bedroom-sized enclosure (referred to as the Edmonton II set of experiments). While full-scale experimental heat release rates could not be obtained in these

fire tests, the heat release rates models were used to predict temperatures for the mattress fires, which were then compared to temperatures measured in field fire tests.

- One of the secondary objectives of this research project was to examine spatial separation requirements, based on current guidelines in the National Building Code of Canada. The spatial separation requirements were examined with respect to a full-scale experimental house burn that was conducted in Edmonton, AB in July 2003, referred to as the Edmonton I set of experiments.
- The secondary objectives also include simply performing full-scale field fire tests and gaining field fire test knowledge. These types of field fire tests have not been performed by the University of Saskatchewan Fire Research Group prior to this work.
- Another secondary objective is to simply perform cone calorimeter small-scale fire tests using a recently acquired cone calorimeter by the University of Saskatchewan Fire Research Group. Very few cone calorimeter tests have been performed at the University of Saskatchewan, allowing this work to contribute to the knowledge of this piece of equipment in the Fire Research Group.

1.9 Overview of Thesis

The next chapter of this thesis will discuss the specific engineering correlations and simple modeling techniques that have been presented in the literature with respect to heat release rate modeling, flashover, flame height and enclosure temperature predictions. Chapter 3 will discuss small-scale fire testing in general and more

specifically the cone calorimeter tests that were performed to gain an understanding of the fire behaviour of mattresses. The results from the full-scale fire tests conducted to investigate the current spatial separation guidelines and the full-scale experimental mattress burn results that were performed will then be presented and discussed in Chapter 4. Comparisons between the modeling techniques and the full-scale experimental results will then be made in Chapter 5 and the appropriateness of the various modeling techniques and implications discussed. Conclusions from this research work are made and related topics for future work discussed in Chapter 6.

CHAPTER 2: FIRE GROWTH MODELING TECHNIQUES AND ENGINEERING CORRELATIONS

As mentioned in Chapter 1, there is currently a considerable amount of research being performed on developing reliable, accurate computer fire models. The current state-of-the-art fire models are classified as field models and rely on CFD techniques in order to discretize the enclosure into many finite volume elements and solve the fundamental differential equations of mass, momentum and energy for each tiny element [33]. While computing power continues to grow, and CFD models become more robust, one of the inherent challenges of accurate fire engineering computational analyses is modeling the fire growth, or heat released by the combustible items, in a compartment both before and after flashover. This research project will focus entirely on the pre-flashover regime, however, it should be noted that correlations have been developed for post-flashover fires.

In a fire protection engineering analysis of an enclosure, especially in a consulting engineering or industry setting, modeling techniques that give timely estimates of fire behaviour and do not involve sophisticated computer programs are often sought. This chapter will focus on reviewing some of the relatively simple techniques that are used by fire protection engineers to predict spatial separation requirements, model fire growth and the resulting fire conditions in enclosures.

2.1 Spatial Separation

In the early stages of a building fire, the flames will largely be contained within the structure by the walls and the roof. The fire spread to the outside of the building will typically occur through broken windows and open doors, referred to as unprotected openings. In a spatial separation analysis, all windows and open doors on a wall are typically combined into a single effective unprotected opening of an equivalent area. An effective peak heat flux is then assumed to be emitted from this single unprotected opening to the surroundings. As a result of the St Lawrence Burns experiments, two fire hazard cases were suggested for spatial separation calculations [23]. It is assumed that building fires will fall into either a “normal” or “severe” fire hazard, where assumed effective peak heat fluxes, q''_o of 180 kW/m^2 and 360 kW/m^2 , respectively, are emitted from the unprotected openings, which is based on experimental results [23]. Assuming a critical incident heat flux, q''_{cr} , of 12.5 kW/m^2 for ignition of adjacent buildings (as discussed in Chapter 1), critical view factors required for ignition of adjacent buildings are calculated.

The view factor for the “normal” and “severe” fire hazard must be reduced to critical view factors of 0.07 and 0.035 respectively to prevent fire spread between buildings (calculated by Equation 2.1 below.) A flame projection, d_f , from the unprotected openings of the burning building of 1.5 m and 2.1 m for the normal and severe fire hazard cases respectively have been suggested [23] and are shown in Figure 2 - 1 below. The actual view factor is calculated from the unprotected opening of the burning building to a point directly opposite the middle of the unprotected opening on the

adjacent building by standard view factor equations such as Equation 2.2 or tabulated data printed in standard heat transfer textbooks (e.g. [5].) Figure 2 - 1, below, describes the variables for this calculation. The view factor equations combined with the assumed peak heat fluxes emitted from the unprotected openings can also be used to calculate the radiation heat flux received at any location outside the building. The following equations are taken from McGuire [23].

$$F_{cr} = \frac{q_{cr}''}{q_o''} \quad (2.1)$$

$$F_u = \frac{2u}{\pi} \left[\sqrt{\frac{\alpha S}{\alpha S + 4}} \arctan \sqrt{\frac{\alpha / S}{\alpha S + 4}} + \sqrt{\frac{\alpha / S}{\alpha S + 4}} \arctan \sqrt{\frac{\alpha S}{\alpha / S + 4}} \right] \quad (2.2)$$

where:

$$S = \frac{L_1}{L_2}$$

$$\alpha = \frac{L_1 L_2}{d^2}$$

$$d = d_a - d_f$$

where:

- F_{cr} = Critical View Factor
- q_{cr}'' = Critical Heat Flux for Ignition (12.5 kW/m^2) [kW/m^2]
- q_o'' = Effective Peak Heat Flux Emitted by Fire [kW/m^2]
- F_u = View Factor from Unprotected Openings to Adjacent Building
- L_1 = Larger of Building Face Width (w) or Height (H) [m]
- L_2 = Smaller of Building Face Width (w) or Height (H) [m]
- d_a = Actual Distance Between Adjacent Buildings [m]
- d_f = Flame Projection Distance [m]
- u = Fraction of Unprotected Openings.

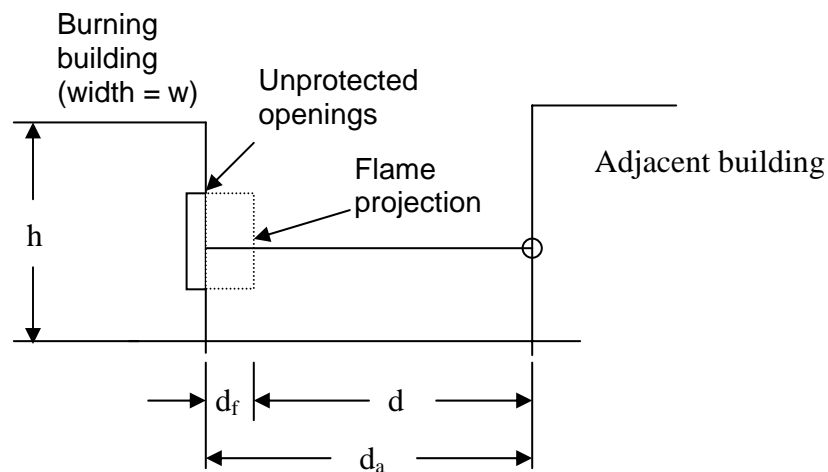


Figure 2 - 1: Schematic Describing Spatial Separation Variables [44]

Canada's National Building Code contains tables that are based on these calculations, where the building designer would choose the height and width of the compartment as well as the percent of unprotected openings and could therefore easily obtain the required separation distance [16,23]. Alternatively, a designer could determine the fraction of unprotected openings for a building face given the separation distance.

2.2 Heat Release Rate Modeling

As described in Chapter 1, the heat release is the most important quantity in describing a particular fire or assessing the fire hazard in a particular enclosure. Most of the techniques that have been developed for predicting fire behaviour have the full-scale heat release rate as the prime input variable [38] as will be discussed in further detail in the following sections. As a result, a reliable technique for estimating the heat release rate as a particular fire grows is extremely important.

There have been many different approaches developed for calculating the energy released when a material burns based on physics, a combination of physics and empirical results or purely empirical results [12,21]. Many computer fire models have been developed that allow users to specify the fire characteristics by selecting an appropriate fire growth model. Most of these computer modeling packages allow the user to either input a data-file with the input heat release rate as a function of time or by selecting one of the programs' built-in fire growth models. Most of the computer programs have adopted relatively simple fire growth modeling techniques based on a combination of physics and experimental results [8].

Krasny et al. [12] indicate that there has been limited experimental work aimed at trying to predict full-scale room fire heat release rates based on cone calorimeter results for mattresses specifically. For the purposes of this research, mattresses are assumed to be similar to upholstered furniture with regards to materials, construction methods and burning behaviour, as much more research has been performed on single upholstered

furniture items. Several other researchers have grouped upholstered furniture and mattresses together for these same reasons (e.g. [27].) While there have been more sophisticated fire growth models examined in the literature (e.g. [12,28,45]), the aim of this work is to investigate a simplified approach to fire growth modeling and temperature prediction. Several of the most relevant fire growth models to this research work will be discussed in the following sections.

2.3 HRR Growth Phase Modeling

Enclosure fires will theoretically grow according to the heat release rate – time history shown in Figure 2 - 2.

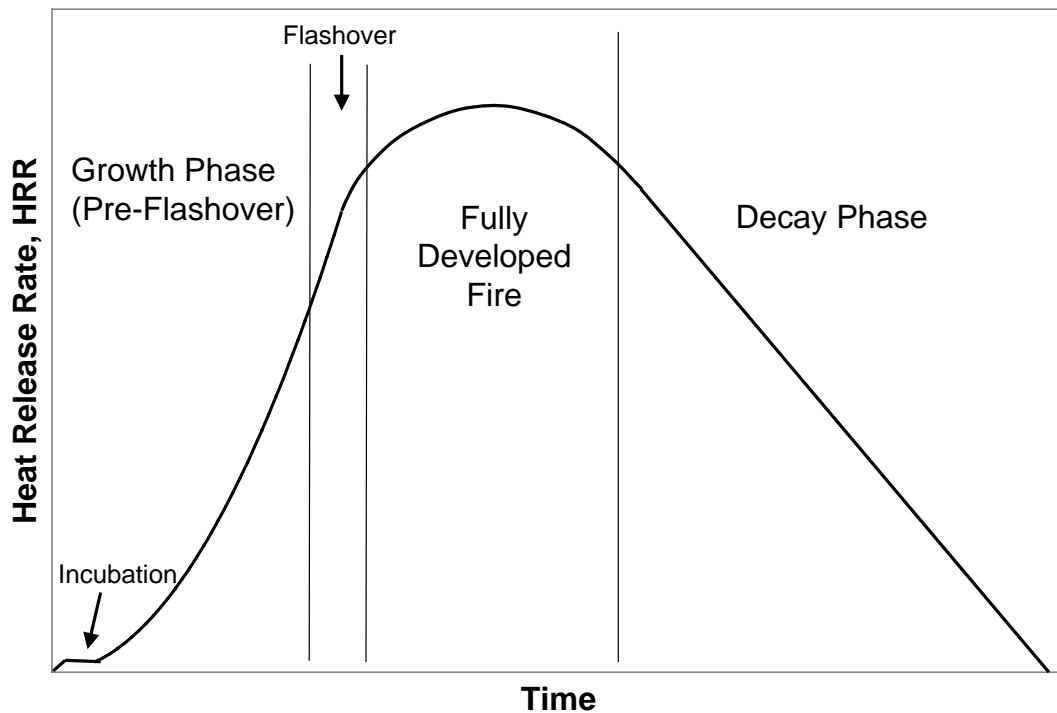


Figure 2 - 2: Theoretical Fire Heat Release Behaviour [5]

This research project is primarily concerned with the pre-flashover or growth phase, although it includes a discussion on the predicted flashover heat release rate for the Edmonton II set of experiments. The following sections will discuss several methods of predicting the fire HRR during the growth phase. Section 2.4 will discuss methods of predicting the maximum HRR and the HRR required to produce flashover.

2.3.1 Combustion Science Theoretical Rate of Heat Release

The theoretical energy released from a burning material during the growth phase of a fire can be obtained, according to combustion chemistry, from the following equation [5]:

$$\dot{Q} = \dot{m}x\Delta H_c \quad (2.3)$$

where:

$$\begin{aligned} \dot{Q} &= \text{Heat Release Rate [kW]} \\ \dot{m} &= \text{Rate of Mass Loss [g/s]} \\ x &= \text{Efficiency Factor} \\ \Delta H_c &= \text{Heat of Combustion [kJ/g]}. \end{aligned}$$

Prior to the development of oxygen consumption calorimetry, which is discussed in more detail in Section 3.1.2, the above equation was one of the primary means by which scientists experimentally obtained the heat release rate of a full-scale burning object [5]. This general approach of modeling fire growth, or a variation of it, is currently used by several computer fire modeling programs including the NIST CFAST program [8].

This equation requires an accurate mass loss rate and heat of combustion to be determined, which is often difficult to acquire, especially for composite samples constructed of several materials, such as a mattress sample. In addition, an efficiency factor is added to the equation to account for incomplete combustion and can vary from 0.35 to 0.99 depending on the fuel being burned [5]. Extensive information regarding the efficiency factor is not readily available for many materials, and especially not composite samples. As a result of the uncertainty in determining the mass loss rate and in the choice of the efficiency factor, other methods of modeling the heat release from a burning object are often preferred.

2.3.2 Semi-Universal Heat Release Model

Another type of fire growth model that has been developed through experimentation is the semi-universal fire specification. This is one of four input fire growth models in the FIRM software package [8], and is intended to provide a generic estimation of fire growth. The heat release rate can be estimated during the growth phase of the fire using the following equations:

$$\dot{Q} = \left\{ \begin{array}{ll} 10 \exp(0.025t) & 0 \leq t \leq 147.6 \\ 400 \exp(0.01(t-145.6)) & 147.6 \leq t \leq 349 \\ 300 \exp(0.005(t-349)) & 349 \leq t \end{array} \right\} \quad (2.4)$$

where:

\dot{Q} = Heat Release Rate [kW]

t = time[s]

This fire growth model is very general and does not account for differences in the fuel being burned and is only intended for a rough estimation of common material burning characteristics.

2.3.3 Generic Upholstered Furniture Fire Growth Model

In the mid-1980's, another generic correlation for modeling the burning characteristics of upholstered furniture was developed. Babrauskas developed the triangular shaped characteristic fire growth model, shown in Figure 2 - 3, while conducting research at NIST [8,12]:

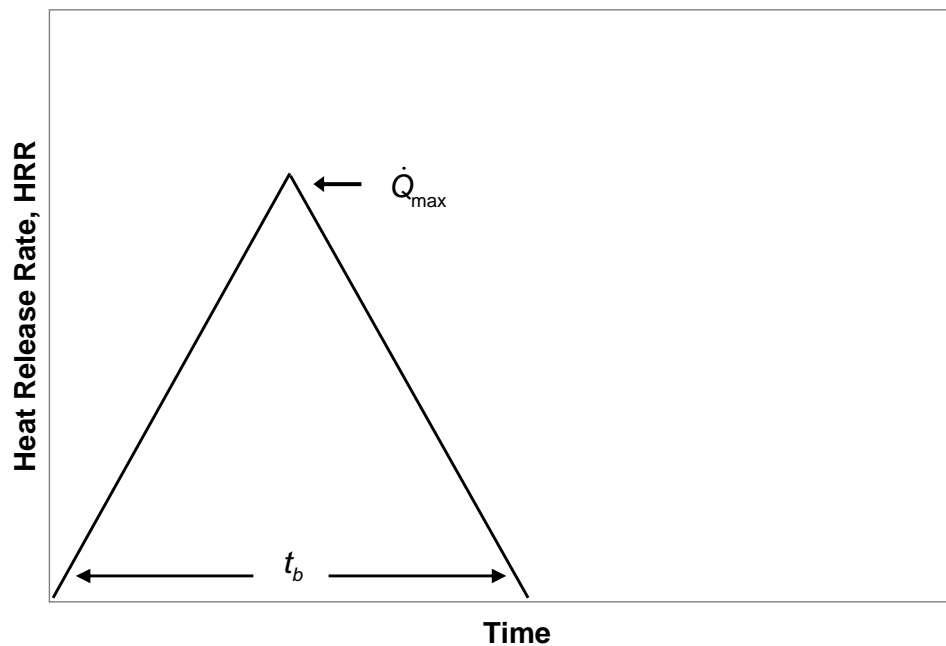


Figure 2 - 3: Generic Upholstered Furniture Fire Growth Model

The maximum heat release rate and triangular base time are given by the following equation, calculated as the product of several dimensionless factors:

$$\dot{Q}_{\max} = 210(FF)(PF)(CM)(SF)(FC) \quad (2.5)$$

where:

\dot{Q}_{\max} =Maximum Heat Release Rate [kW]

FF =Fabric Factor

PF =Padding Factor

CM =Combustion Mass [kg]

SF =Style Factor

FC =Frame Combustibility Factor.

This model assumes a triangular shaped growth phase heat release curve, with the maximum heat release rate occurring at half of the following burn time, t_b :

$$t_b = \frac{(FM)(CM)\Delta h_{c,net}}{\dot{Q}_{\max}} \quad (2.6)$$

where:

t_b =Burn Time [s]

FM =Frame Material Factor

ΔH_c =Heat of Combustion [kJ/kg].

The factors listed in the above equations are explained in more detail in the following table.

Table 2 - 1: Suggested Input Values for Generic Upholstered Furniture Fire Growth Model [12]

Factor	Description	Suggested Value in Literature
Fabric (FF)	Thermoplastic Fabrics	1.00
	Cellulosic Fabrics	0.40
	PVC or Polyurethane Film Coverings	0.25
Padding (PF)	Polyurethane Foam or Latex Foam	1.00
	Cotton Batting	0.40
	Neoprene Foam	0.40
	Mixed Materials (i.e. both polyurethane and cotton)	1.00
Frame (FC)	Non-Combustible	1.66
	Melting Plastic	0.58
	Wood	0.30
	Charring Plastic	0.18
Style (SF)	Ornate, Convolute Shapes	1.50
	Intermediate Shapes	1.2-1.3
	Plain, Primarily Rectilinear Construction	1.00
Frame Material (FM)	Metal, Plastic	1.80
	Wood	1.30

The challenge, and possibly the downfall of this model, is the inability to accurately classify the burning item based on the various dimensionless input factors that range from 0 to 1.0. This fire growth model is included in the FIRM computer package as an input fire growth model [8].

2.3.4 Time-Squared (t-Squared) HRR Fire Models

One of the most popular methods of predicting fire growth for fire protection engineering purposes is to assume a power-law relationship for heat release rate as a function of time. This approach has been well-supported by experimental data [46] and is commonly used by engineers to estimate the fire hazard of a specific enclosure and

fuel. This method is also incorporated into fire protection engineering standards and design methods such as the NFPA 72, National Fire Alarm Code [47].

Through experimentation, it has been found that the heat release growth rate of the majority of flaming fires of common materials, with the exception of flammable liquid fires, follows a parabolic profile, and has the following power-law relationship, commonly referred to as the t-squared fire model:

$$\dot{Q} = \alpha(t - t_o)^2 \quad (2.7)$$

where:

- \dot{Q} = Full-Scale HRR [kW]
- α = Fire Growth Coefficient [kW/s²]
- t_o = Incubation Time [s]
- t = Time [s].

The incubation time refers to the length of time from initial ignition required before significant flame spread occurs, typically associated with smouldering combustion.

When using the t-squared fire model, a fire is usually assumed to fall into one of the following categories of the fire growth coefficient:

Table 2 - 2: Typical Materials Associated With t-Squared Fires [5,29]

t-Squared Fire Classification	α (kW/s²)	Typical Materials
Slow	0.00293	Solid Wood Cabinetry, Densely Packed Paper
Medium	0.01172	Upholstered Furniture, Traditional Mattress/Boxspring
Fast	0.0469	Wood Pallets, Thin Plywood Wardrobe, Polyurethane Foam Mattress
Ultra-Fast	0.1876	High-rack storage, Some Polymers

The t-squared fire growth model has proven to be a good fire growth modeling technique and has become quite popular in modeling full-scale heat release rate. One advantage of this model is that it requires only an estimation of a fire growth coefficient to obtain the heat release rate history, which can be estimated based on an established list of typical materials. One of the problems associated with this model is that it does not allow for prediction of the maximum heat release rate, although that can be estimated based on the prediction of flashover and other factors as will be discussed in the following sections. The t-squared fire model also assumes that the fire is fuel-controlled.

2.3.5 Ventilation vs. Fuel Controlled Fires During Fire Growth Phase

The growth of any fire is limited by the amount and type of fuel and the amount of oxygen available for combustion reactions. Fires can either fall in the fuel-controlled or ventilation-controlled regimes, meaning that the fire growth is either limited by the amount of fuel or by the amount of oxygen respectively. Through experimental research, it was found in the late 1950's [5] that one could determine if a fire would be fuel or ventilation-controlled based on experimental evidence of burning behaviour and of the geometry of the enclosure openings (windows and doors). The following correlation was found to be a good predictor of fuel or ventilation-controlled burning [5]:

$$\begin{aligned} \dot{Q}_{vc} &= 3000 \cdot \dot{m}_a && \text{[kW]} \\ \dot{m}_a &= 0.5 A_o H_o^{1/2} && \text{[kg/s]} \end{aligned} \tag{2.8}$$

where:

\dot{Q}_{vc} = HRR Required for Onset of Ventilation-Controlled Fire [kW]

\dot{m}_a = Mass Flowrate of Air [kg/s]

A_o = Area of Ventilation Openings [m^2]

H_o = Height of Ventilation Openings [m].

The above empirical correlation can be used, in addition to a fire growth phase model such as t-squared, to determine if a particular enclosure fire will transition between the fuel-controlled and ventilation-controlled regimes. If the predicted HRR is below the HRR required for the onset of a ventilation-controlled fire, the fire is said to be fuel controlled. This is a very important transition, as fires can become much more dangerous when they approach ventilation-controlled. Ventilation-controlled fires can result in the fire phenomena known as backdraught, in which an oxygen-deprived fire has a sudden influx of oxygen (such as opening a door) causing a fierce flare-up of the fire [5].

A fire will remain fuel-controlled if the HRR remains below that predicted by the above correlation. Equation 2.9 is valid for most fuels, as it has been found that the majority of fuels release an approximately constant amount of heat per unit mass of oxygen consumed [21].

2.4 Maximum HRR (Post-Flashover Fire Region)

There have been several empirical correlations developed for predicting the heat release rate required for flashover, which are generally accepted and are included in many fire

protection engineering handbooks (e.g. [29].) The prediction of flashover is very valuable, as it is a very dangerous, critical transition in a fire in regards to life safety.

2.4.1 McCaffrey Prediction of Flashover

Experimental work by several researchers including McCaffrey has resulted in the following correlation that is generally accepted for prediction of flashover [5,38]. The constant in Equation 2.7 assumes a temperature rise of 500°C at the ceiling indicating the onset of flashover and uses the values for the density and specific heat of air are at room temperature.

$$\dot{Q}_{FO} = 610(h_k A_T A_o H_o^{1/2})^{1/2} \quad (2.9)$$

where:

\dot{Q}_{FO} = HRR Required for Flashover [kW]

h_k = Enclosure Conductance (defined below) [kW/m²/K]

A_T = Internal Enclosure Area Excluding Openings [m²]

A_o = Area of Ventilation Openings [m²]

H_o = Height of Ventilation Opening [m].

The enclosure conductance is calculated as follows:

$$h_k = \left\{ \begin{array}{ll} \left(\frac{k_{thermal} \rho C}{t} \right)^{1/2} & t \leq t_p \\ k_{thermal} / \delta & t_p \leq t \end{array} \right\} \quad (2.10)$$

$$t_p = \frac{\rho C}{k_{thermal}} \left(\frac{\delta}{2} \right)^2$$

where:

$k_{thermal}$ = Thermal conductivity [kW/m · K]

ρ = Density [kg/m³]

c = Thermal capacity[kJ/kg · K]

t = Time [s]

t_p = Thermal penetration time [s]

δ = Wall thickness [m].

This correlation assumes that onset of flashover occurs when the hot gas layer in the enclosure rises by 500°C beneath the ceiling, based on experimental evidence. The data used for the development of this correlation was obtained from fires that were set in the centre of a cubic shaped enclosure with ceiling heights of approximately 2.4 m. This correlation should not be used in enclosures with ceiling heights significantly greater than 2.4 m, for elongated enclosures and for fires started against a wall or in a corner.

2.4.2 NIST/CBHF Upholstered Furniture and Mattress Peak HRR Correlation

In the early 1990's, NIST and the California Bureau of Home Furnishings (CBHF) were involved in an experimental research project aimed at investigating the relationship between the HRR of upholstered furniture tested according to several different standard test methods including the ASTM full-scale room test, a furniture calorimeter and the cone calorimeter. One of the major findings of this work, which is relevant to this research project, was that the three-minute average cone calorimeter HRR was a very good predictor of full-scale peak HRR in a full-scale room test [27,48]. The three-minute average cone calorimeter HRR is obtained by averaging the first three minutes of

data obtained during a cone calorimeter test done according to the standard test methods described in Section 3.2.

The NIST/CBHF research also suggests that there are three distinct full-scale regions based on cone calorimeter results, and that the full-scale HRR can be predicted fairly accurately in two of these regions. The regions are classified as non-propagating fires, transition and self-propagating fires as shown in the following figure.

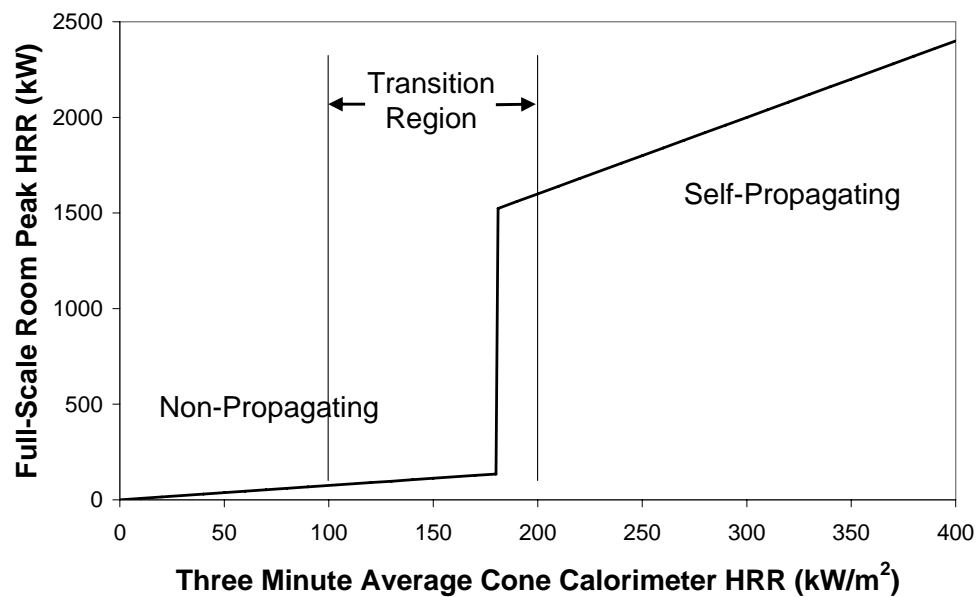


Figure 2 - 4: NIST/CBHF Upholstered Furniture and Mattress HRR Correlation [27]

The research suggests that a cone calorimeter three-minute average HRR of less than approximately 100 kW/m² will produce a non-propagating full-scale fire, which is defined as a fire not releasing enough energy to allow further fire growth and will therefore smoulder and possibly self-extinguish. The research also suggests that a cone calorimeter three-minute average HRR of greater than approximately 200 kW/m² will

result in a self-propagating full-scale fire, which will release enough energy in the vicinity of the flaming region to ignite the surrounding material and allow the fire to grow. There is an abrupt transition region which falls between 100 and 200 kW/m², where it was not possible to obtain an accurate correlation to predict the full-scale HRR from cone calorimeter results during this series of tests.

The correlations obtained from the NIST/CBHF research for upholstered furniture and mattresses are shown below:

$$\dot{Q}_{FullScalePk} = \begin{cases} 0.75\dot{Q}_{3MinCone}'' & \text{Non-Propagating} \\ 4\dot{Q}_{3MinCone}'' + 800 & \text{Self-Propagating} \end{cases} \quad (2.11)$$

where:

$\dot{Q}_{FullScalePk}$ = Full-Scale Peak Heat Release Rate [kW]

$\dot{Q}_{3MinCone}''$ = 180 second Average Cone Calorimeter HRR [kW/m²].

These correlations require the three-minute average cone calorimeter HRR to be obtained by standard test methods at an incident heat flux of 35 kW/m². This approach seems to show much promise as a method of predicting full-scale HRR from bench-scale experiments. Some of the downfalls of these correlations are that they only give the peak heat release rate and not the heat release rate history and they do not give a time to peak heat release rate. Another disadvantage of these correlations are that they cannot predict the heat release rate in the transition region between non-propagating and self-propagating fires.

2.5 FPE Empirical Temperature Correlations

The ability of fire protection engineers to predict enclosure temperatures during the various stages of a fire is important for several reasons. One of the major reasons is that these temperatures are used to predict fire sprinkler activation times. Another important reason for the ability to determine enclosure temperatures is the effect of fire on building structural components, as it is known that structural materials, such as steel, begin to drastically lose strength at elevated temperatures.

This section will focus on the prediction of the fire plume temperature within a compartment as a fire grows. The equations presented here are the general, very common and well accepted correlations that are often included in fire protection engineering handbooks [29,38]. Several other similar temperature correlations have been developed such as those developed by Heskestad and Delichatsios and the Factory Mutual Research Corporation [29]. NIST conducted a study aimed at comparing several temperature correlation methods for a high bay hangar facility, where they found that the Alpert ceiling temperature correlation predicted enclosure temperatures that were close to other methods such as Heskestad and Delichatsios and were all within reasonable accuracy of experimental results [39].

2.5.1 Alpert Ceiling Temperature Correlation

In the early 1970's, the Factory Mutual Research Corporation was involved in the development of empirical temperature correlations to predict the response time of ceiling-mounted fire detectors [49]. This work is still accepted today and is included in

many of the existing fire protection design handbooks and codes such as the SFPE Handbook [29] and the NFPA 72 standard [47]. The correlations were developed by Alpert and are shown below [5,29,49]:

$$T - T_{\infty} = \begin{cases} \frac{5.38(k\dot{Q}/r)^{2/3}}{H} & \text{if } r > 0.18H \\ \frac{16.9(k\dot{Q}^{2/3})}{H^{5/3}} & \text{if } r \leq 0.18H \end{cases} \quad (2.12)$$

where:

T = Temperature at Location of Interest [°C]

T_{∞} = Ambient Temperature [°C]

\dot{Q} = HRR [kW]

H = Distance from Fire Base to Ceiling [m]

r = Radial Distance from Fire Axis to Location of Interest [m]

k = Configuration Factor

= 1 if fire located in centre of room

= 2 if fire located against a flat wall

= 4 if fire located in a 90° corner

Equation 2.10 assumes that the HRR input variable is constant, however, the SFPE Handbook of Fire Protection Engineering indicates that the Alpert equation can still be used with a variable HRR, such as a t-squared fire, thereby following a quasi-steady analysis [29].

The heat release rate is the prime input variable of interest in the above correlations.

This is the most difficult of the input quantities in Equation 2.10 to obtain

experimentally, however, for the purposes of this research work, the methods in

Section 2.4 of modeling the HRR during the growth phase of the fire will be used. The radial distance, r , in Equation 2.10 can also be difficult to estimate for many fuels such as the mattresses burned in this investigation. The difficulty arises when the flames spread across the surface and the diameter of the fire does not remain constant. When burning a liquid fuel in a pool fire such as gasoline, the diameter of the fire will remain constant and equal to the size of the gasoline pool, and therefore the radial distance, r , is easier to estimate.

The correlations in Equation 2.10 were developed using data obtained during experimental testing of wood, cardboard, plastic materials and liquid pool fires with heat release rates ranging from 668 kW to 98 MW in enclosures with ceiling heights ranging from 4.6 to 15.5 m [49]. These correlations are only valid during the initial growth phase of a fire, before there has been a significant build-up of hot gases at the ceiling. In addition, these correlations are intended for fires where the fire source is located a distance of 1.8 times the ceiling height away from the enclosure walls, resulting in a configuration factor, k , of 1. For situations where the fire is located directly against a flat wall or in a 90° corner, the effective result is an increased HRR due to mirroring effects represented by a configuration factor of 2 and 4, respectively. The configuration factor is intended to account for both re-radiation effects from wall surfaces to the fuel and reduced entrained air when a fire is located against a wall or in a corner, thereby increasing the fire temperature.

It takes a great deal of interpretation to determine exactly when Alpert's correlations are suitable for predicting temperatures in enclosures. One needs to use judgement when

considering the assumption that there has not been a significant build-up of hot gases in the enclosure. In addition, these correlations assume that an accurate heat release rate history can be determined for the fire, which relates back to the previous sections in this chapter.

2.5.2 Average Hot Upper Gas Layer Temperature Correlation

In order to determine the temperature of the upper gas layer that develops in an enclosure fire, another empirical correlation has been developed by McCaffrey et al. [29]. The following correlation allows an average hot gas layer to be estimated during a pre-flashover, fuel-controlled fire and is a rearranged version of the McCaffrey flashover prediction formula presented in Equation 2.7:

$$\Delta T_g = 6.85 \left(\frac{\dot{Q}^2}{A_o \sqrt{H_o} h_k A_t} \right)^{1/3} \quad (2.13)$$

where:

ΔT_g = Average Hot Upper Gas Layer Temperature [°C]

\dot{Q} = Fire HRR [kW]

h_k = Enclosure Conductance (defined in Eq'n 2.10) [kW/m²/K]

A_t = Internal Enclosure Area Excluding Openings [m²]

A_o = Area of Ventilation Openings [m²]

H_o = Height of Ventilation Opening [m].

Equation 2.11 can be used to estimate the average upper hot gas layer temperature. This correlation assumes that there will be sufficient mixing of the hot upper gas layer, and it can be approximated by an average temperature. As opposed to the correlation

developed by Alpert, which is only valid at the beginning of a fire, this correlation can be used for all times in the pre-flashover fire regime.

This correlation was developed using data obtained by conducting many fires using different fuels placed in the centre of an enclosure. It is intended for enclosures where the thermal properties of the wall materials are known and the temperature rise in the hot upper gas layer does not exceed approximately 500-600°C, the range commonly associated with flashover. This correlation, once again, requires the heat release rate of the fire to be known.

2.6 Flame Height Correlation

In addition to methods developed to predict the heat release rate of a fire and temperature in an enclosure, correlations for predicting flame height have also been developed. Several flame height correlations have been developed and reviewed by other researchers (e.g. [5,9,29,50]), however one method suggested by Heskestad will be summarized here. The height of the flames above a fire can be estimated by the following equation [51]:

$$H_f(t) = 0.1743(k\dot{Q}(t))^{0.4} \quad (2.14)$$

where:

H_f = Flame Height [m]

k = Configuration Factor (Defined in Eq'n 2.12)

\dot{Q} = Fire HRR [kW].

Here, the configuration factors are identical to that presented in Section 2.3.1. The flame height predicted using this correlation is for the continuous flame, shown in Figure 1-1, and is only valid when the flame height is less than that of the ceiling height.

2.7 Summary

This chapter serves to highlight the challenges that exist in trying to determine fire behaviour. The majority of the tools that fire protection engineers use to assess burning behaviour are based on full-scale experiments. It is difficult, if not impossible, to perform full-scale experiments to characterize all materials and enclosure sizes, and therefore, all of the correlations presented here must be assessed for their validity in a certain set of circumstances before being used. They all have inherent assumptions built in to them and limitations on their accuracy. The temperature correlations and the flame height correlations presented here all have the fire heat release rate history as an input variable, and therefore highlight the importance of accurately modeling the heat release rate of fires, as discussed in Sections 2.3 and 2.4.

While sophisticated computational fluid dynamics computer fire modeling software packages have been developed and successfully implemented, ultimately their ability to predict fire behaviour depends on characterizing the fire in terms of its heat release rate. Accurately characterizing the heat release rate of a fire is a challenge for fire protection engineers and researchers and is one of major aspects of this thesis.

CHAPTER 3: SMALL-SCALE FIRE TESTING

In recent years, there has been much work focused on developing methods to predict large-scale fire behaviour based on conducting small-scale fire experiments. With respect to this research work, the term laboratory-scale refers to tests that are performed on a small portion of a larger item (e.g. a piece of the sofa covering/construction material), and the term large-scale refers to tests that are performed on the entire item (e.g. the entire sofa.) The laboratory based tests can be performed much more easily than full-scale tests and researchers also have the ability to control atmospheric test variables, which are often difficult to control during full-scale testing. In addition, small-scale tests are typically much more cost effective to perform.

The largest disadvantage, and currently the limiting factor in conducting many types of small-scale tests, is that it can be very difficult to model the full-scale scenario accurately based on the fire behaviour of the small-scale test specimen. For example, it is often difficult to overcome scaling issues between large-scale tests and small-scale tests such as the burning of household furniture. Many household items are composed of several different materials which burn differently, release different amounts of energy and are arranged in different orientations such as vertical or horizontal. Therefore, if small-scale fire tests were to be performed on a piece of furniture, questions arise as to how to combine the different materials into a representative composite sample for fire testing.

3.1 Introduction to the Cone Calorimeter

The cone calorimeter apparatus is one of the most useful pieces of laboratory scale fire testing equipment and is the focus of this laboratory scale research work. The cone calorimeter, shown in Figure 3 - 1 below, was developed in the late 1970s and early 1980s by the National Institute of Standards and Technology (NIST) in the United States [21] and is described in detail in ASTM E 1354 [24]. Previously, there had been many attempts at designing a small-scale calorimeter for measuring the heat release rate in fire research such as the Stanford Research Institute (SRI) Calorimeter and the Ohio State University (OSU) Calorimeter, which were largely unsuccessful [12,21]. The importance of the HRR variable was known at this time, however, most of the early attempts at designing an apparatus to measure this variable were complicated and ultimately unreliable. The cone calorimeter design was first described in 1982 in a NIST publication [21]. Since this time, the cone calorimeter has become commercially available to the research community and its popularity has grown due to its wide range of uses.

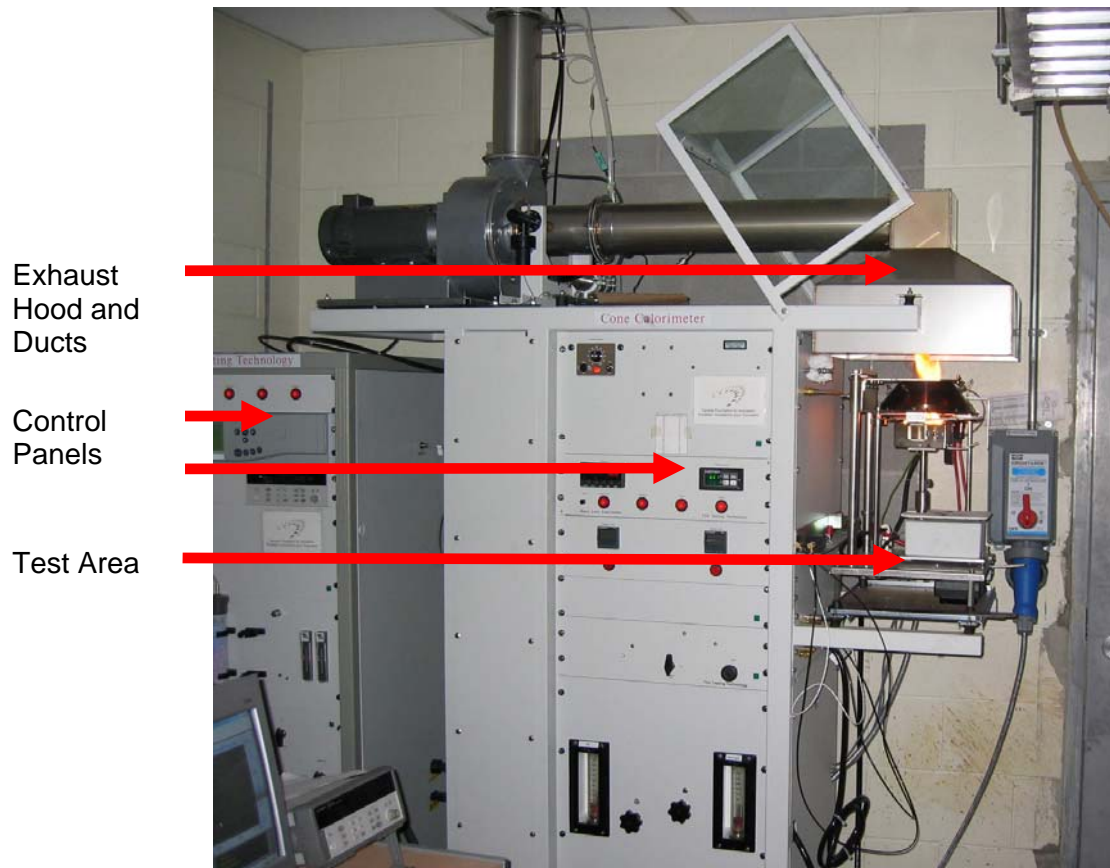


Figure 3 - 1: University of Saskatchewan Cone Calorimeter

The cone calorimeter can be used by fire researchers to obtain many important quantities including the heat (energy) release rate, smoke production, mass loss, carbon monoxide and carbon dioxide yield and time to ignition, which are all described in ASTM E 1354 [24]. Other information such as the total heat evolved as well as the heat of combustion can also be obtained from the experimental results. Some cone calorimeters have also been fitted with additional instrumentation in order to perform exhaust gas corrosivity and species analysis studies by adding equipment such as a Fourier Transform InfraRed Spectrometer (FTIR) which would allow for real-time gas analysis of numerous species.

The University of Saskatchewan cone calorimeter is a Fire Testing Technology (Fire Testing Technology Ltd, West Sussex, UK) Dual Analysis Cone Calorimeter model. The cone calorimeter is fitted with a Servomex 4100 Gas Purity Analyzer (Servomex Group Ltd, East Sussex, UK) which measures the concentration of oxygen, carbon dioxide and carbon monoxide as discussed in Section 3.1.2. An Agilent 34970A Data Acquisition and Control Unit (Agilent Technologies Inc, Palo Alto, CA) is used to record data and display test results in real-time using the cone calorimeter software program.

3.1.1 Description of Cone Calorimeter Equipment

Samples with dimensions of 100 mm by 100 mm ranging up to 50 mm thick, of any solid, non-explosive combustible material can be inserted into the cone calorimeter specimen holder and exposed to a purely radiant heat flux that is relatively constant in both time and across the surface of the specimen. The cone calorimeter allows for very repeatable burning conditions as a result of the precise heater control and the ability to control the atmospheric conditions.

The source of the heat flux is a resistance coil heater (seen in Figure 3 - 2) which is in a conical shape, giving a spatially constant heat flux under the specimen testing area. The temperature of the coil heater is held constant to within one degree Celsius by the use of a feedback control system.

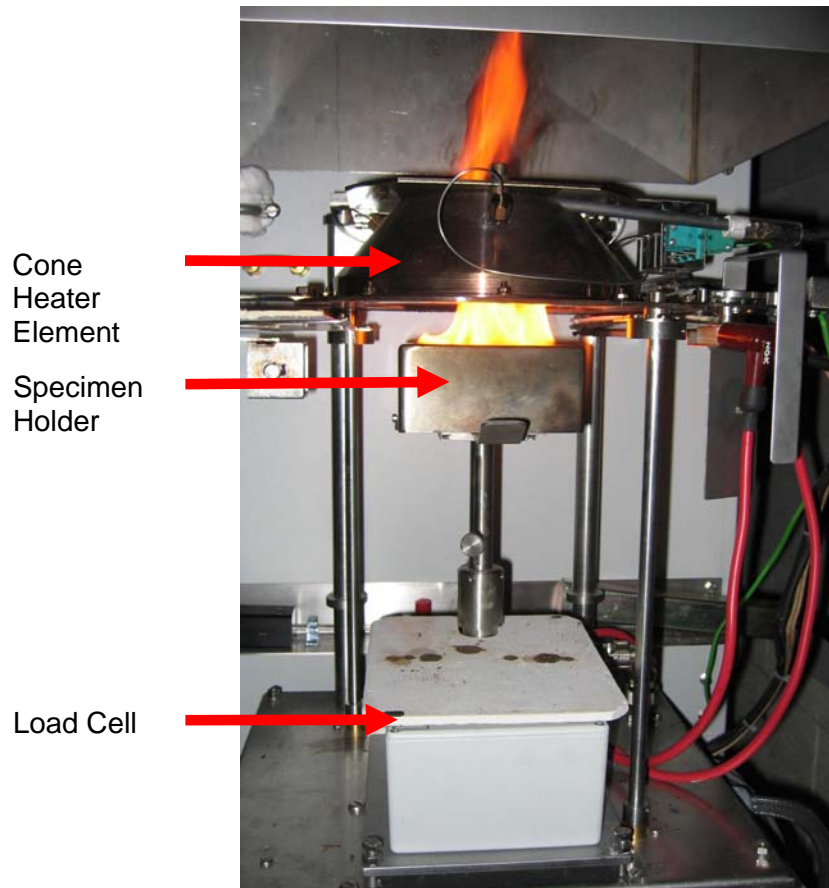


Figure 3 - 2: Cone Calorimeter Specimen Test Area

In order to set the heat flux that is emitted from the cone calorimeter, a temperature is input to the front panel heater control. The cone calorimeter then ramps the temperature of the heater to this set point and then maintains it. After the temperature of the heater has had sufficient time to settle, the incident heat flux is measured by placing a factory-installed 13 mm diameter Schmidt-Boelter heat flux sensor (Medtherm Corp., Huntsville, AL) at a distance of 25 mm from the base of the cone heater. Software supplied by the manufacturer of the cone calorimeter converts the voltage output to heat flux in an on-screen, real-time display.

The specimen is inserted in a stainless steel specimen holder, shown below in Figure 3 - 3, and then placed on a load cell (shown in Figure 3 - 2), which allows real-time measurement of mass as the test proceeds. The load cell also allows for calculation of mass-dependent properties such as the heat of combustion, which is defined as the “total amount of heat released when a unit quantity of a fuel is oxidized completely [21].” Many materials will not ignite, and will simply smoulder, without the addition of a spark, as very high surface temperatures and suitable ventilation conditions are required for spontaneous ignition [5]. The cone calorimeter, therefore, is fitted with a spark ignition system that is used as a pilot in order to ignite the combustible exhaust gases that are emitted by the heated specimen during chemical decomposition. This initiates the flaming combustion that is seen during testing.

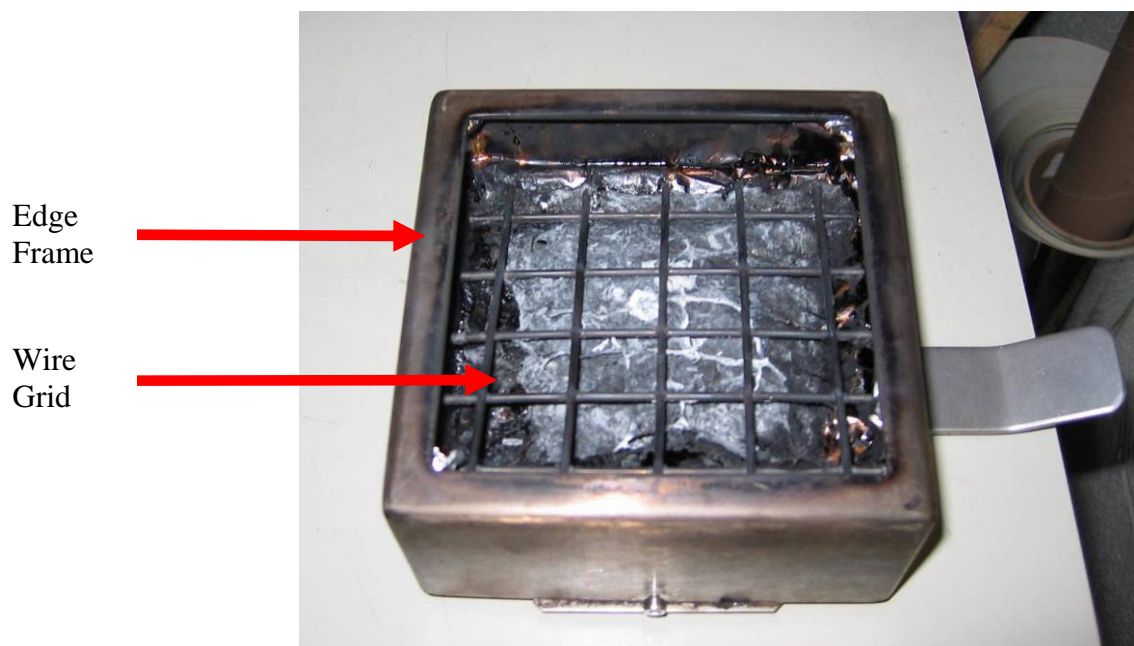


Figure 3 - 3: Cone Calorimeter Specimen Holder
(Shown With Wire Grid over Burned Specimen)

The cone calorimeter is fitted with an exhaust fume hood and exhaust fan, which collects the products of combustion for gas analysis. The exhaust gas is passed through a carbon dioxide, carbon monoxide and oxygen gas analyzer which collects the required information for calculation of the heat release rate and other variables as described in the following section on oxygen consumption calorimetry. A laser used for smoke obscuration analysis is also fitted on the cone calorimeter. The laser is used to measure the optical density of the smoke in the exhaust duct.

3.1.2 Oxygen Consumption Calorimetry

The oxygen consumption technique for measuring the energy released by burning materials has evolved over the past century. In the early 20th century, Thornton demonstrated that a relatively constant amount of energy was released per unit of oxygen consumed during combustion of organic liquids and gases [52]. Another researcher, Huggett, in the early 1980s, extended Thornton's findings to include organic solids and found with very few exceptions that the average constant value to be 13.1 MJ per kilogram of oxygen consumed to an accuracy of $\pm 5\%$ [52]. The oxygen consumption technique has become the standard method for obtaining both full-scale and laboratory-scale heat release and the constant proposed by Huggett is commonly accepted by researchers.

The equation that the cone calorimeter uses to calculate the heat release rate is as follows [24].

$$\dot{Q} = (1.10)(13.1 \times 10^3)(XO_2^a)\dot{m}_e \left[\frac{\phi - 0.172(1 - \phi) \frac{X_{CO}}{X_{O_2}}}{(1 - \phi) + 1.105\phi} \right] \quad (3.1)$$

where:

$$\dot{m}_e = C \sqrt{\frac{\Delta P}{T_e}}$$

$$\phi = \frac{X_{O_2}^o (1 - X_{CO_2} - X_{CO}) - X_{O_2} (1 - X_{CO_2}^o)}{X_{O_2}^o (1 - X_{CO_2} - X_{CO} - X_{O_2})}$$

$$XO_2^a = (1 - X_{H_2O}^o) X_{O_2}^o$$

\dot{Q} = Heat Release Rate [kW]

C = Orifice Flow Constant Determined Daily

ΔP = Pressure Drop Across Orifice [Pa]

T_e = Exhaust Gas Temperature at Orifice Plate [K]

X_{CO} = Mole Fraction of Carbon Monoxide in Exhaust

X_{O_2} = Mole Fraction of Oxygen in Exhaust

X_{CO_2} = Mole Fraction of Carbon Dioxide in Exhaust

$X_{H_2O}^o$ = Initial Mole Fraction Water Vapour in Exhaust

$X_{O_2}^o$ = Initial Mole Fraction Oxygen in Exhaust.

In 1999, Enright and Fleischmann [53] presented an uncertainty analysis for the cone calorimeter based on the instrument and calculations. The uncertainty analysis does not include operational uncertainty or random uncertainty between specimens. The findings indicate that typical cone test results have uncertainties in the vicinity of less than 1% to approximately 10%. The standard test method describing the cone calorimeter equipment and operating procedure, ASTM E 1354 [24], has more detailed information

on precision errors, bias errors, repeatability and inter-laboratory reproducibility based on a series of multi-laboratory round robin tests.

In all fire tests, regardless if they are full-scale or small-scale, the heat release rate is often measured and represents the single most descriptive quantity to fire researchers. This is a difficult quantity to measure directly by an energy balance, especially in the field. Drysdale [5] describes another method of predicting the energy released during an enclosure fire that several researchers have developed. It is based on the heat released due to combustion, the heat loss due to the interaction between hot and cold gases, the heat loss through the enclosure boundaries and the heat loss by radiation through the enclosure openings. This alternative method to oxygen consumption calorimetry is much more complex and difficult to implement and highlights the difficulty of measuring the heat release rate of a fire. With respect to standard, laboratory based tests, oxygen consumption calorimetry is primarily used to determine the heat release rate.

3.2 Edmonton II Mattress Sample Cone Calorimeter Testing

As described in Chapter 1, two sets of full-scale experimental fire tests were performed in Edmonton in July 2003 and September 2004, referred to as Edmonton I and Edmonton II respectively. This section will describe the small-scale tests that were performed on mattress samples that were obtained prior to the full-scale fire tests performed in the Edmonton II set of experiments. Before the mattresses were burned in the Edmonton II set of experiments, a relatively small, but representative sample, was

cut from each of the three mattresses with the intent to perform laboratory-scale testing in the cone calorimeter.

Two of the three mattresses that were burned during the Edmonton II set of experiments were of polyurethane foam and fibre backing material over steel spring construction as seen in Figure 3 - 4 and Figure 3 - 5. The other mattress was an older mattress constructed of steel springs and a dense fibre material without any foam as seen in Figure 3 - 6, following. Table 3 - 1 describes the three mattresses that were burned during the full-scale tests and subsequent laboratory-scale testing.

Table 3 - 1: Mattress Description

Mattress (Test No)	Size, m (ft)			Mattress Construction Materials			Composite Density* (kg/m ²)
	Width	Length	Thickness	Layer 1	Layer 2	Layer 3	
1	1.35 (4.4)	1.93 (6.3)	0.15 (0.5)	Polyester	Polyurethane Foam	Reclaimed Fibre Cotton Batting	1.42
2	1.55 (5.1)	2.0 (6.7)	0.15 (0.5)	Polyester	Polyurethane Foam	With Plastic Grid	2.04
3	1.55 (5.1)	2.0 (6.7)	0.15 (0.5)	Rayon	Reclaimed Fibre	Fibre	2.43

*Note: Composite Density only includes the combustible materials and not the steel springs and is on a per unit mattress top surface area basis

The following figures show the combustible components construction of the three mattresses and also show the composite sample used during cone calorimeter testing. In all three mattresses, the composite samples shown in Figure 3 - 4, Figure 3 - 5 and Figure 3 - 6 below were placed over a steel spring inner core.

Outer Fabric Layer
(Polyester)

Polyurethane Foam
(2 Layers)
28.5 mm thick (total)

Reclaimed Fibre
Backing
6.4 mm thick

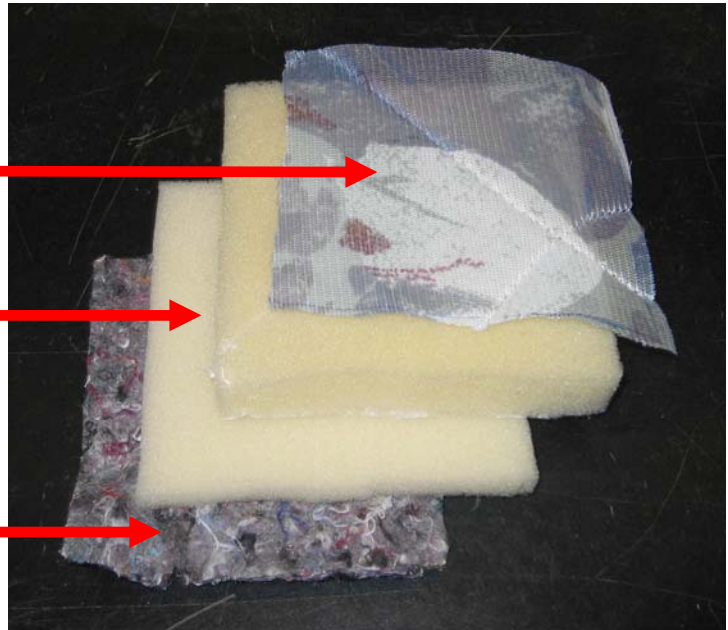


Figure 3 - 4: Mattress 1 Cone Calorimeter Composite Sample Showing Different Components

Outer Fabric Layer
(Polyester)

Polyurethane Foam
(1 Layer)
28.5 mm thick

Reclaimed Fibre
Backing
(White Backing)
19.0 mm thick

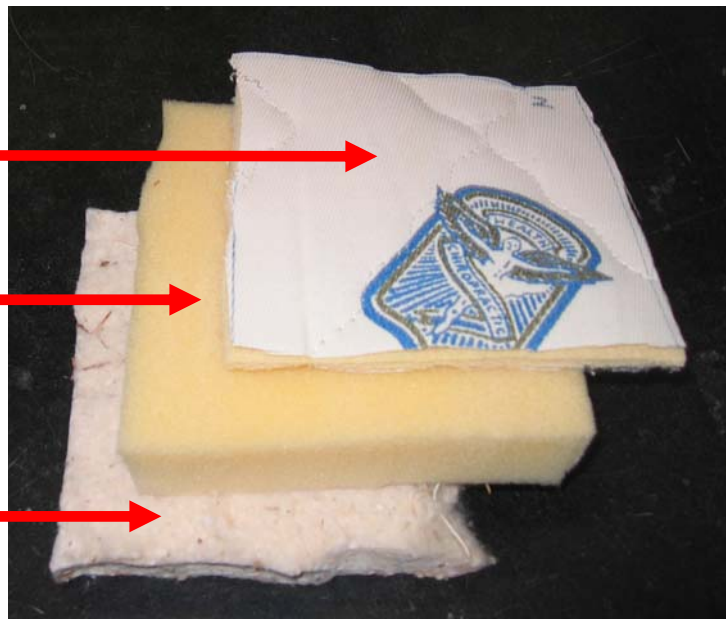


Figure 3 - 5: Mattress 2 Cone Calorimeter Composite Sample Showing Different Components

Outer Fabric Layer
(Rayon)

Reclaimed Fibre
28.5 mm thick

Fibre Backing
15.0 mm thick

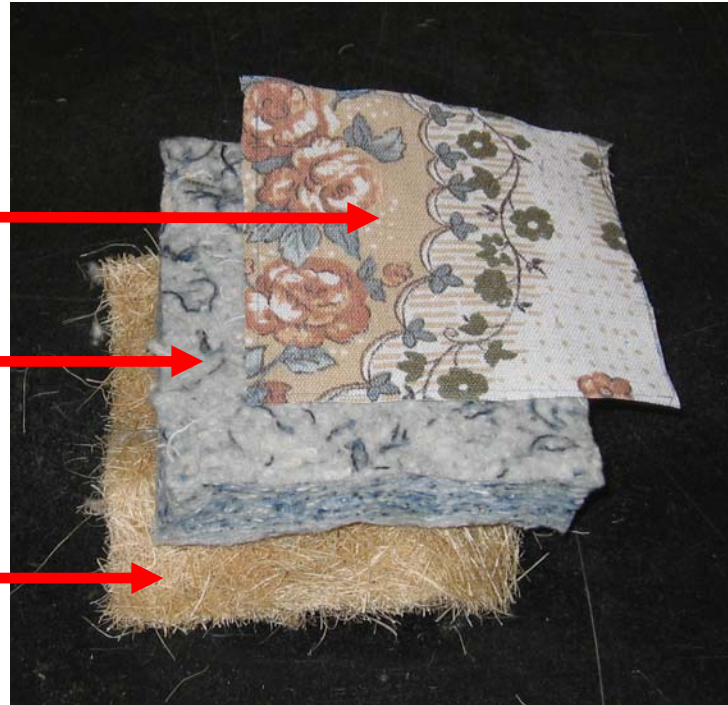


Figure 3 - 6: Mattress 3 Cone Calorimeter Composite Sample Showing Different Components

The exact chemical composition or type of fabric and foam of each of the mattresses were not known as they were obtained from second-hand stores.

3.2.1 Mattress Sample Preparation

One of the many challenges of laboratory-scale fire testing is to choose a material sample that accurately reflects the properties and burning behaviour of the parent material. Considering that mattresses are three-layer composite materials, selecting samples for testing is difficult. For the purposes of this investigation, ASTM E 1474 [54] was used as a basis, with some modifications, for the laboratory-scale testing. This standard describes the conditions and sample preparation that will be used for cone calorimeter testing and is quite descriptive in its treatment of upholstery

and mattress components as it has different preparation procedures for loose-fill and other types of materials.

Several researchers have examined the effect of sample preparation, specifically regarding upholstered items and mattresses, on cone calorimeter results (e.g. [40,55]) and have found that results can vary significantly from test to test and can vary due to differences in test method. For example, Fritz et al. [55] found there to be differences based on which of the ASTM E 1474 [56] sample preparation method is used. In addition, Fritz et al. found significant differences, varying as much as approximately 67% [55], between tests performed with and without the edge frame (shown in Figure 3 - 3).

The modifications to the ASTM E 1474 [56] test standard used during this study were due to the limited amount of material that could be cut from the mattresses prior to full-scale testing. According to the ASTM E 1474 standard, a 200 mm by 200 mm sample is to be cut from the parent material and then formed into a block using a prescribed method of cutting and gluing or stapling. In order to acquire statistically significant cone-calorimeter data, at least five small-scale tests were to be performed on each of the three mattresses. Considering the number of required tests, and the fact that each sample would require a 200 mm by 200 mm area if the ASTM E1474 standard were followed, it was felt that the material removed from the mattresses to conduct five cone calorimeter tests according to the ASTM E 1474 standard would be excessive and would affect the full-scale results. Therefore, it was decided that a modified small-scale sample

preparation method would be followed, whereby a sample area of 100 mm by 100 mm would be used.

The primary reason for the large sample area and the involved process of cutting and gluing the sample into a block in the ASTM E 1474 standard is to prevent the top fabric layer from swelling and shrinking immediately upon exposure to the heat source. The intent is to keep the top fabric layer pulled tight until it burns, similar to what happens during full-scale testing. In order to reproduce this effect during small-scale tests, a wire grid was placed between the edge frame and the mattress sample in order to hold the top layer taut as seen in Figure 3 - 7.

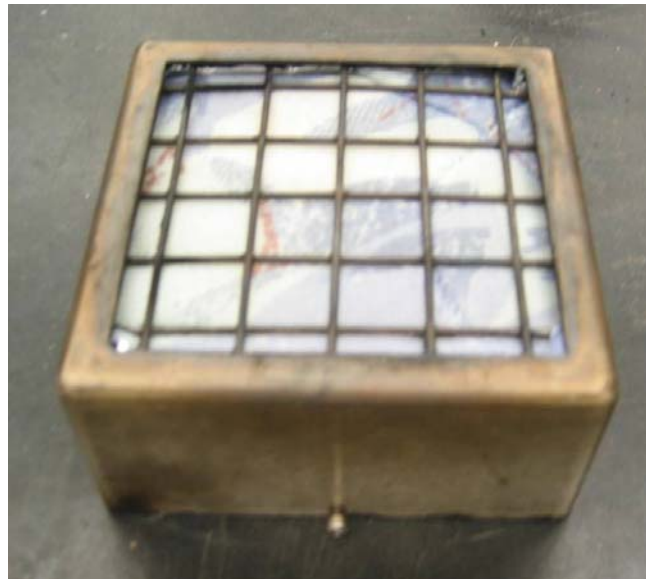


Figure 3 - 7: Specimen Holder With Wire Grid

During testing, it was found that this method produced results within approximately 20% of the five-test average as seen in Figure 3 - 8, below.

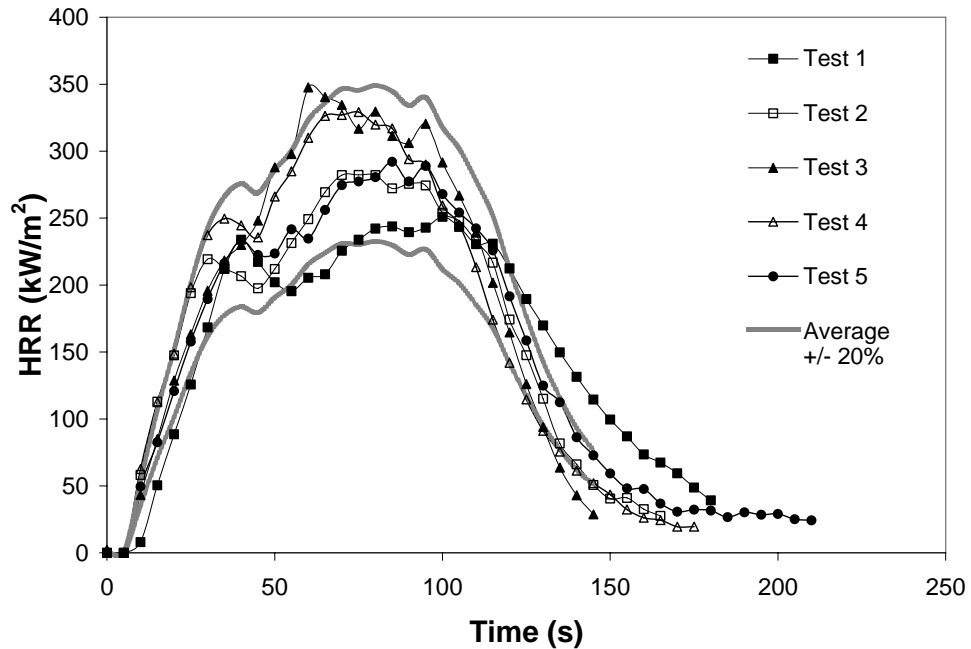


Figure 3 - 8: Individual Mattress Test Results (Mattress 1 Tests Shown)

Similar results were obtained regarding the repeatability of Mattresses 2 and 3 with the five tests falling within approximately 20% of the five-test mean. Considering the challenge of testing the mattress composite samples and the similar level of repeatability found by other researchers (e.g. [55]) the repeatability of the mattress tests found during cone calorimeter testing were considered to be acceptable for the purposes of this research work.

Polymethyl methacrylate (PMMA) is commonly tested in the cone calorimeter because it is known to produce extremely repeatable results. This material is typically burned for calibration purposes in order to test the repeatability of the testing apparatus and ensures that the equipment is performing properly [57]. Figure 3 - 9 below, shows the results from a set of calibration burns of PMMA before and after the five trials performed on

Edmonton II Mattress 1 specimens. As seen Figure 3 - 9, the repeatability of the cone calorimeter equipment is validated by the good agreement between these tests. Similar calibration burns were performed before and after the other mattress specimens were tested, producing similar repeatability.

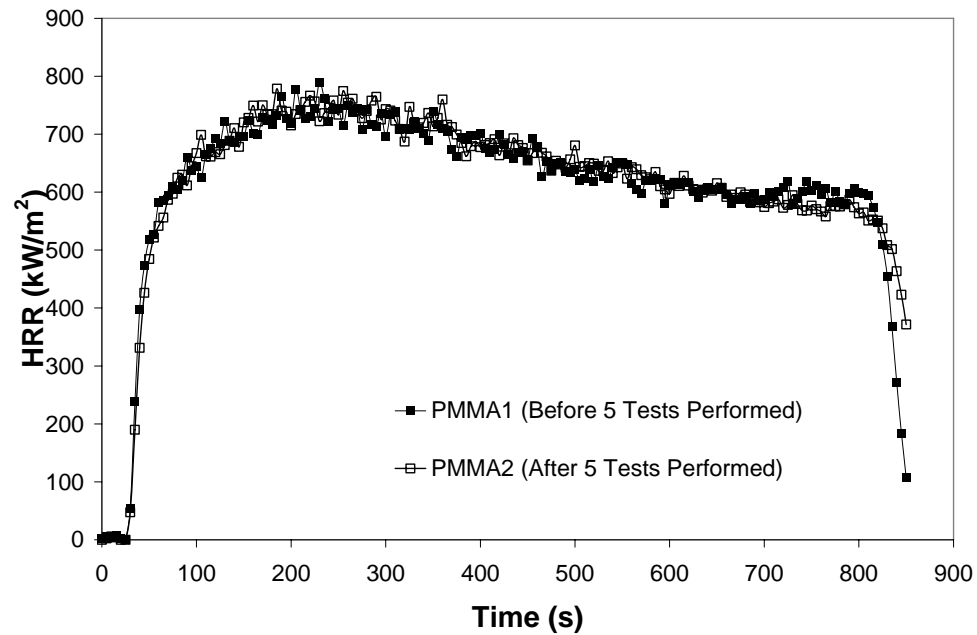


Figure 3 - 9: Individual PMMA Calibration Sample Test Results (Before and After Mattress 1 Tests Shown)

There were only two differences in sample preparation procedure used in this study versus the ASTM E 1474 standard. These involved cutting a 100 mm by 100 mm sample of the mattress composite (3 layers) rather than the larger 200 mm by 200 mm sample and the addition of the wire grid to prevent vertical movement of the sample during burning. The remainder of the specimen preparation was performed in accordance with the standard. It should be noted, however, that this modified sample preparation and test procedure could affect the results versus the standardized

ASTM E 1474 tests. This involved wrapping the mattress layers in aluminum foil to reduce heat transfer to the edge frame and to help control the burning process [40], as shown in Figure 3 - 10. The specimens were all tested at 35 kW/m^2 , according to the ASTM E 1474 test standard [56], and were conditioned at $50\% \pm 5\%$ relative humidity for at least 24 hours prior to testing in accordance with ASTM E 1474. The samples were conditioned at 50% relative humidity using the environmental chamber located in the University of Saskatchewan Thermodynamics Laboratory.

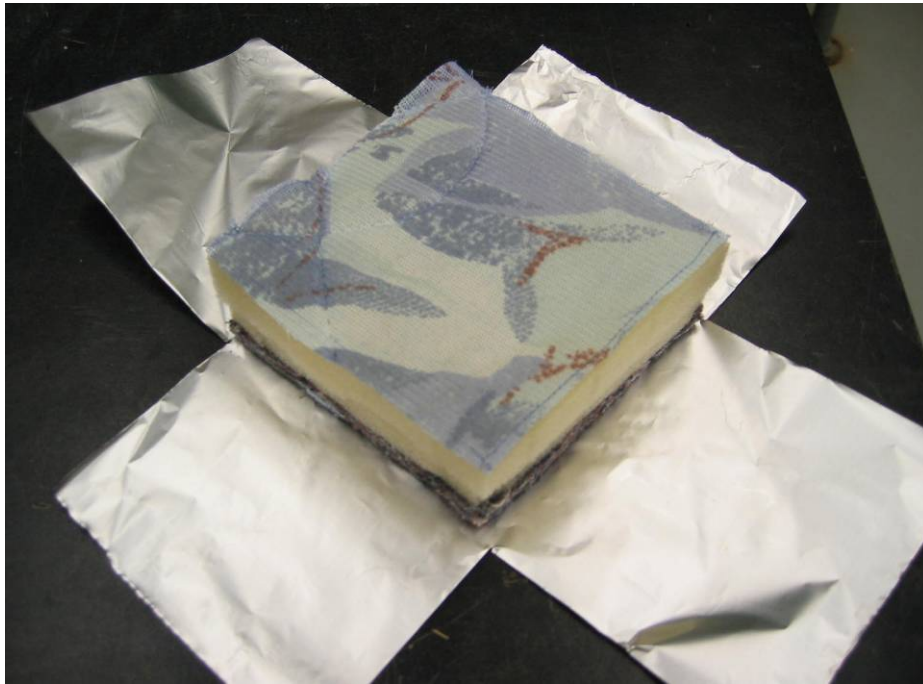


Figure 3 - 10: Mattress 1 Sample Wrapped in Aluminum Foil

3.2.2 Cone Calorimeter Heat Release Rate and Total Heat Release Results

As mentioned previously, the most important variable in fire protection engineering and the primary data of interest measured by the cone calorimeter is the heat release rate.

Figure 3 - 11, which follows, shows the average heat release results from the five cone

calorimeter tests performed on each of the mattresses. The repeatability of the five tests performed on each of the three mattresses was consistent with that presented in the literature (e.g. [57]) as all five tests fell within approximately 20% of the average.

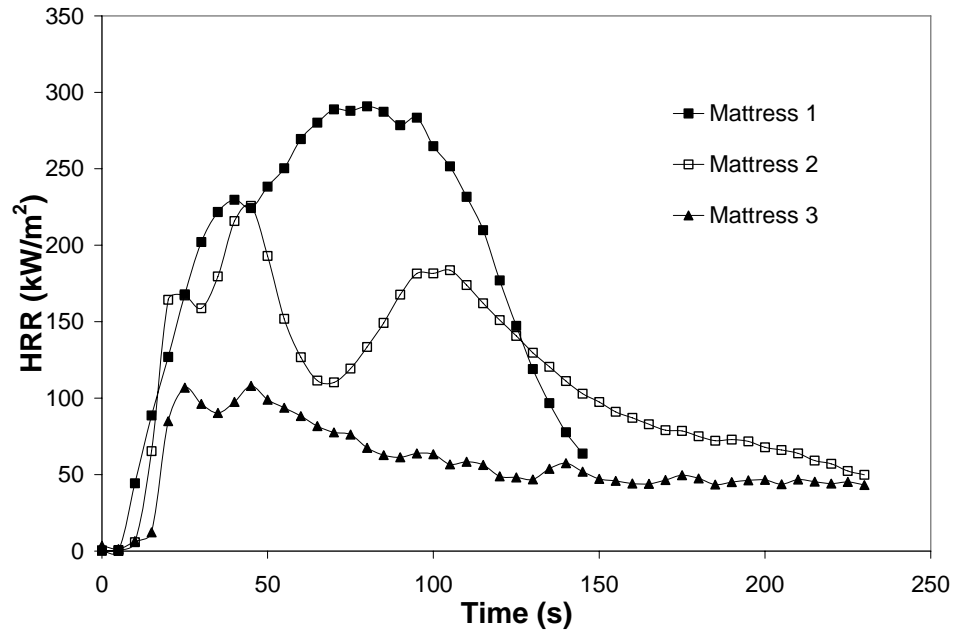


**Figure 3 - 11: Average Cone Calorimeter HRR Results
(5 Test Average Shown for Each Mattress)**

This figure indicates that there was a large difference in energy released between the three mattresses, which would suggest that there should be a difference in their full-scale fire behaviour. A further discussion regarding the comparison between full and small scale results follows in Chapter 5. For each of the three mattress results presented in Figure 3 - 11, several peaks during the HRR – time history exist. Mattress 1 and 3 have two distinct peaks, whereas Mattress 2 has three distinct peaks at approximately 25 s, 50 s and 100 s. These can be explained by the burning of the different layers in the

composite cone calorimeter samples. As each layer burns, it releases energy, contributing to a peak associated with that layer.

Upon examination of Figure 3 - 11, one can see that Mattress 1 has a much higher peak heat release rate than the other two and also burns much quicker from ignition to flame-out. Table 3 - 2 following, shows the average ignition time for each of the mattresses. Mattress 1 ignites faster than the other two mattresses, and also has the smallest scatter in ignition times, having a standard deviation of 1.1 seconds. Mattresses 2 and 3 have longer times to ignition and also have more scatter, with standard deviations of 2.7 and 3.5 seconds respectively. Also shown are two of the most important HRR quantities obtained from cone calorimeter testing, which will be discussed in more detail in Chapter 5. The three-minute or 180 second average HRR has been found to predict full-scale burning behaviour quite well [12,27], and has therefore been included in Table 3 - 2.

Table 3 - 2: Summary of Edmonton II Mattress Cone Calorimeter Mattress Results

Mattress	Time to Ignition (s)	5-Test Average Peak HRR (kW/m²)	5-Test Average 180 sec Avg HRR (kW/m²)
1	6.2	290.9	190.0
2	11.0	225.7	126.4
3	15.0	114.6	61.2

The total heat released during the test, or the area under the HRR curve was also determined for each of the three mattresses, and is shown in Figure 3 - 12 below.

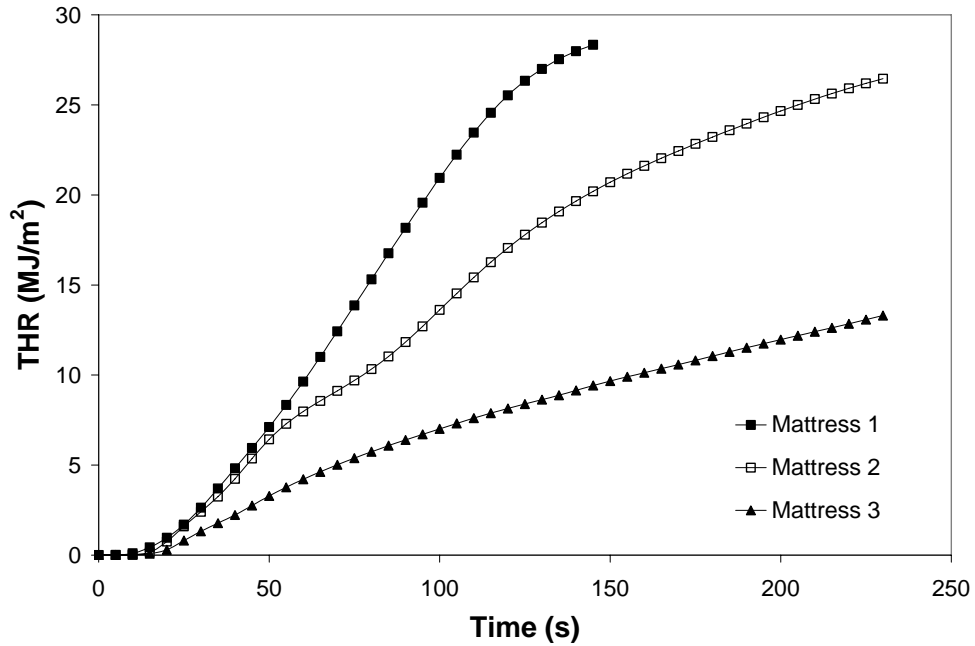


**Figure 3 - 12: Average Cone Calorimeter THR Results
(5 Test Average Shown for Each Mattress)**

The above figure shows that Mattress 1 releases a larger amount of total energy than the other two mattresses in addition to burning the fastest.

3.2.3 Cone Calorimeter Smoke Production Results

The cone calorimeter is fitted with a laser system to measure smoke obscuration. The quantity that is typically quoted in the literature is the specific extinction area (SEA) and is expressed in units of square metres per kilogram. The SEA can be explained by imagining that spherical particles (the smoke) are released from the burning object and obscure a beam of light in the cone calorimeter exhaust duct [21]. The attenuation of the light beam becomes a function of the overall effective cross-sectional area of the obscuring smoke particles and the SEA quantity refers to the area of smoke particles in

the exhaust duct normalized by the mass of the test sample resulting in the units of square metres per kilogram.

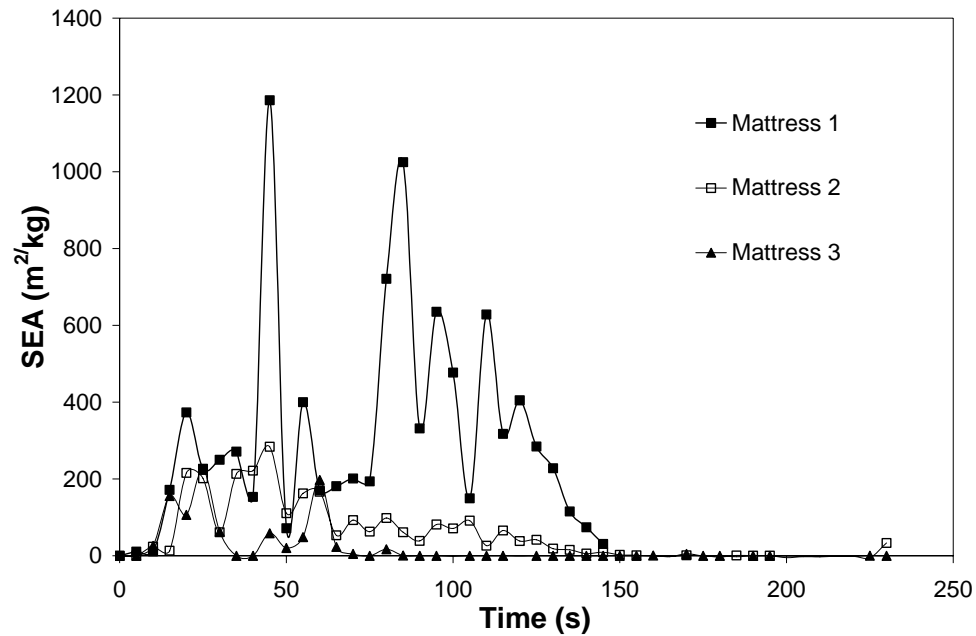


**Figure 3 - 13: Average Cone Calorimeter Smoke Production Results
(5 Test Average Shown for Each Mattress)**

As seen in the above figure, Mattress 1 consistently produces more smoke than the other two mattresses, especially at later stages of the test. The smoke production from each of the three mattress samples was not overly important for purposes of comparison to full-scale results or for fire behaviour modeling, however, it has been included here as a qualitative comparison between the burning behaviour of the mattresses.

3.2.4 Effect of Moisture Content on Cone Calorimeter Heat Release Results

During the full-scale testing in Edmonton, the exact humidity level in the testing room was unknown. As a result of the previous burns that were done and the action by the

firefighters, there was a significant amount of water in the building, and it is thought that the humidity level would therefore be quite high. During cone calorimeter testing, the effect of the humidity level on the burning behaviour of the mattresses was investigated. It has been shown that a higher amount of energy is released during burning as the sample moisture level is decreased by other researchers (e.g. [58].) The moisture in the sample requires energy in order to evaporate, which is defined as the heat of vaporization and is approximately 40.8 kJ/kmol [5].

The magnitude of the effect of the moisture level was investigated in the cone calorimeter using a set of polyurethane foam composite mattress samples obtained locally from Sleepers Mattress Factory (Sleepers Mattress Factory Inc., Saskatoon, SK.) The same preparation procedure was used as described in Section 3.2.1.

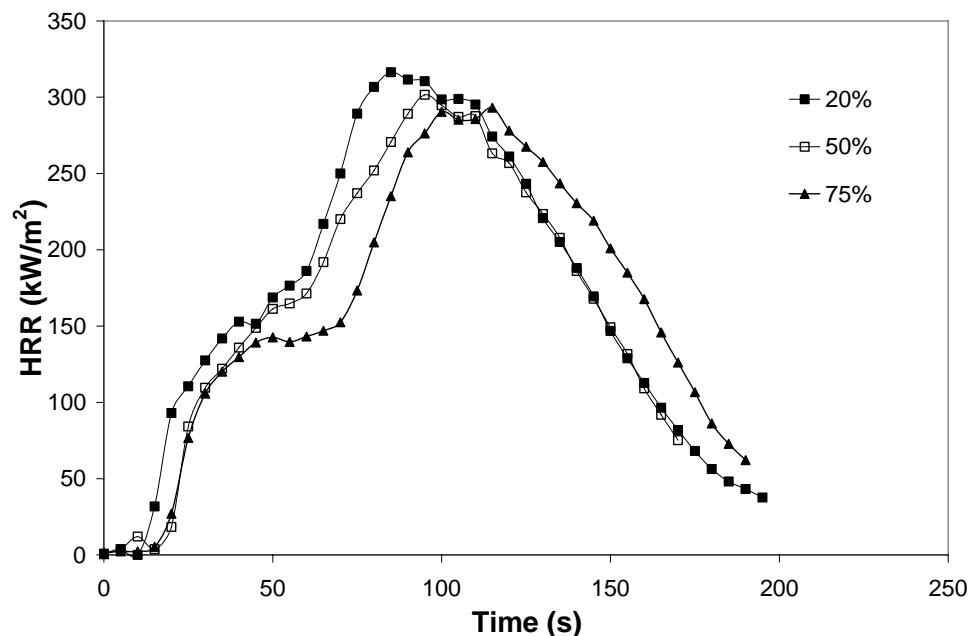


Figure 3 - 14: Effect of Relative Humidity on Cone Calorimeter Results (3 Test Average)

As seen in Figure 3 - 14 above, the lowest moisture content is associated with the highest heat released during combustion as expected and the highest moisture content is associated with the lowest heat released. The information shown in Figure 3 - 14 above, demonstrates that there is a noticeable effect of moisture content on heat release rate results with results differing by a maximum of approximately 60% for the majority of the test duration.

3.2.5 Effect of Incident Heat Flux on Cone Calorimeter Heat Release Results

It has been suggested by several researchers (e.g. [45]) that the heat released by a burning sample has a limited dependency on the cone calorimeter irradiance level. It is intuitive, however, that a larger incident heat flux would produce larger heat release results, as more energy is input to the system, and therefore more energy will be released. Similar to the effect of moisture content, the magnitude of the difference in heat release results based on incident heat flux level used in the cone calorimeter was investigated and is shown in Figure 3 - 15 below. Similar to the investigation of the effect of relative humidity on HRR results, the investigation of incident heat flux on HRR results used composite mattress samples of a polyurethane foam mattress obtained locally in Saskatoon from the Sleepers Mattress Factory and the same preparation procedure was used as described in Section 3.2.1.

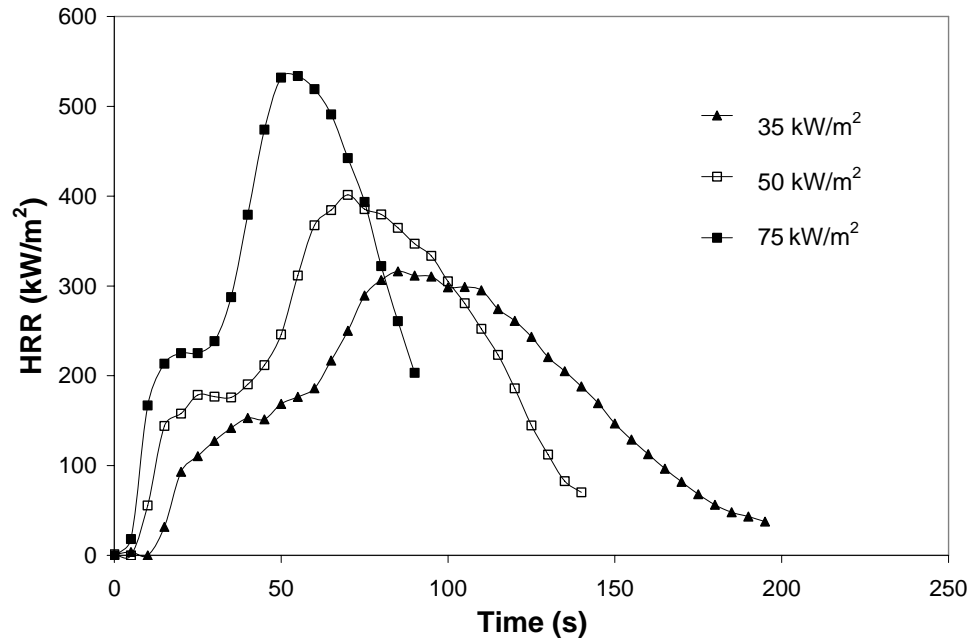


Figure 3 - 15: Effect of Heat Flux on Cone Calorimeter Results (3 Test Average)

Figure 3 - 15 indicates that higher levels of heat flux incident on the specimen surface produced higher heat release rates as measured with the cone calorimeter, which supports the results obtained by other researchers (e.g. [58]). With respect to correlating full-scale and cone calorimeter test results, the selection of incident heat flux for cone calorimeter testing is another major challenge as it is difficult to choose a constant incident heat flux that accurately replicates the heat flux emitted by a full-scale fire.

3.2.6 Investigation of Individual Mattress Layer Component Heat Release Rates

The heat release rate contribution of each layer in the Edmonton II composite mattress samples was also examined. The results follow in Figure 3 - 16 and Figure 3 - 17 for Mattresses 1 and 2 respectively. Mattress 3 has not been included because it was not a

polyurethane foam mattress, and because it did not produce any significant temperature results during full-scale field fire testing as will be discussed in Chapters 4 and 5.

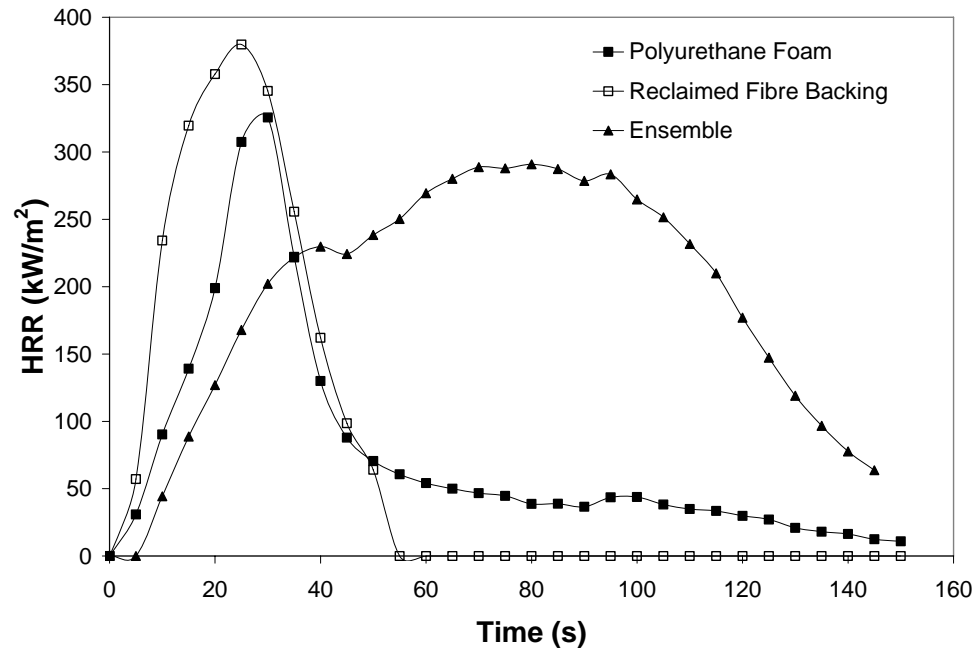


Figure 3 - 16: Mattress 1 Comparison of Individual Mattress Layer Tests versus the Entire Ensemble (3 Test Average)

Figure 3 - 16 can be used to help explain the different peaks that are seen in the composite sample cone calorimeter results seen in Figure 3 - 11. As seen in Figure 3 - 16 with respect to Mattress 1, the reclaimed fibre backing had a higher HRR than the polyurethane foam. The reclaimed fibre backing corresponds to the second peak in the ensemble, as it is the last layer to be ignited during the ensemble tests.

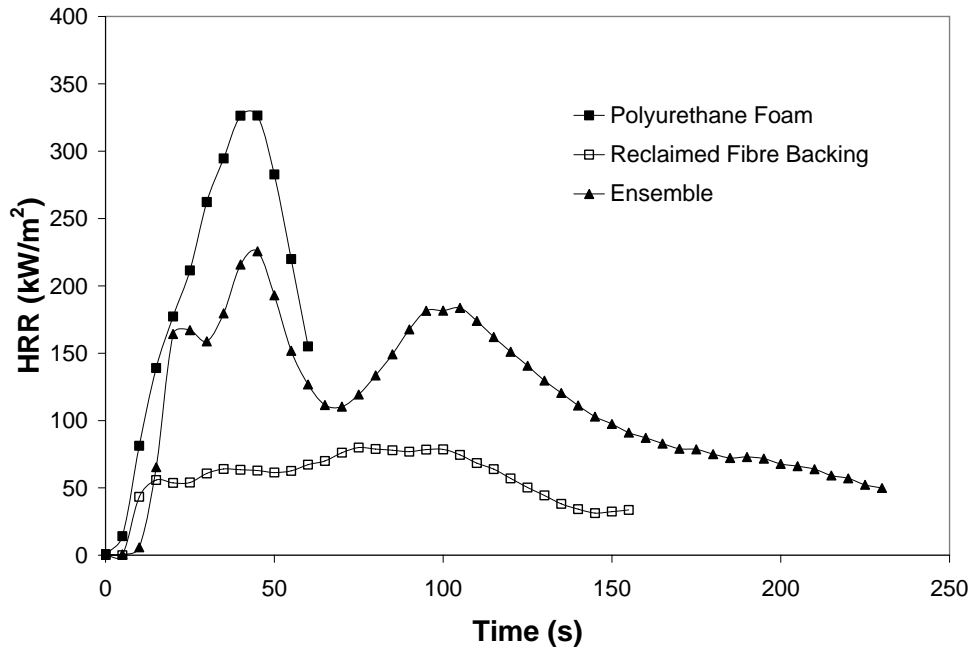


Figure 3 - 17: Mattress 2 Comparison of Individual Mattress Layer Tests versus the Entire Ensemble (3 Test Average)

Figure 3 - 16 and Figure 3 - 17 demonstrate the complexity of the heat release rate curve for a composite sample, as the component HRR curves cannot simply be superimposed or added to obtain the total ensemble sample HRR curve. Heat release rate is not strictly a material property as indicated by these results; but is more of a combination of effects based on the material, sample configuration and burning behaviour. With reference to Mattress 1 shown in Figure 3 - 16, the results presented here indicate that the polyurethane foam and backing material each have a larger HRR and burn quicker than the three-layer ensemble of the backing material, polyurethane foam and top fabric layer. The top fabric layer (which was not tested alone in the cone calorimeter due to difficulties testing fabric materials that burn extremely quickly and due to the precision of the load cell used to measure mass) is typically constructed of a flame-resistant material or has a fire retardant applied to the surface during manufacturing. This

explains the increased time to ignition for the three-layer ensemble versus the polyurethane foam and backing material, as it takes time for the heat and flame to penetrate this protective barrier.

With reference to Mattress 2, shown in Figure 3 - 17, the polyurethane foam has a higher HRR than the ensemble, however, unlike Mattress 1, the reclaimed fibre backing (which is different than the material used in Mattress 1) burns with a much lower HRR as seen in Figure 3 - 18, below, which compares the difference in heat released by the backing material.

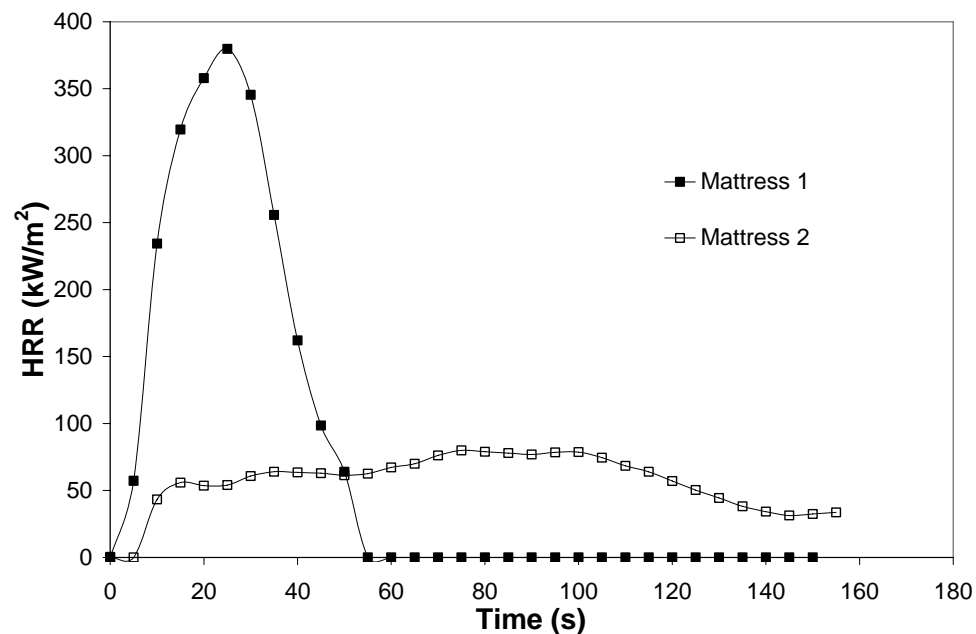


Figure 3 - 18: Comparison of Backing Material Heat Release (3 Test Average)

Figure 3 - 19, below, indicates that the two polyurethane foams had similar heat release rates during the tests.

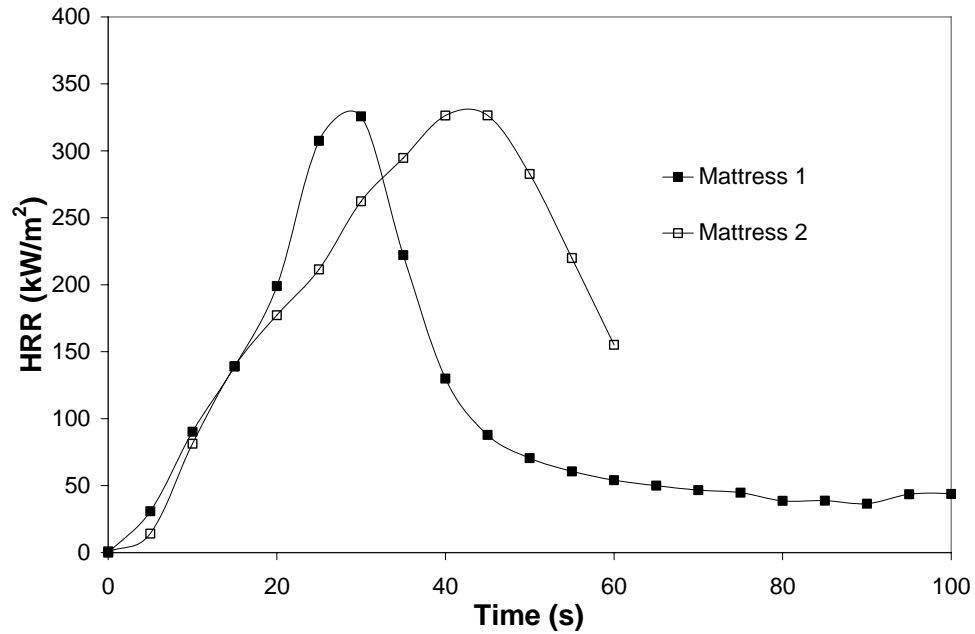


Figure 3 - 19: Comparison of Polyurethane Foam Heat Release (3 Test Average)

The differences in HRR between the backing material for Mattress 1 and Mattress 2, seen in Figure 3 - 18, help to explain the differences in the ensemble cone calorimeter HRR results seen in Figure 3 - 11. The two backing materials were constructed of different materials and different thicknesses with Mattress 1 being constructed of a 6.4 mm thick reclaimed fibre and Mattress 2 being constructed of a 19.0 mm thick cotton batting reinforced with a plastic grid. The polyurethane foam layer for both Mattress 1 and Mattress 2 gave similar HRR results as seen in Figure 3 - 19 and were both constructed of 28.5 mm thick foam.

3.3 Summary

The burning behaviour of the mattresses examined in the Edmonton II set of experiments were investigated through cone calorimeter testing. One of the challenges of cone calorimeter testing is selecting a representative sample of the full-scale product for laboratory-scale testing. Composite mattress samples composed of a covering fabric layer, a padding layer and a layer of backing material were chosen for cone calorimeter testing and results indicated that Mattress 1 posed the most significant fire hazard in terms of heat release rate, total heat released and smoke produced followed by Mattress 2 and Mattress 3 respectively. It was found that the moisture content and cone calorimeter incident heat flux level had a significant effect on the heat released by the mattress samples, as increasing moisture content levels resulted in decreasing sample heat release rates and increasing incident heat flux resulted in increasing sample heat release rates.

CHAPTER 4: FULL-SCALE FIRE TESTING

As mentioned previously, full-scale fire testing is often one of the most important tools for fire researchers. With the improvement of small-scale or laboratory-scale fire test equipment and methods as well as the advances in computer modelling, the necessity of conducting full-scale tests has somewhat diminished in recent years. Full-scale fire testing does, however, remain the standard to which most other test methods and models are compared. Due to the nature of fire and associated scaling issues, it is often difficult to model the burning behaviour of three-dimensional objects in a laboratory. With respect to laboratory-scale experiments of combustible objects, there are many variables such as air currents, three-dimensional fire spread effects and construction techniques that are difficult to account for, as will be discussed further in the following chapter on laboratory scale testing.

This chapter will present common types of full-scale fire experimental methods and will discuss two sets of experiments that were conducted in Edmonton, Alberta in July 2003 (Edmonton I) and in September 2004 (Edmonton II.)

4.1 Standardized Full-scale Tests

There are many different types of standard full-scale fire tests that are commonly performed [5,21]. These tests are performed in order to obtain quantities such as the

heat release, hot gas temperature, smoke production, ignitability and combustion product composition and toxicity [12]. Full-scale fire testing is often performed in accordance with a specific standard developed by organizations such as ASTM, ISO and the Underwriters' Laboratory of Canada (ULC).

One of the most widely used full-scale fire tests that is performed to evaluate enclosure fire behaviour is described in ASTM E 2067: Standard Practice for Full-Scale Oxygen Consumption Calorimetry Fire Tests [19], as shown below in Figure 4 - 1 and Figure 4 - 2. This standard fire test is commonly performed in order to acquire test results for wall covering materials (described by the ISO 9705 standard [20]) and furnishings such as mattresses (described by the ASTM E 1590 standard [59]). The ASTM E 2067 test standard describes how the 3.6 m by 2.4 m by 2.4 m (12ft x 8ft x 8ft) enclosure should be constructed and the instrumentation that will be used. The enclosure has a single opening, which is a doorway at one of the ends with dimensions of 0.8 m by 2.0 m.



Figure 4 - 1: ISO 9705 Standard Test Apparatus

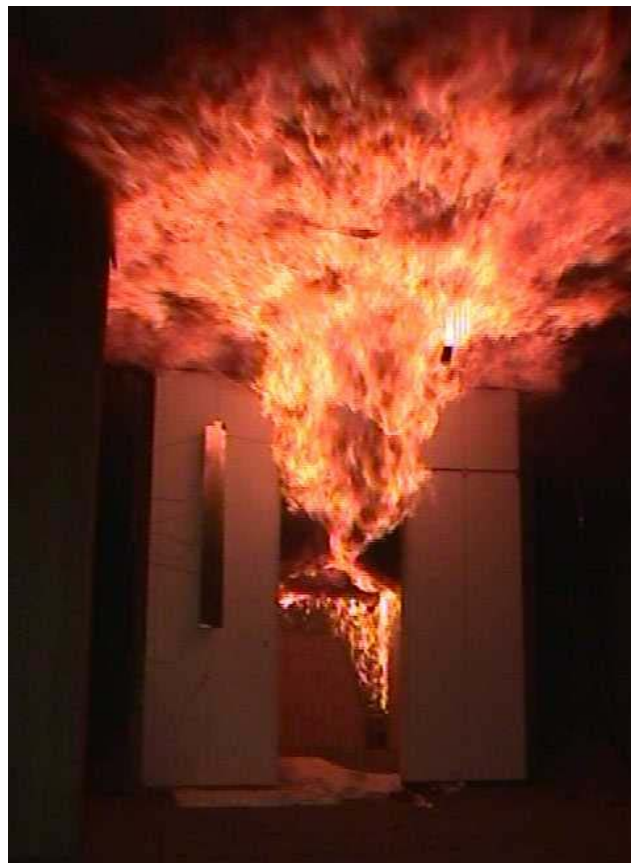


Figure 4 - 2: Front View of ISO 9705 Standard Test Room During Flashover Fire

In this test, products can be evaluated for their fire performance in terms of heat release rate, products of combustion, time to flashover, smoke production and temperature measurements in the room [19]. The specimen is placed in the test room, ignited and then allowed to burn until a specified end-of-test criterion is met such as time, flameout or flashover. The fume hood, located outside of the doorway, as seen in Figure 4 - 1 above, is used to collect the combustion products for species analysis, smoke production and for measurement of the fire heat release rate by means of the oxygen consumption calorimetry technique discussed in Section 3.1.2.

Full-scale laboratory fire tests, such as ASTM E 2067, are conducted in a more controlled manner than field fire tests. As a result, this type of fire testing is often very expensive and can be quite difficult to perform. There are very few facilities in Canada that have the ability to perform controlled full-scale fire tests according to standards such as the ISO 9705 Room/Corner Test Standard. NRC is one of the facilities in Canada that has a dedicated full-scale, ISO 9705, fire test apparatus. Field fire tests are another type of full-scale fire test that can be performed in addition to the standardized full-scale fire tests.

4.2 Building Field Fire Tests

Field fire tests can often be performed in abandoned buildings slated for demolition or in firefighters' training facilities. The St Lawrence Burns [22], discussed in Chapter 1, is one of the most famous and useful set of field fire tests that has been performed, and highlights the benefits of this type of full-scale fire test. A field fire test does not

necessarily follow a prescribed method or standard, however, it can still be a valuable tool in experimental fire research. Field fire testing allows for testing to be performed, which otherwise may not be able to be done at dedicated laboratory full-scale fire testing facilities for various reasons including cost and facility constraints. Field fire tests are performed in buildings according to the researchers' requirements. One advantage of field fire tests are that they may better represent real-life scenarios than tests in laboratories for several reasons including the addition of real-life environmental variables such as wind effects, which may help the fire to grow faster and that field fire tests can often be performed on larger buildings than laboratory-based full-scale tests. Disadvantages of this type of testing can include the inability to control environmental variables such as wind, temperature and humidity and also limited instrumentation due to difficulties in set-up and the fact that very few tests may be conducted in the same location, therefore increasing costs.

4.3 Small-Scale and Full-Scale Heat Flux Test Instrumentation

The type of instrumentation used during fire testing can vary depending on the type of test being conducted and the quantities of interest. Whether a full-scale fire test or a laboratory-scale test is being performed, the two most common quantities include temperature and heat flux. Temperature is a fairly descriptive quantity to fire researchers and is relatively easy to obtain using thermocouples. Heat flux, however, is a more challenging quantity to obtain. The following sections will discuss the heat flux and temperature instrumentation that is commonly used in fire testing.

4.3.1 Heat Flux Sensors

Heat flux, which is defined as the rate of thermal energy transferred per unit area across a surface, is a difficult quantity to measure directly. Many different techniques of measuring heat flux have been explored with varying degrees of success [60].

Diller [60] discusses the challenges of measuring heat flux and describes that heat flux is a difficult quantity to measure because it requires an inverse approach – a measurable quantity, such as temperature, has to be sampled and then converted to heat flux by knowing the nature of the heat transfer in the sensor.

An ideal heat flux sensor is able to obtain an accurate measurement while being non-invasive [60]. The heat flux gauge should not affect the heat transfer characteristics on the surface of the object. The gauges should be flush mounted with flat surfaces and should be of similar thermal and surface properties as the object they are mounted on. The gauges used in this investigation fall under two general categories of heat flux measurement devices: measuring a change in temperature during a known change in time and measuring a change in temperature over a known distance in a material with known thermal properties.

During fire testing, the heat flux gauges are placed in an insulating block in order to promote one-dimensional heat transfer in the sensor and to reduce the edge effects of the sensor. The insulating blocks are constructed from a solid insulation board of 22 mm thickness and are machined in order for mounting of the sensor (pictured in Figure 4 - 3, following.) In addition to the insulating block, the incident faces of the gauges are

painted with a high temperature black paint in order to increase the emissivity close to 1.0, approaching a black body radiation receiver.

4.3.2 Skin Simulant Sensor (Thin Film)

Skin simulant sensors measure a change in temperature over a certain duration of time and then convert this to a heat flux using standard heat transfer equations and have been developed for thermal mannequin protective clothing tests performed at the University of Alberta Fire Research Department [61]. The skin simulant sensor used during this project were manufactured at the University of Alberta and were machined to be approximately 22 mm diameter and 19 mm long out of colceran, a material that has similar thermal properties to human skin. A T type thermocouple is flush mounted to the front of the cylinder and measures the temperature of the exposed surface.

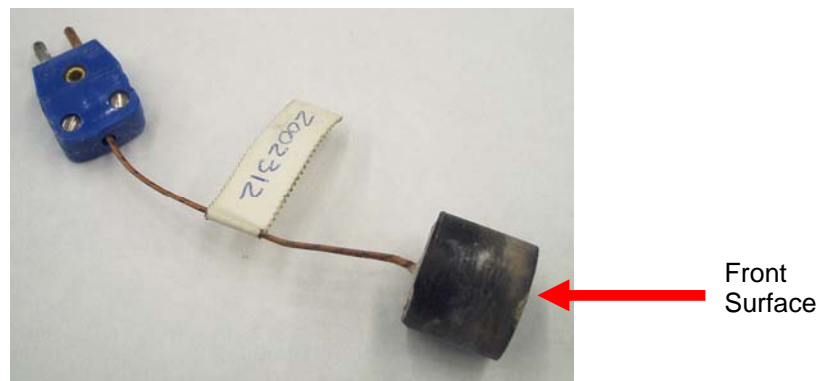


Figure 4 - 3: Skin Simulant Sensor

In order to acquire heat flux from this type of sensor, a semi-infinite solid transient heat conduction problem is assumed. A semi-infinite solid assumption is based around the fact that the material is quite thick (in this case, the cylinder is long) and the material has

a low thermal diffusivity. Relatively short exposure times are also part of the semi-infinite solid assumption as seen in the following criterion formula presented in common heat transfer textbooks, for constant heat fluxes: (e.g. [5]):

$$\frac{L}{2\sqrt{\alpha_{th}t}} > 2 \quad (4.1)$$

where:

L = Length [m]

t = Time [s]

α_{th} = Thermal Diffusivity [$m^2/2$].

If the criteria in Equation 3.1 is true, the heat flux from the Fourier Field equation can be determined to be [5]:

$$q_{total}'' = \frac{(\Delta T)\sqrt{\pi}\sqrt{k_{thermal}\rho c}}{2\sqrt{t}} \quad (4.2)$$

where:

q_{total}'' = Total Heat Flux [W/m^2]

t = Time [s]

$k_{thermal}$ = Thermal Conductivity [$W/m \cdot K$]

ΔT = Temperature Change on Surface [K]

c = Specific Heat [$J/kg \cdot K$]

ρ = Density [kg/m^3].

To determine the heat flux measured by the skin simulant sensor, the temperature rise, exposure time and the other thermal properties of the sensor are entered into Equation 3.2. The sensors were calibrated to find the value of $\sqrt{k\rho c}$. For time-dependent heat fluxes, a more complex equation, using Duhamel's Theorem, is required

to determine the heat flux measured by the skin simulant sensor, described in the following equation [60]:

$$q_{total}''(t) = \sqrt{\frac{k_{thermal}\rho c}{\pi}} \left[\frac{1}{2} \int_0^t \frac{T_s(t) - T_s(\tau)}{(t - \tau)^{3/2}} d\tau + \frac{T_s(t) - T_i}{t^{1/2}} \right] \quad (4.3)$$

where:

- q_{total}'' = Total Heat Flux [W/m^2]
- t = Time [s]
- $k_{thermal}$ = Thermal Conductivity [$W/m \cdot K$]
- c = Specific Heat [$J/kg \cdot K$]
- ρ = Density [kg/m^3]
- τ = Dummy Variable of Integration
- T_s = Surface Temperature [K]
- T_i = Initial Temperature [K].

For the purposes of this work, a computer program using Equation 4.3 was used to calculate the time-dependent heat flux to the skin simulant sensors as outlined in [62].

4.3.3 Schmidt-Boelter Gauge

Schmidt-Boelter (SB) gauges (MedTherm Corp., Huntsville AL) are commercially available in many sizes and heat flux measurement ranges. As Diller [60] describes, a SB gauge is used to determine heat flux by measuring the temperature difference across some known thermal resistance. The thermal resistance material (or wafer) used in SB gauges is a high thermally conductive material such that there is a quick time response to changes in heat flux. The wafer is then wrapped with a thermocouple wire, and a thermopile is created. The thermopile allows small changes in temperature across the

wafer to be detected, allowing for sensitive measurements. The thermopile and wafer are connected to a liquid-cooled (usually water) heat sink such that a constant temperature is maintained on the back of the wafer. This prevents the gauge from becoming damaged due to high temperatures and prevents losses from the wafer becoming significant and thus introducing errors. An example of the Schmidt-Boelter gauges used in this work is shown in Figure 4 - 4 below. The face of the sensor is approximately 25 mm in diameter and 22 mm long.

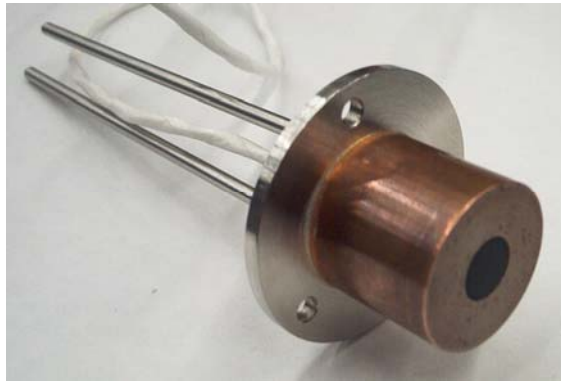


Figure 4 - 4: Schmidt-Boelter Gauge

The Schmidt-Boelter gauge measures a change in temperature as a function of distance as explained above. The gauges, which were calibrated by the manufacturer, output a linear relationship between voltage and heat flux with calibration constants of $6.12 \text{ kW/m}^2/\text{mV}$.

4.3.4 Gardon Gauge

The Gardon gauge is similar to the Schmidt-Boelter gauge in that it measures a change in temperature over a certain distance and then uses the geometry of the heat transfer to calculate the heat flux. A Gardon gauge operates by measuring the temperature difference between the centre of a disk and the edge of the disk using a thermocouple [60]. This type of gauge, probably more so than the others, requires a uniform heat flux across the 25 mm diameter face of the sensor due to the fact that the heat transfer within the disk is perpendicular to the incident heat transfer (the water-cooling is along the circumference of the disk). The Gardon gauge is pictured below in Figure 4 - 5, when mounted in an insulating block, and looks identical to the Schmidt-Boelter gauge with the same dimensions. As with the Schmidt-Boelter gauge, the Gardon gauge outputs a voltage, which has been calibrated by the manufacturer in terms of a linear relationship between heat flux and voltage output of $9.823 \text{ kW/m}^2/\text{mV}$.

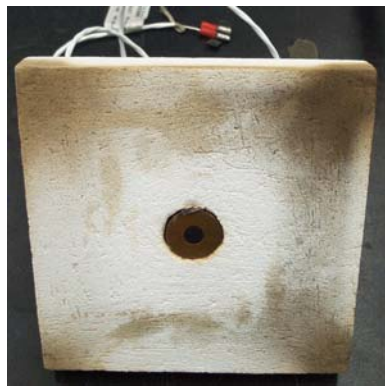


Figure 4 - 5: Gardon Gauge in Insulating Block

4.4 Edmonton I

In July 2003, researchers from the Universities of Alberta and Saskatchewan conducted a set of field fire tests in an abandoned building in Edmonton, AB. Threlfall et al. [44] and Dale et al. [63] summarize this test; additional details are included here. The building used for the fire tests was a single story dwelling with a floor area of 68 m² (732 ft²) as seen in Figure 4 - 6 below. Additional details of the building are located in Appendix A. In order to replicate a real-life scenario, the house was fitted with typical appliances and furnishings during a set of four separate test burns, summarized in Table 4 - 1 . During three of the four burns, the fire was contained to a single room by the Edmonton Fire Department. The last of the test fires was allowed to progress until the entire house was destroyed. Appendix A contains additional data recorded during the Edmonton I set of burns that is not presented here as well as drawings of the house floor plan used in the fire tests.

Table 4 - 1: Summary of Edmonton I Experiments

Test Burn	Room of Fire Origin	Details
1	South Bedroom	Started at 9:47 AM, July 8, 2003 Extinguished by Edmonton Fire Department
2	Living Room	Started at 12:45 PM, July 8, 2003 Extinguished by Edmonton Fire Department
3	Basement	Started at 2:44 PM, July 8, 2003 Extinguished by Edmonton Fire Department
4	Living Room	Started at 3:42 PM, July 8, 2003 Allowed to burn to the ground



Figure 4 - 6: House Used In Full-scale Tests

The first of the four test burns was performed in the South bedroom as seen below in Figure 4 - 7. The second and third test burns were performed in the living room and basement respectively. The final burn was started in the living room and allowed to proceed until the house was entirely burned.

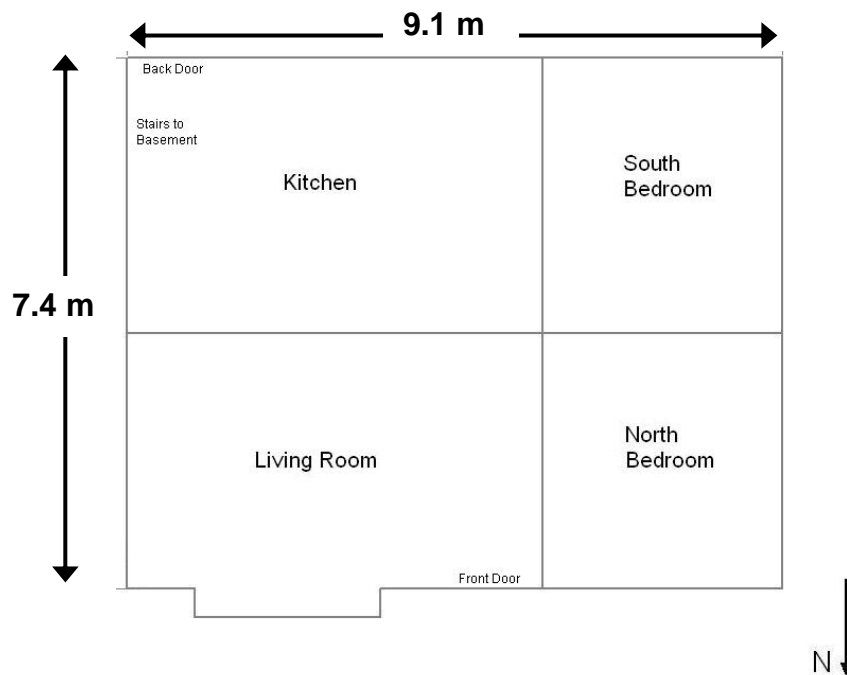


Figure 4 - 7: Edmonton I House Floor Plan

This work was primarily concerned with investigating the spatial separation requirements that are in Canada's National Building Code [34]. The Building Code requires that structures have a specific minimum separation distance between them in order to reduce the likelihood of fire spread to a neighbouring building. The principal methods of fire spread between buildings can be by flying brands, which were not investigated in this work, and radiation heat transfer.

4.4.1 Edmonton I Instrumentation

During this series of experiments, the temperatures and heat fluxes inside the building were measured in addition to the exterior heat fluxes emitted from the burning building. The temperature was measured in three different rooms with type K, chromel-alumel, 24 AWG thermocouple wire. At each location where the temperature was measured, a thermocouple tree was used. The thermocouple tree was constructed by attaching a steel wire from the floor to the ceiling and then fastening three thermocouples at specific vertical distances from the floor. The locations chosen for the thermocouples were at distances of 0.15 m, 1.37 m and 2.7 m. Figure 4 - 8 shows one of the partially completed thermocouple trees.

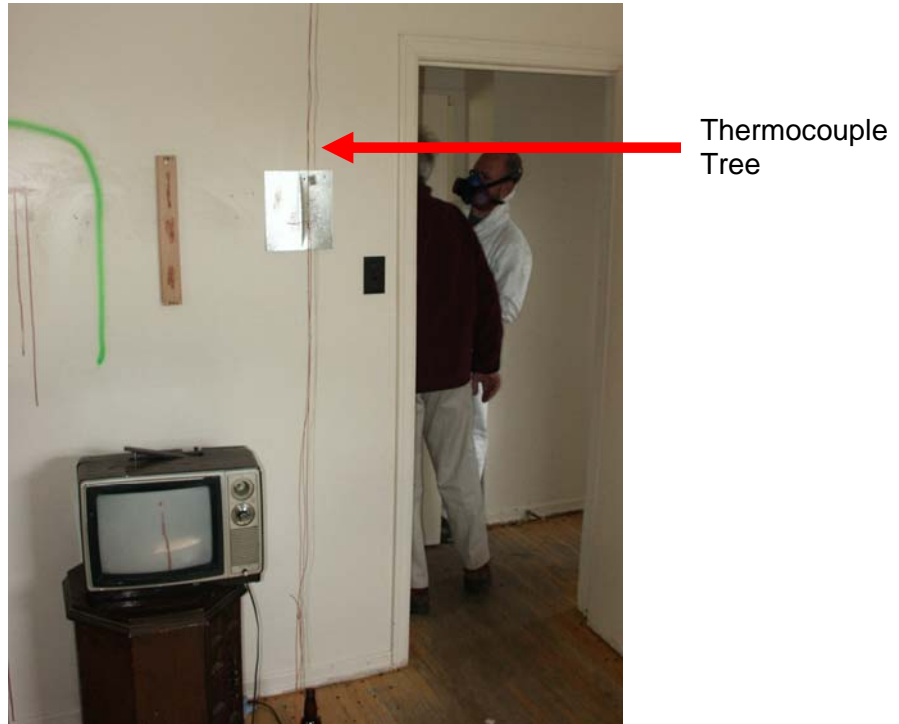


Figure 4 - 8: Thermocouple Tree Located in North Bedroom

Skin simulant heat flux sensors were placed in insulating boards as described in Chapter 3 and then attached to the interior walls at several locations throughout the house. In order to examine the radiant heat flux emitted by a burning building and received by surrounding structures, heat flux gauges were located at a distance of 4.0 m from the window and 1.84 m above the ground during this series of experiments. The bottom of the 1.8 m wide by 1.2 m high window was 1.94 m from the ground. Four heat flux gauges: a Gardon gauge, Schmidt-Boelter gauge and two skin simulant sensors were mounted in an insulating board on a tripod opposite the burning building in order to record heat flux data and to also investigate differences in sensor results as seen in Figure 4 - 9.

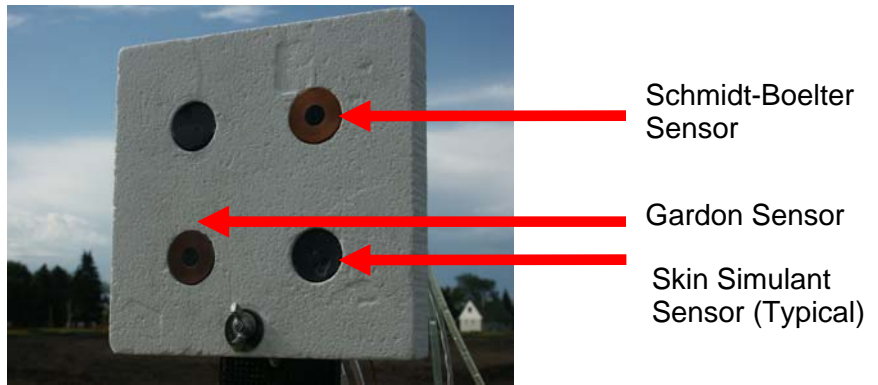


Figure 4 - 9: Thermal Insulating Board with Heat Flux Gauges

The Gardon and Schmidt-Boelter gauges both require the use of cooling water as previously discussed. Figure 4 - 10 shows the support structure used for the sensors during the testing.



Figure 4 - 10: Support Structure for Heat Flux Gauges (Back Showing)

Several small, battery-operated, data loggers were used to log the data taken by the various test sensors at a sampling rate of 60 Hz per channel. These data loggers were located at several locations both inside and outside the house. The data loggers, seen in Figure 4 - 11, were manufactured at the University of Alberta. The results were stored

on the data loggers and later downloaded to a PC for analysis. In addition, an Agilent model 34970A data logger (Agilent Technologies Inc, Palo Alto, CA) was used to record the radiant heat flux data from the sensors located on the tripod.



Figure 4 - 11: Data Acquisition System (Data Logger)

4.4.2 Edmonton I Results

The most significant results were obtained during the first test and the final test. Other results are located in Appendix A. During the first burn, a fire was set in a bedroom by igniting a mattress with a propane burner. The fire was contained to a single room.

During this experiment, the heat flux was measured opposite the window at a distance of 4.0 m and height of 1.84 m, as seen in the following figure. Figure 4 - 12 following, shows a sequence of pictures qualitatively demonstrating the fire growth rate.



Approx. time after ignition: 4 min



Approx. time after ignition: 8 min



Approx. time after ignition: 9 min



Approx. time after ignition: 11 min



Approx. time after ignition: 15 min



Approx. time after ignition: 18 min

Figure 4 - 12: Sequence Showing Single Room Fire Growth and Location of Sensors

The exterior heat flux measured by the skin simulant and Schmidt-Boelter sensors on the tripod is shown in Figure 4 - 13. The results from the second skin stimulant sensor and Gardon gauge have been left off Figure 4 - 13 for clarity, as they were virtually identical to the presented skin stimulant sensor and Schmidt-Boelter gauge results respectively. The maximum heat flux reached during this test was approximately 2 kW/m^2 , which is

much lower than the heat flux required for unpiloted ignition of neighbouring cellulosic materials [5,23]. Figure 4 - 13 also indicates that there is a difference in the measured radiant heat flux between the skin stimulant sensor and Schmidt-Boelter gauge. This will be explored in more detail in the following section, 4.4.

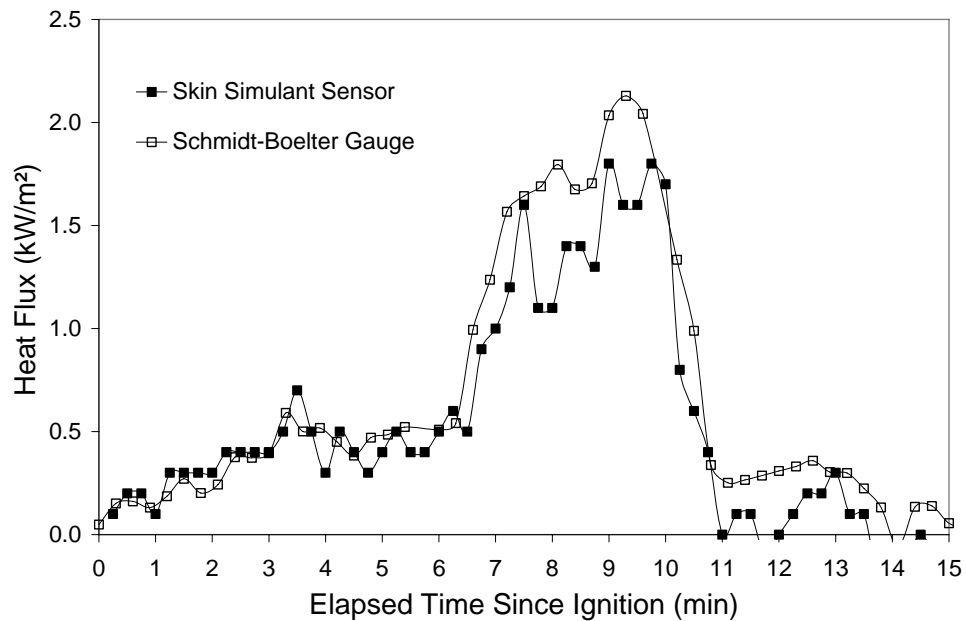


Figure 4 - 13: Exterior Heat Flux Measured During Single Room Fire

During the final fire test, shown in Figure 4 - 14, the entire house was allowed to completely burn to the ground. Gasoline was used as an accelerant in order to help the fire to get started.



Approx. time after ignition: 2 min



Approx. time after ignition: 4 min



Approx. time after ignition: 4 min



Approx. time after ignition: 7 min



Approx. time after ignition: 10 min



Approx. time after ignition: 14 min



Approx. time after ignition: 24 min



Approx. time after ignition: 32 min

Figure 4 - 14: Sequence Showing Entire House Fire Growth and Location of Sensors

The exterior heat flux measured by the sensors on the tripod during the initial portion of the full house burn follows in Figure 4 - 15. The sensors were located at horizontal and vertical distances of 4.0 m and 1.84 m, respectively, opposite the large window at the front of the building. The sensors were removed after approximately 11 min for fear the equipment may be damaged as a result of the intense heat.

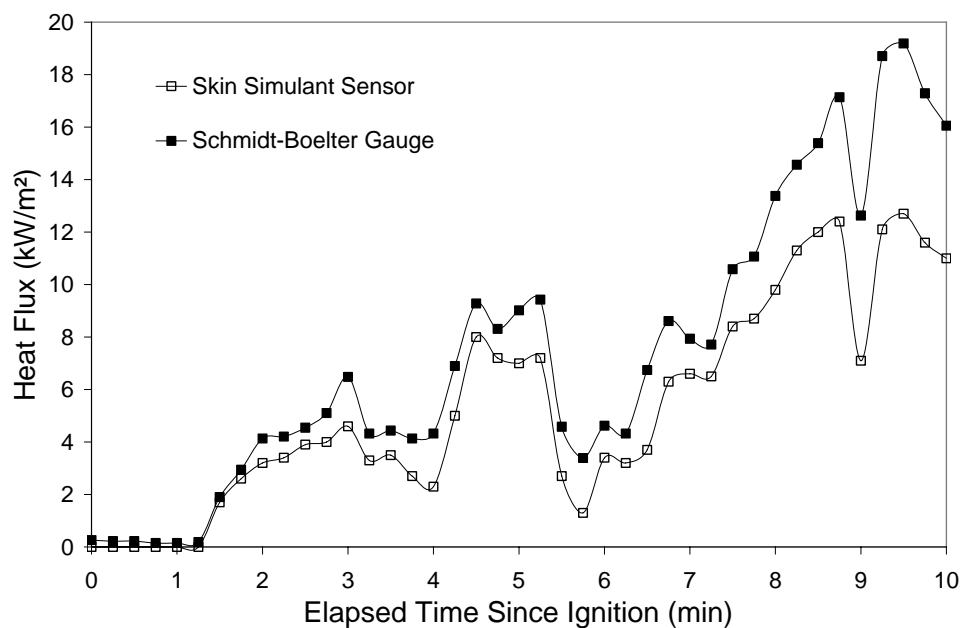


Figure 4 - 15: Exterior Heat Flux During Initial Portion of Full House Burn

As evident in Figure 4 - 15 above, the heat flux as measured by the sensors continued to increase until the equipment was removed. There was an increase in the measured heat flux when the window broke, at approximately 1.5 to 2.0 minutes, as the fire grew with the influx of oxygen and flames began to project from the window.

The results from the full house burn indicate that another structure or object located at the same distance as the sensors (4.0 m) would likely have been subjected to heat fluxes greater than the required heat flux for ignition, as radiant heat fluxes exceeding the 12.5 kW/m² limit for ignition of cellulosic materials. Further discussion and analysis of the required spatial separation for this building is located in Section 5.1.

4.5 Edmonton I Heat Flux Sensor Response

The cone calorimeter was used to investigate the difference in sensor response exhibited during the Edmonton I full-scale tests performed in July 2003, presented in Figure 4 - 13 and Figure 4 - 15 above. As previously mentioned, a significant difference in measured heat fluxes between some of the individual sensors can be seen. The Schmidt-Boelter and Gardon gauges seem to give approximately the same results for the majority of the test, as do the two skin stimulant sensors. The disparity between the two types of gauges (Schmidt-Boelter and Gardon versus skin stimulant) seems to be greatest at the maximum heat flux reached at approximately ten minutes as seen in Figure 4 - 15 above. At an elapsed time of ten minutes, the difference in measured results reaches a maximum of approximately 30%. It is evident that the differences are a result of the measurement technique and operation of the type of heat flux sensor. The differences between the Schmidt-Boelter and Gardon gauges and the skin stimulant sensors were examined in more detail during laboratory-scale testing and is described in more detail in the following sections.

The cone calorimeter was used to examine the differences between the results measured by the two different types of heat flux gauges seen during the Edmonton I experimental testing. The cone calorimeter, being able to provide a constant heat flux in time, was an ideal piece of equipment for examining the behaviour demonstrated during full-scale testing. The cone calorimeter was used to expose each type of sensor used during full-scale testing to a constant, radiant heat flux, and determine the response characteristics of each type of gauge. Heat flux levels ranging from 5 kW/m² to 80 kW/m², representing the range of heat fluxes typically encountered in both full-scale and small-scale fire testing, were set in the cone calorimeter using the factory-installed and calibrated cone calorimeter Schmidt-Boelter gauge. Heat fluxes of less than 5 kW/m² are difficult to accurately obtain in the cone calorimeter, which is why this value was chosen for the minimum heat flux.

The cone calorimeter heat fluxes were set using the factory-installed and calibrated Schmidt-Boelter sensor. This factory-installed Schmidt-Boelter sensor is a 13 mm diameter gauge. The purpose of the heat flux sensor response study is to assess the reason for the differences between the Schmidt-Boelter and Gardon type gauges versus the skin stimulant sensors.

4.5.1 Heat Flux Exposure Level of 5 kW/m²

Shown below is the graph that compares the responses of each gauge at an exposure level of 5.0 kW/m².

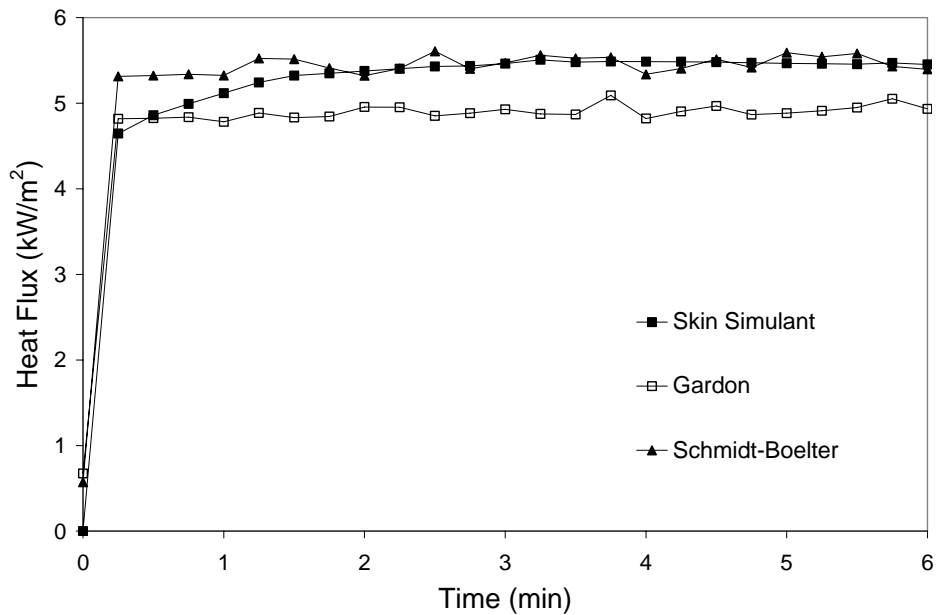


Figure 4 - 16: Comparison of Sensor Response at 5 kW/m²

As seen in Figure 4 - 16 above, the skin simulant sensor measures a fairly constant heat flux over the entire test duration. It takes this sensor approximately 1 min in order to start displaying a constant heat flux of approximately 5.5 kW/m² (9% difference as compared to nominal value of 5.0 kW/m²).

At an exposure level of 5 kW/m², both the Gardon and Schmidt-Boelter gauges perform much better than the skin simulant sensor. The Gardon gauge performs the best, as it quickly rises to an approximate constant heat flux of 4.9 kW/m² (-2.0 % difference). The Schmidt-Boelter also performs quite well as it displays a constant heat flux of approximately 5.5 kW/m² giving a difference of 9%.

From the results, it definitely appears as though the Gardon and Schmidt-Boelter sensors produce the most accurate results. This is especially true for long duration experiments exceeding a few seconds. The skin simulant sensor also did reasonably well during this test considering the relatively low cost of producing these sensors compared to the Schmidt-Boelter and Gardon gauges.

4.5.2 Exposure level of 20 kW/m²

The results for the sensor evaluation at 20 kW/m² is seen in Figure 4 - 17 below.

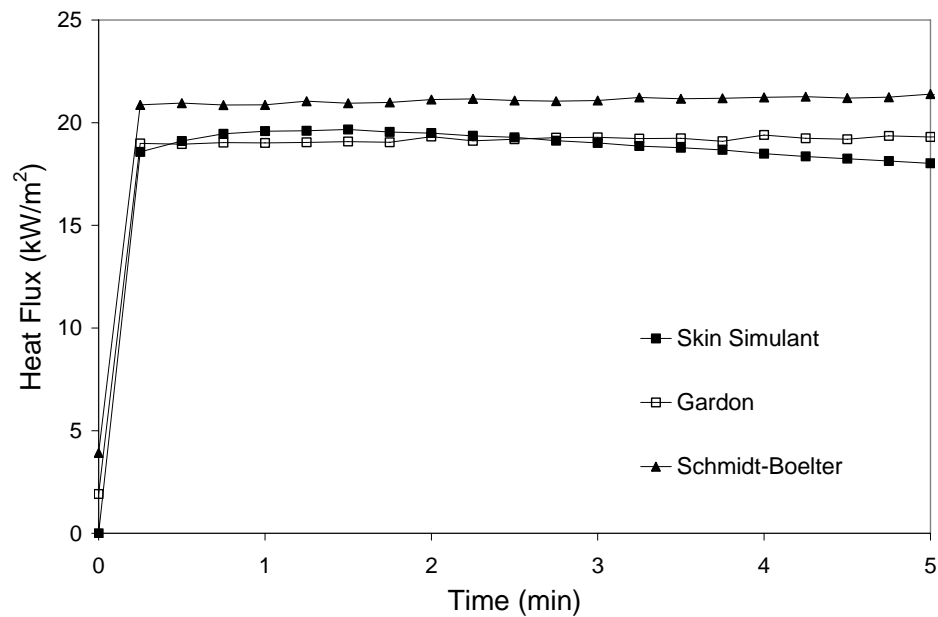


Figure 4 - 17: Comparison of Sensor Response at 20 kW/m²

The skin simulant sensor performs quite well at this exposure level. It takes this gauge some time to start giving approximately constant results. After 50 s of exposure, the skin simulant sensor displays a heat flux of approximately 19.5 kW/m² (-2.3%

difference) and after approximately 100 s, the gauge seems to start linearly decreasing to 17.8 kW/m² (-11% difference) at 5 min.

The Gardon gauge performs the best during this test over the entire duration of exposure. For most of the test, the Gardon gauge gives approximately constant results of 19.3 kW/m² (-3% difference). The Schmidt-Boelter gauge consistently gives results above 20 kW/m² as it gave a heat flux of approximately 21.2 kW/m² (6% difference).

4.5.3 Exposure level of 40 kW/m²

The results for an incident heat flux of 40 kW/m² follow in Figure 4 - 18.

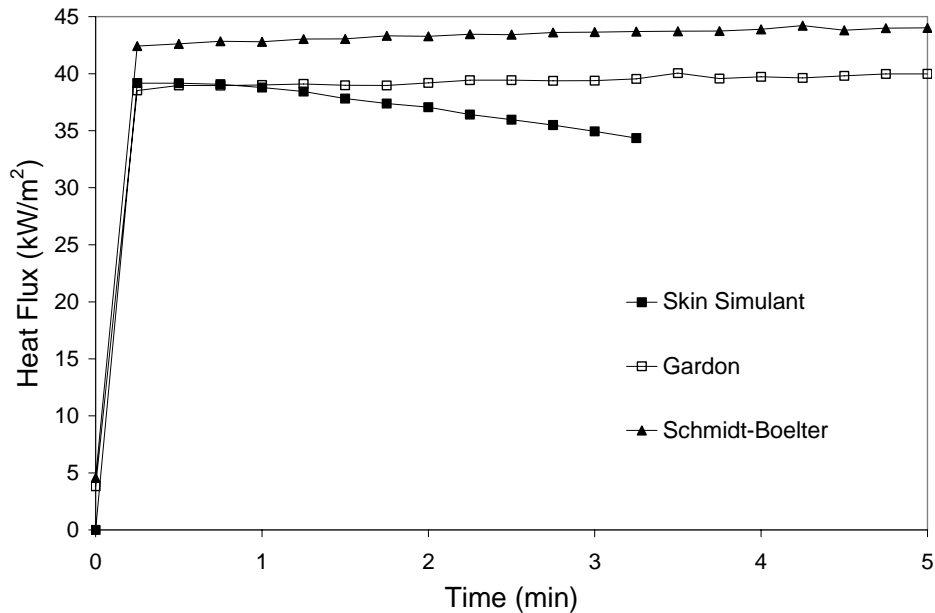


Figure 4 - 18: Comparison of Sensor Response at 40 kW/m²

Once again, the skin simulant sensor displayed very accurate results after about 20 s, however, the heat fluxes obtained from this sensor began to decrease significantly after

about 75 s. The reason for the gradual decline in the accuracy of this gauge is due to the assumption of a semi-infinite solid discussed in Section 4.3.2. During the portion where the skin simulant sensor results remain approximately constant, a heat flux of 39.3 kW/m² (-1.7% difference) is given. This accuracy decreases over the duration of the test until the gauge gives a reading of 34 kW/m² (-15% difference) at 200 s exposure. At approximately 220 s, the skin simulant sensor test was terminated as it was felt (based on experience) that damage to the sensor was imminent due to high temperature. Both the Gardon and Schmidt-Boelter gauges gave consistent results during the tests producing heat flux readings of 39.6 kW/m² (-1% difference) and 43.5 kW/m² (8.8% difference) respectively.

4.5.4 Exposure level of 80 kW/m²

A comparison of the results for the four gauges follows in Figure 4 - 19 below.

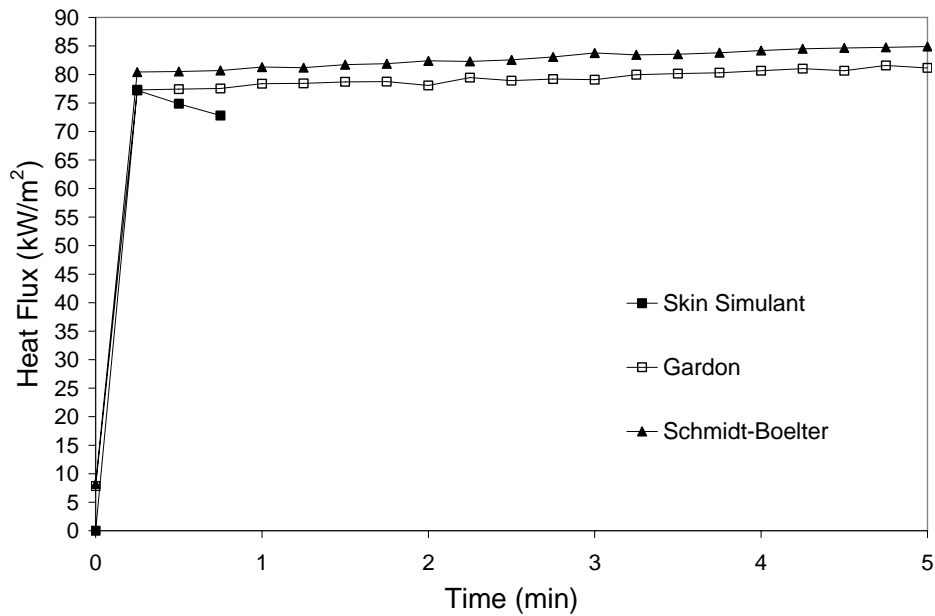


Figure 4 - 19: Comparison of Sensor Response at 80 kW/m²

Similar to the 40 kW/m^2 incident heat flux exposure level, the skin simulant sensor seemed to perform fairly well over the first few seconds and then perform poorly as the temperatures of the sensor began to approach the dangerous level for damage to the gauge. The skin simulant sensor started off giving results of 80.2 kW/m^2 (0.3% difference) and then seemed to linearly decline until a value of 73.0 kW/m^2 (-9% difference) was given approximately 45 s after the test began due to a breakdown in the assumption of a semi-infinite solid.

The Gardon and Schmidt-Boelter gauges both gave results that increased linearly by about 5 kW/m^2 over the duration of the tests. The Gardon gauge started at approximately 77.0 kW/m^2 (-3.7% difference) and then increased to 81.3 kW/m^2 (1.6% difference) after 5 min exposure. The Schmidt-Boelter gauge started at approximately 79.8 kW/m^2 (-0.3% difference) and then increased to 85.0 kW/m^2 (6.2% difference) at the end of the test.

4.5.5 Discussion of Cone Calorimeter Heat Flux Sensor Test Results

At the lower heat flux exposure levels of less than 20 kW/m^2 , a constant heat flux reading was measured by the skin simulant sensor for the majority of the test duration. At exposures of 20 kW/m^2 and higher, the measured skin simulant heat flux reached a constant value and then began to decrease as the test proceeded. The reason for this gradual, and linear, decrease in heat flux is due to the breakdown of the assumption of a semi-infinite solid and the heat losses from the gauge due to conduction into the insulation board and convection and radiation heat transfer to the surroundings. For the

calculation of heat flux, the temperature of the back of the sensor was assumed to stay constant at room temperature. With increased levels of heat flux, heating of the sensor material was increased and the temperature of the back of the sensor material is presumed to have not remained at room temperature.

The results for the skin simulant sensor were, however, quite accurate for low incident heat flux exposures after the initial settling period. The results were also accurate for higher heat flux exposures after the initial settling period and if the test did not proceed very long. A method for correcting the heat flux at long exposure times should be explored. As mentioned, if a thermocouple were attached to the back surface, and this information used somehow to adjust the heat flux reading, more accurate results may be produced.

The Gardon gauge was consistently the most accurate gauge used during this investigation. The results were within 5% of the incident heat flux level for all exposure levels. As with the Schmidt-Boelter gauge, the water cooling of this gauge is a definite advantage, as constant heat flux results are almost always reported. Also, the water cooling and the design of the gauge allows for an almost instantaneous reaction to a heat flux change. The results produced by the Schmidt-Boelter sensor are similar to those from the Gardon gauge in that they were very consistent. The Schmidt-Boelter gauge always produced readings within 10% of the cone calorimeter incident heat flux level.

4.6 Edmonton II

In September 2004, researchers from several organizations including the Fire Research Groups from the University of Alberta and University of Saskatchewan performed another set of full-scale field fire experiments in an abandoned building in Edmonton, AB. The Edmonton Fire Department was on location to assist and to start and control the fires. Interior temperature and heat flux data was recorded for three separate mattress fires, which can pose a significant fire threat in the home. The tests were performed in order to collect full-scale experimental temperature results that will be compared with temperatures predicted using the techniques outlined in Chapter 2. The experiments were conducted in a single room of an office building, shown below in Figure 4 - 20. The office building, which was slated for demolition, was located in an old section of the Canadian Forces Base Edmonton Garrison in approximately the same location as the Edmonton I set of experiments.



Figure 4 - 20: Abandoned Office Building Used for Edmonton II Fire Tests

All of the tests were performed in the same bedroom-sized enclosure, instrumented with several thermocouples and heat flux gauges to monitor conditions during the experiments. The room had dimensions of approximately 3.7 m by 4.3 m (12 ft. by 14 ft.) and a ceiling of 2.7 m (9 ft). Two of the walls were of drywall construction and the other two were of sheet metal construction, and there was a single door-sized opening approximately 2.0 m by 0.8 m (7 ft by 3 ft.) There were no combustibles in the enclosure, except a single mattress sitting on a boxspring.

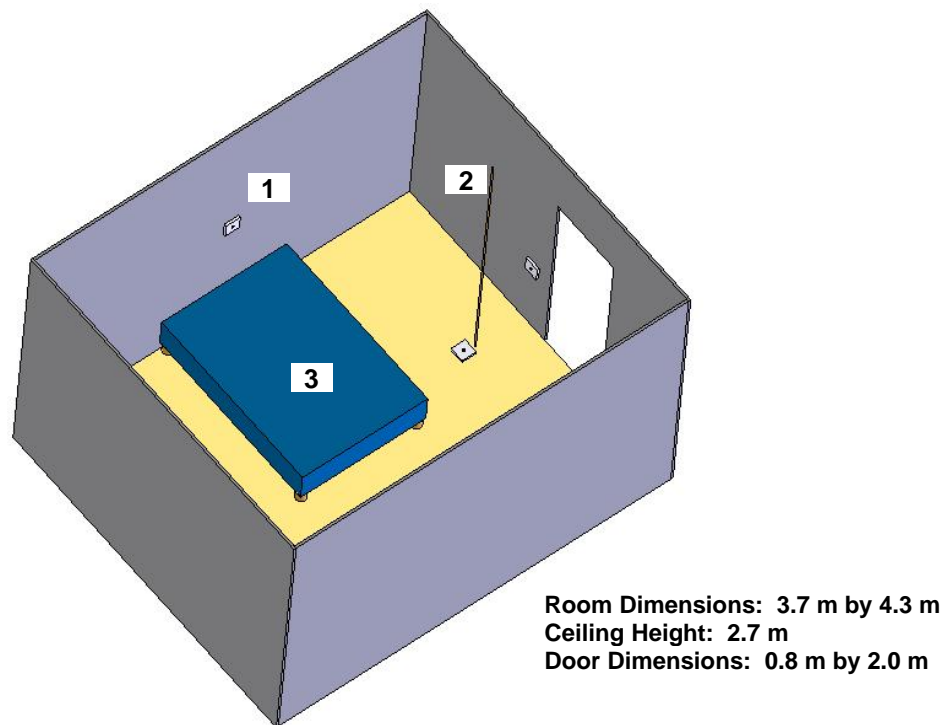
The Mattress 1 and Mattress 2 fire tests, started at 2:00 PM and 7:30 PM on September 13, 2004, respectively, were allowed to proceed until the mattress was completely burned. The Mattress 3 fire test was started at 10:00 AM on September 14, 2004 and was extinguished by the firefighters after it became apparent that it would only smoulder and not effectively burn by flaming combustion. In each case, the fire was lit on the edge at the centre of the foot of the bed and firefighters stopped the flames before the fire destroyed the boxspring. The boxspring was re-used for all three tests as it was not significantly damaged. The tests were captured on both regular and infrared video camera. The infrared video camera, which was not capable of outputting a data-file, provided a useful method of approximate temperature analysis.

The three mattresses used for this investigation were acquired second-hand in Edmonton. Detailed information as to their age and composition was not available, however, it was assumed that these samples represent typical mattresses that are used in Canadian homes. All three were spring mattresses, having the steel springs sandwiched

by an ensemble of materials ranging from cotton batting, reclaimed fibres, polyester, rayon and polyurethane foam as discussed in Section 3.2.

4.6.1 Edmonton II Instrumentation

As mentioned, both temperature and heat flux data were recorded during the tests. The enclosure chosen for this series of fire tests was instrumented with five thermocouples located at the ceiling (described in Table 4 - 2) and a thermocouple tree extending from the floor to the ceiling, consisting of four thermocouples located at distances of 0.6 m, 1.2 m, 1.8 m and 2.4 m (2 ft., 4 ft., 6 ft. and 8 ft.) from the floor. Five skin simulant heat flux sensors were also used to monitor interior conditions; the sensors were mounted in the centre of each of the four walls and 0.8 m (2.5 ft.) above the floor, and one located at the base of the thermocouple tree as shown in Figure 4 - 21, following.



1 – Typical Heat flux sensor location (5 total); 2 – Thermocouple tree location; 3 – Mattress & boxspring

Figure 4 - 21: Plan View of Test Room Showing Location of Sensors

The mattress was located at approximately the centre of the room, with the head against one of the long walls as seen in Figure 4 - 21. Mattress 1 had dimensions of approximately 1.3 m (4.4 ft.) by 1.9 m (6.3 ft.) and Mattress 2 and 3 both had dimensions of 1.2 m (5 ft.) by 2.0 m (6.7 ft.) All three mattresses and the boxspring were approximately 0.2 m (0.5 ft.) thick. The bottom of the boxspring was located approximately 0.1 m (0.3 ft.) off the floor for all three tests.

Table 4 - 2: Radial Distances from Centre of Bed to Ceiling Thermocouples

Thermocouple (T/C) Number	Radial Distance From Centre of Mattress, r (m)
1	1.125
2	2.358
3	0.710
4	2.190
5	0.855

The data was recorded by the same battery operated data loggers used in the Edmonton I set of experiments described in Section 4.4.1. Once again, a sampling frequency of 60 Hz per channel was used during this series of experiments.

4.6.2 Edmonton II Results

Figure 4 - 22 shows the extent to which the mattresses were destroyed during the testing. As seen, the entire mattress was destroyed except for the steel springs. Figure 4 - 23 and Figure 4 - 24 show the temperatures measured in the first of the three tests.



(a)



(b)

Figure 4 - 22: Example of Mattress (a) Before and (b) After Test (Mattress 1 shown)

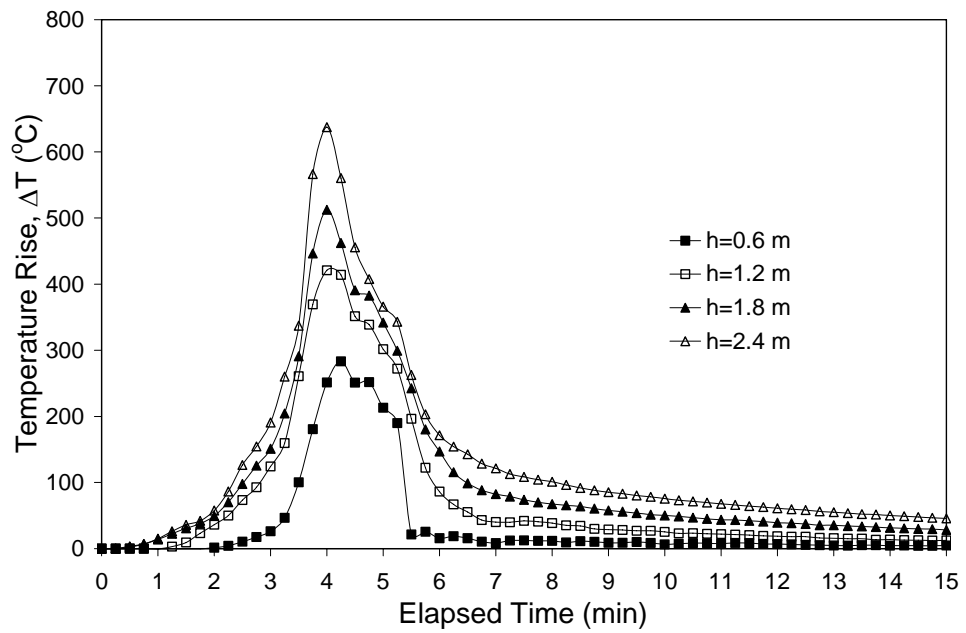


Figure 4 - 23: Test 1 Thermocouple Tree Temperature Measurements (h=vertical distance from floor)

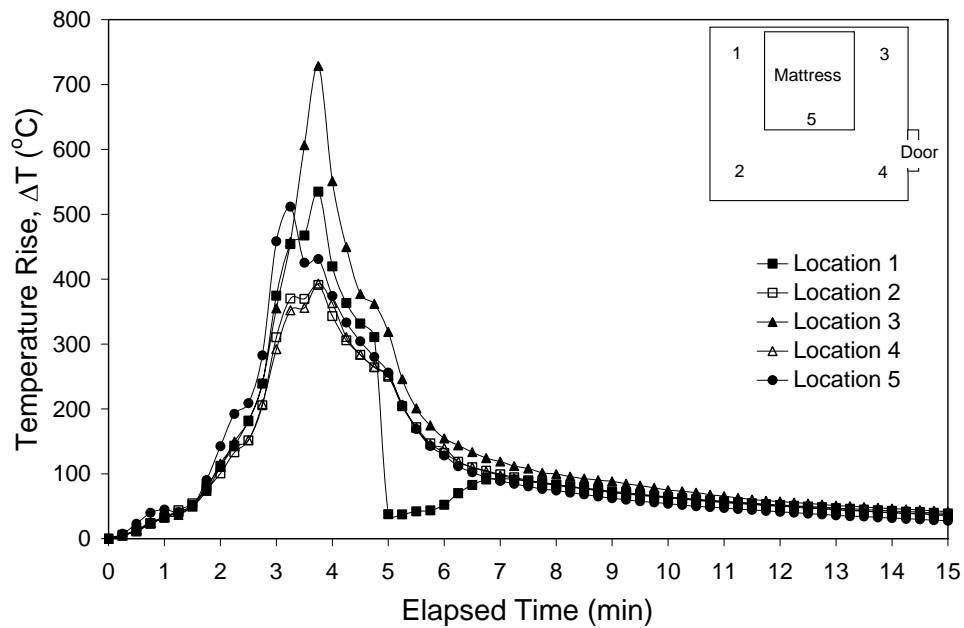


Figure 4 - 24: Test 1 Ceiling Temperature Measurements

The skin simulant sensors located in the room did not record any significant heat flux results during the test, due to damage of the heat flux sensor wires as a result of the fire. As expected, the temperature measured by the thermocouple tree indicated that the temperature was lowest near the ground and progressively increased with increasing distance above the floor.

Figure 4 - 25 and Figure 4 - 26, which follow, show the temperature measured during the test of Mattress 2. Once again, no significant results were obtained from the heat flux sensors located in the room.

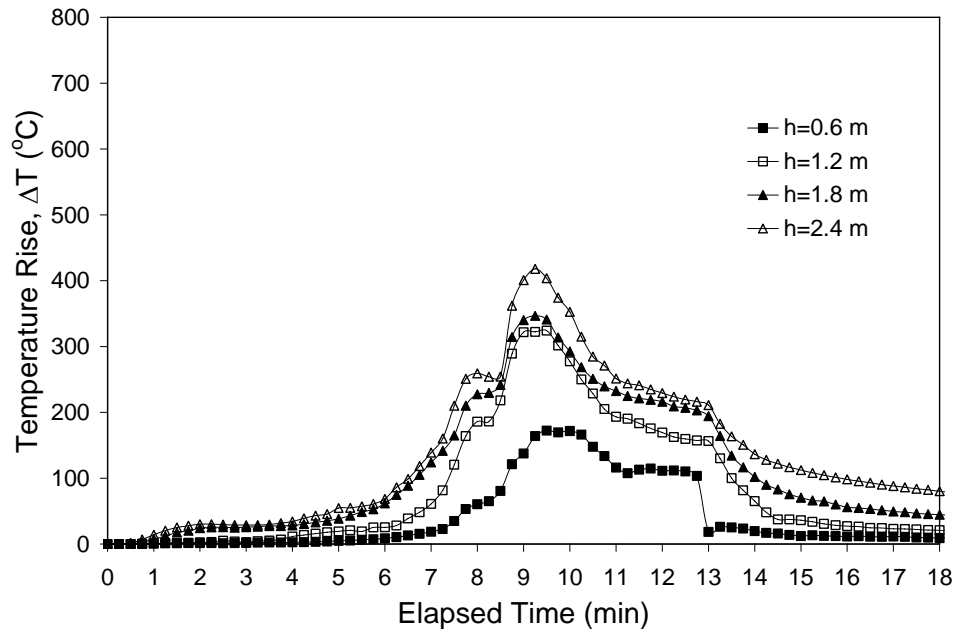


Figure 4 - 25: Test 2 Thermocouple Tree Temperature Measurements
(h=vertical distance from floor)

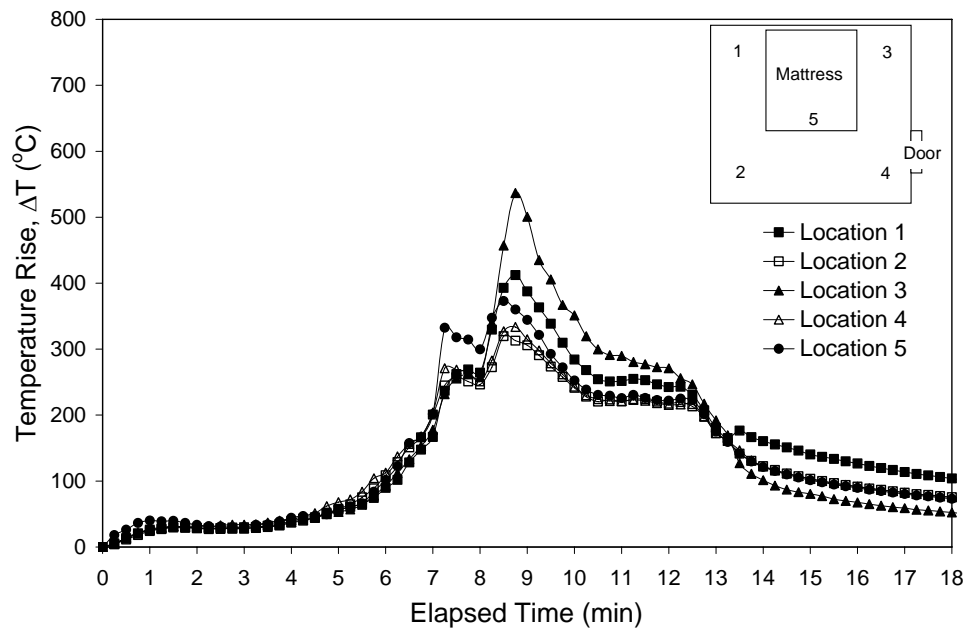


Figure 4 - 26: Test 2 Ceiling Temperature Measurements

The third mattress was constructed of different types of materials than Mattress 1 and Mattress 2 and as a result, did not burn very well. Mattress 3 simply smouldered for several minutes producing a significant amount of smoke and never burned with prolonged flaming combustion, until it was extinguished by the firefighters. As a result, the mattress did not produce any significant results that can be used in this investigation of fire modeling techniques as will be discussed in further detail in Section 5.5.

Figure 4 - 27 through Figure 4 - 30 compare the thermocouple tree results for Mattress 1 and Mattress 2.

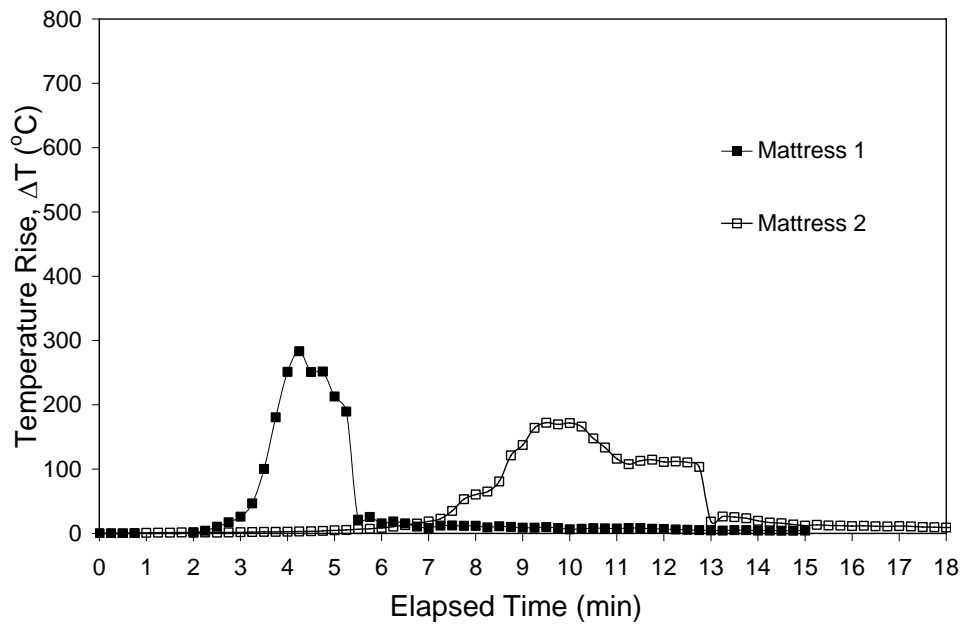


Figure 4 - 27: Comparison of h = 0.6 m Thermocouple Tree Results

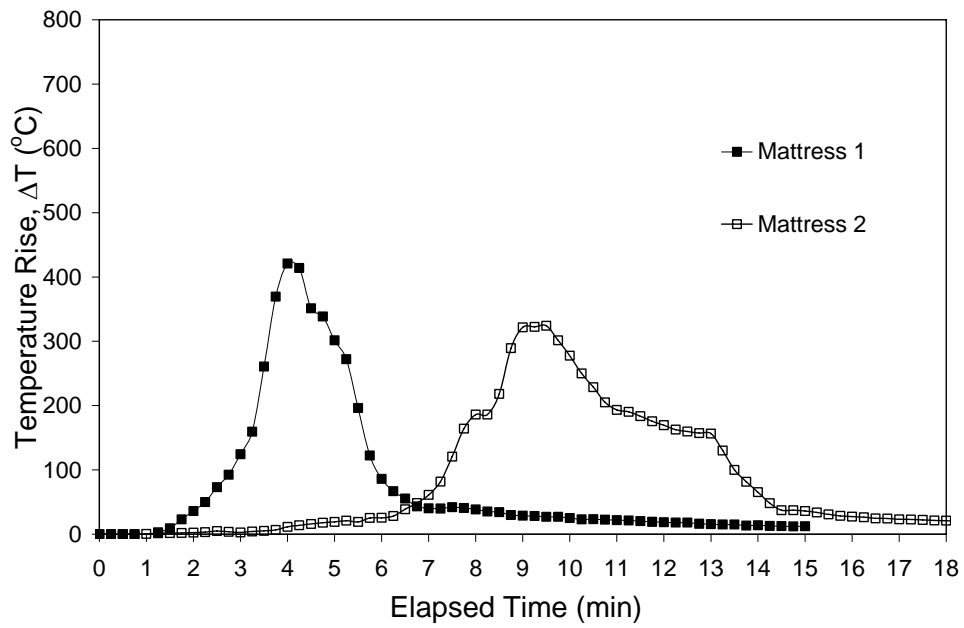


Figure 4 - 28: Comparison of h = 1.2 m Thermocouple Tree Results

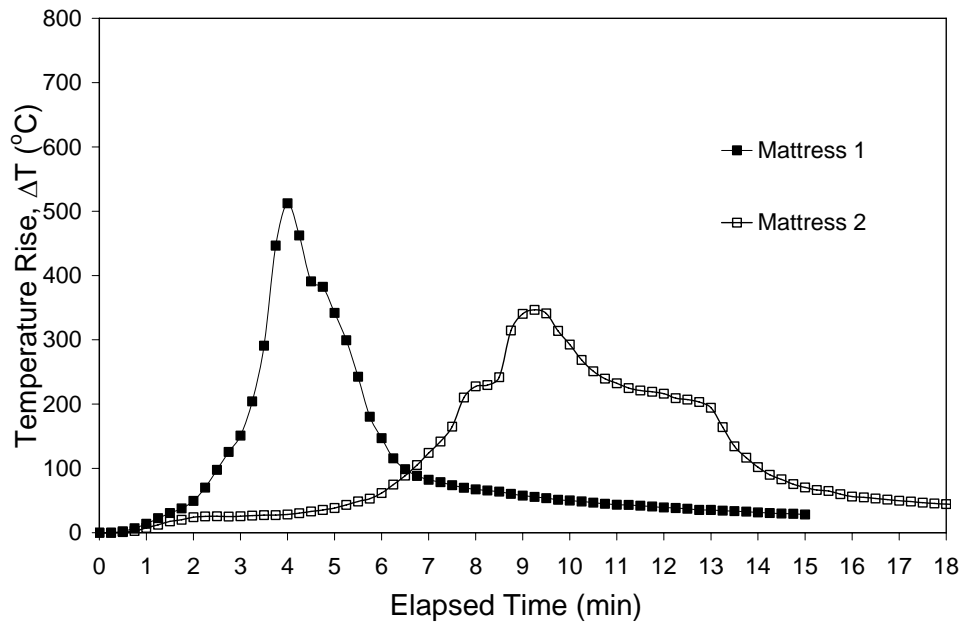


Figure 4 - 29: Comparison of h = 1.8 m Thermocouple Tree Results

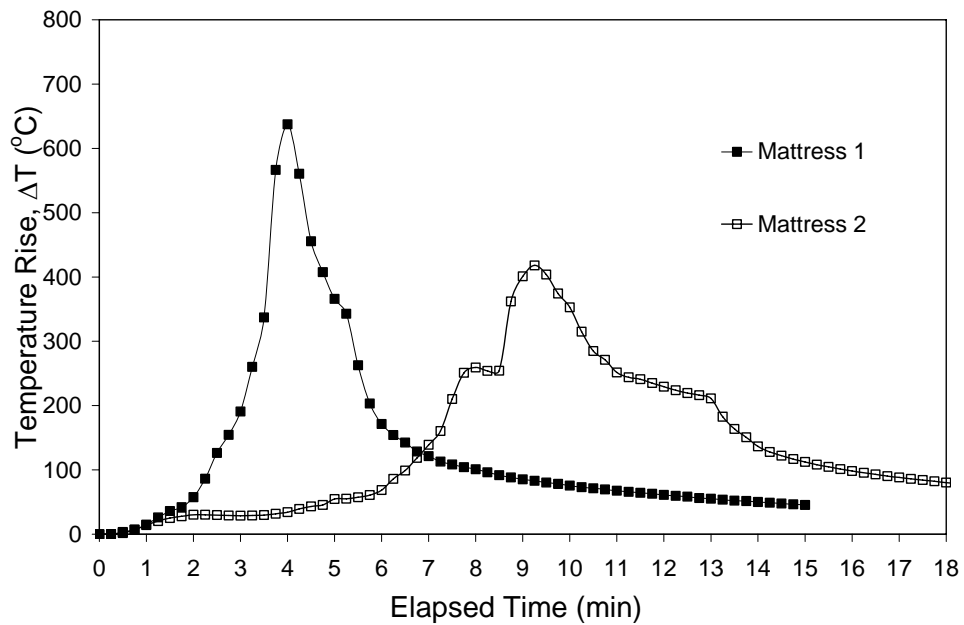


Figure 4 - 30: Comparison of h = 2.4 m Thermocouple Tree Results

Figure 4 - 31 through Figure 4 - 35 compare the ceiling temperature results for Mattress 1 and 2 for the five ceiling thermocouple locations. As with the thermocouple tree results, it is clear that Mattress 2 has a longer incubation time, as it takes longer for the fire to grow.

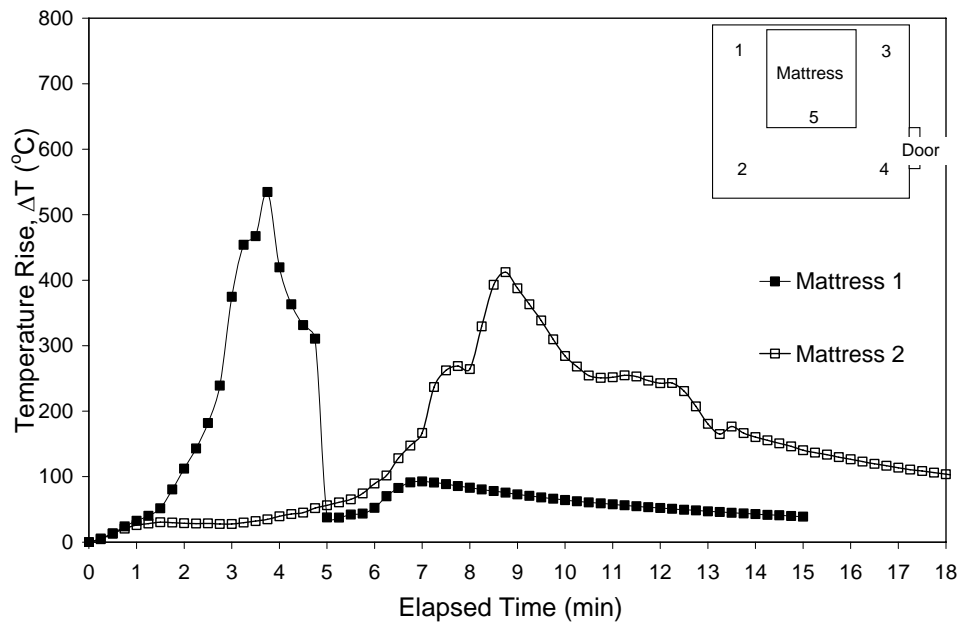


Figure 4 - 31: Comparison of Ceiling Thermocouple Location 1 Results

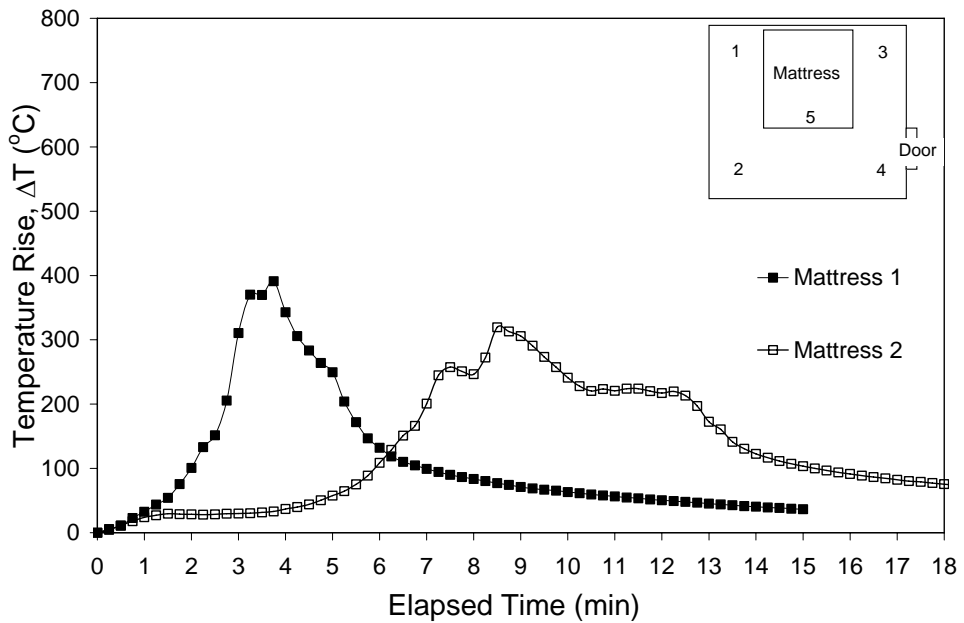


Figure 4 - 32: Comparison of Ceiling Thermocouple Location 2 Results

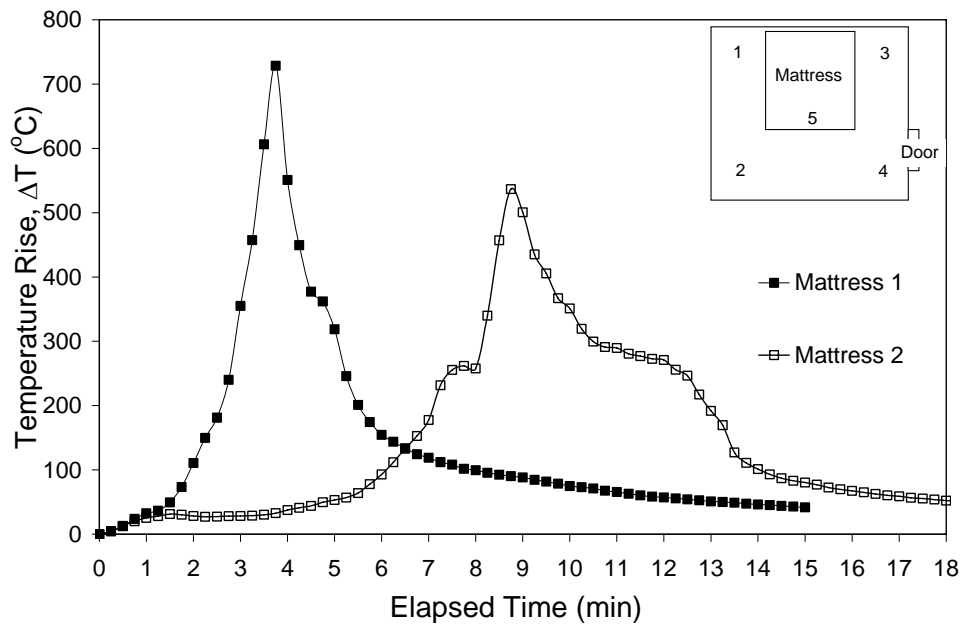


Figure 4 - 33: Comparison of Ceiling Thermocouple Location 3 Results

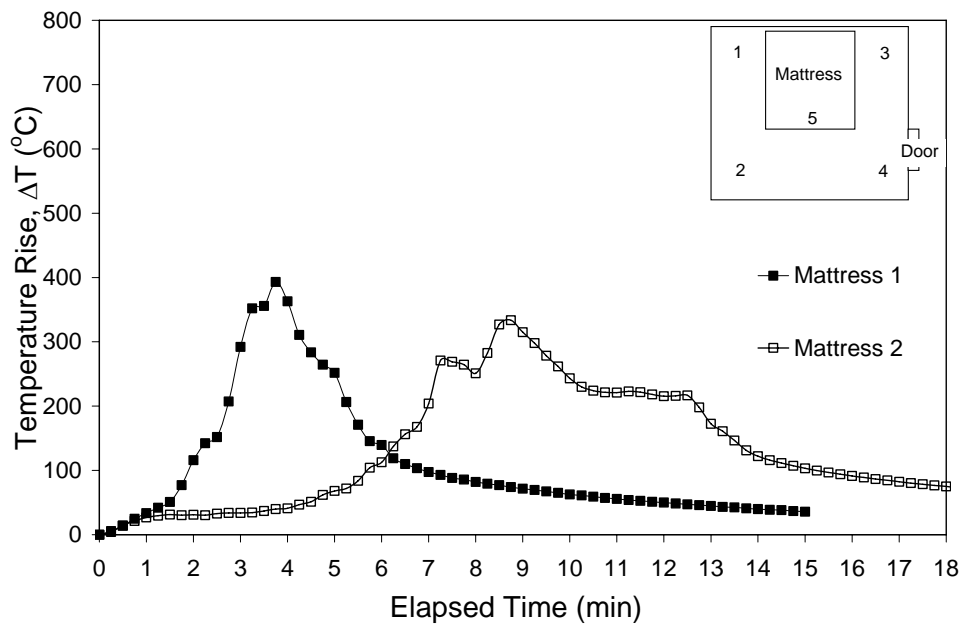


Figure 4 - 34: Comparison of Ceiling Thermocouple Location 4 Results

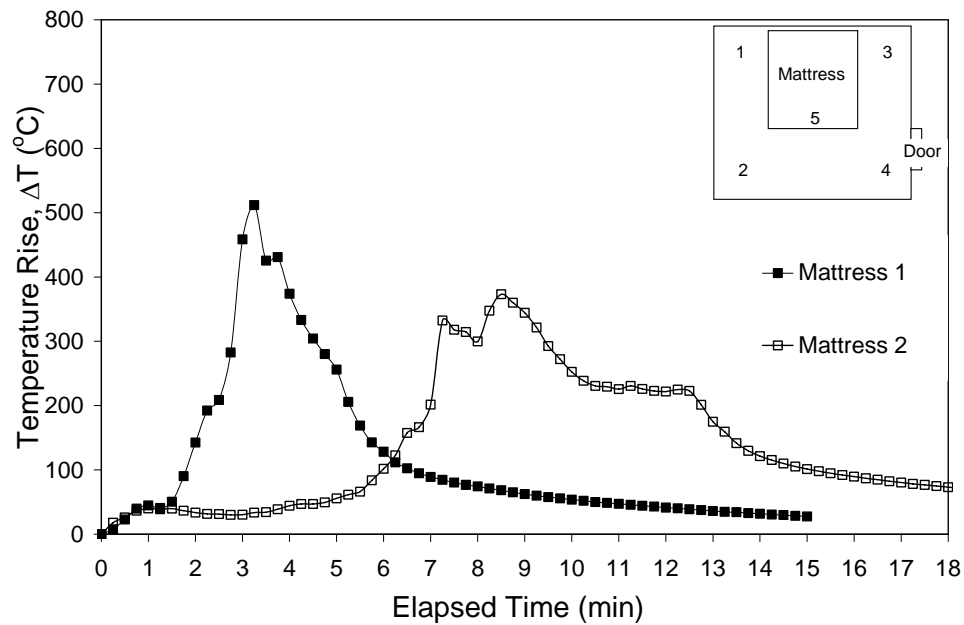


Figure 4 - 35: Comparison of Ceiling Thermocouple Location 5 Results

4.7 Summary

Both sets of fire tests conducted in Edmonton served as useful exercises in conducting field fire testing. Significant results were obtained for these tests which will be used in this work and by future researchers in examining topics such as predictive models and spatial separation guidelines. Field fire testing can be difficult to accomplish, and these tests allowed the Fire Research Group at the University of Saskatchewan to gain valuable experience in conducting this type of testing that will prove useful in future field fire tests.

CHAPTER 5: FIRE GROWTH MODEL AND TEMPERATURE PREDICTIONS COMPARED TO EXPERIMENTAL RESULTS

The focus of this research was to investigate several relatively simple correlations and modeling techniques that predict fire behaviour in enclosures. The development of improved fire modeling techniques will lead engineers to design safer, more efficient and economical fire protection systems and occupancies. There were three major areas of this research project – the investigation of spatial separation requirements, mattress heat release rate modeling techniques and enclosure temperature predictions. This chapter will explain the methods of analysis used in the various areas of the research and will highlight the major results obtained from the different methods. Where possible, the predictions will be compared to experimental results that were obtained.

5.1 Edmonton I Spatial Separation Calculations

As discussed in Chapter 1, fire spread between buildings is a major concern of fire service personnel and occupants during any building fire. Minimum separation distances, also known as spatial separation, between buildings have been included in Canada's National Building Code (NBC) [34] in order to prevent fire spread between buildings in the event of a large scale building fire. This section will discuss radiation heat transfer measurements that were obtained during the Edmonton I set of experiments

with respect to the spatial separation requirements of the NBC. The approach taken for this part of the analysis is similar to one that a fire protection engineer would take for this building. The objective was to calculate what the minimum separation distance between adjacent buildings should be in this case. Also, it was to compare the radiant heat flux that the spatial separation correlations would predict at the location of the heat flux sensors to the heat flux measured during the field fire tests.

5.1.1 Minimum Separation Distance

The front wall of the house burned in the Edmonton I set of experiments, thought to represent a “normal” fire hazard, was 9.1 m wide by 2.7 m high with two windows with dimensions of 1.8 m by 1.2 m and 0.8 m by 1.2 m for the bay window and bedroom window respectively as seen in Figure 5 - 1.



Figure 5 - 1: Edmonton I House Used for Test Burns

For the purposes of spatial separation calculations, the two windows (unprotected openings) are combined into one which is centred on the wall as shown in the following schematic, which also shows the important dimensions of the building. The door has not

been included in this calculation of the unprotected openings as video evidence suggests that the door did not fail during the initial stages of the fire.

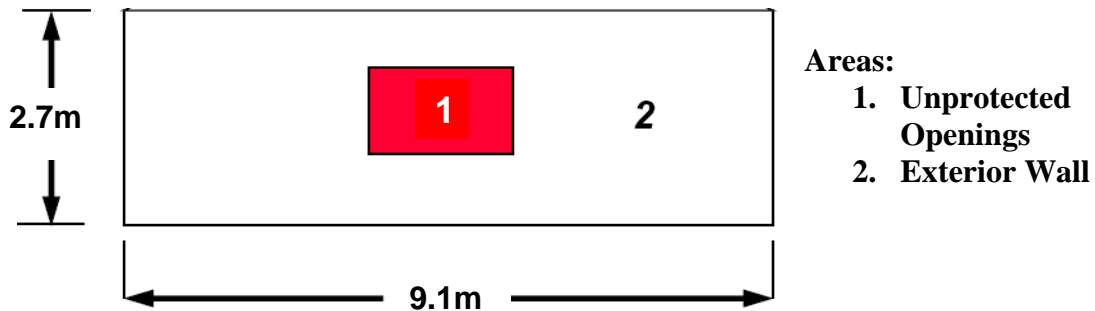


Figure 5 - 2: Schematic of House Used for Spatial Separation Calculations

The two windows seen in Figure 5 - 1 above are combined into Area 1 (unprotected openings) as labelled in Figure 5 - 2, with an area of 3.1 m². The fraction of unprotected openings of the wall were calculated to be 0.13 as seen in Appendix A.

Using the spatial separation correlation and assuming a flame projection of 1.5 m corresponding to a “normal” fire hazard, a minimum separation distance of 3.5 m is calculated for this fraction of unprotected openings. Similarly, a spatial separation distance of 6.3 m is calculated for a “severe” fire hazard, which includes a “severe” flame projection of 2.1 m. A detailed sample calculation of the spatial separation is found in Appendix A.

5.1.2 Spatial Separation Correlations Compared to Experimental Measurements

The experimental heat flux results measured during the Edmonton I full house burn are presented in Figure 5 - 3 below (also presented in Chapter 4.) These experimental

results were measured at a distance of 4 m, and clearly show that the heat fluxes exceed the critical heat flux for ignition of cellulosic materials of 12.5 kW/m^2 after approximately 8 minutes. As shown in Appendix A, a heat flux of 15.4 kW/m^2 is predicted at the sensor location when the spatial separation assumptions for a normal fire hazard are used assuming the front bay window is the only area radiating energy (during the initial portions of the fire, the other unprotected openings were not significantly involved in the fire.) This is relatively close to the peak experimental heat fluxes measured during the Edmonton I full house burn.

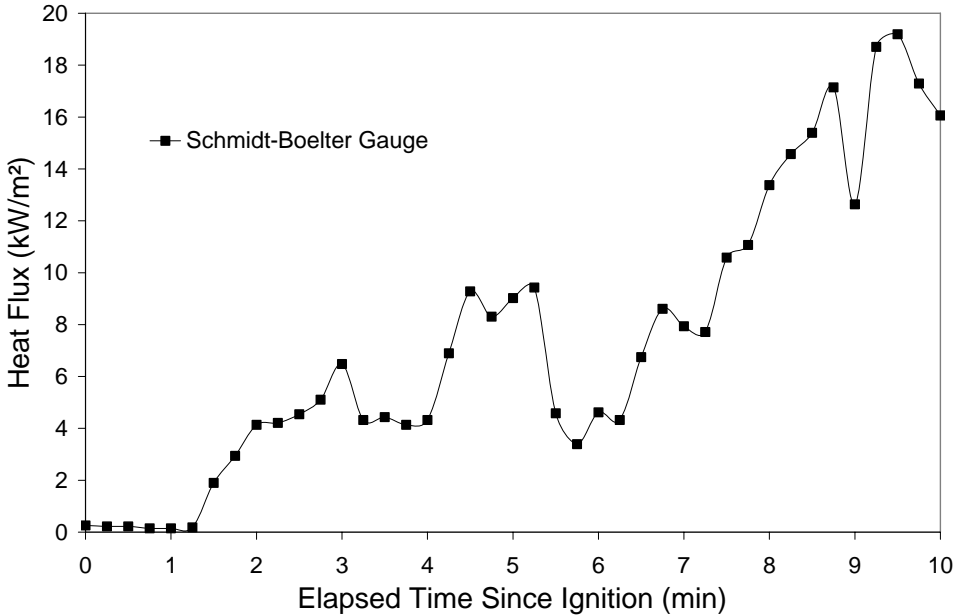


Figure 5 - 3: Edmonton I Radiation Heat Flux Results

5.1.3 Discussion

The method used in the NBC guidelines for spatial separation underestimates the heat fluxes emitted by the burning building during the first 10 min. A peak heat flux of approximately 19 kW/m^2 was measured during experimental testing, however, the spatial separation calculations predict a peak heat flux of approximately 15.4 kW/m^2 for a normal fire hazard. The spatial separation guidelines are based on the initial stages of a fire before the fire spreads from the unprotected openings to the other portions of the building exterior, causing a significant increase in the area emitting thermal radiation and therefore, the radiation view factor and heat transfer to adjacent structures. The assumption is that the fire department will arrive and suppress the fire during the initial stages, before the fire has had a chance to significantly spread to the exterior of the building.

The separation distance required to reduce the heat flux received by a neighbouring structure to 12.5 kW/m^2 was found to be 3.5 m for a normal fire hazard. This value is below the 4.0 m distance between the house and the heat flux gauges. Peak heat fluxes of greater than 12.5 kW/m^2 were measured, likely due to the fact that the view factor from the source to the receiver increases as the fire progresses due to flame spread to other combustible items such as the roof. In addition, the spatial separation method calculates the heat flux to a point opposite the unprotected openings of the burning building in the middle of the wall, versus a point opposite one window as was done in this investigation. It is also difficult to estimate the view factor from the flames to adjacent buildings as the location of the flames changes with time.

5.2 Edmonton II Heat Release Modeling

As discussed in Chapter 1, the heat release rate is the single most important quantity used to describe a fire [6]. With respect to fire protection engineering analyses, modeling the heat release from a fire is extremely important in terms of understanding the fire risk presented in a specific enclosure given a combination of combustible items. The following sections will discuss the heat release rates predicted using the methods presented in Chapter 2, for the Edmonton II set of mattress burns. As discussed in Section 4.5.2, the third mattress test conducted during the Edmonton II set of experiments did not produce a significant temperature increase in the room, and therefore, will largely be ignored in this section. The fire behaviour of the third mattress observed in the Edmonton II set of experiments will be discussed in Section 5.5.2.

The theoretical fire heat release rate was discussed in Section 2.3 and is also shown below in Figure 5 - 4. During this study, only the pre-flashover fire region was investigated, as none of the mattress fires reached the point of flashover.

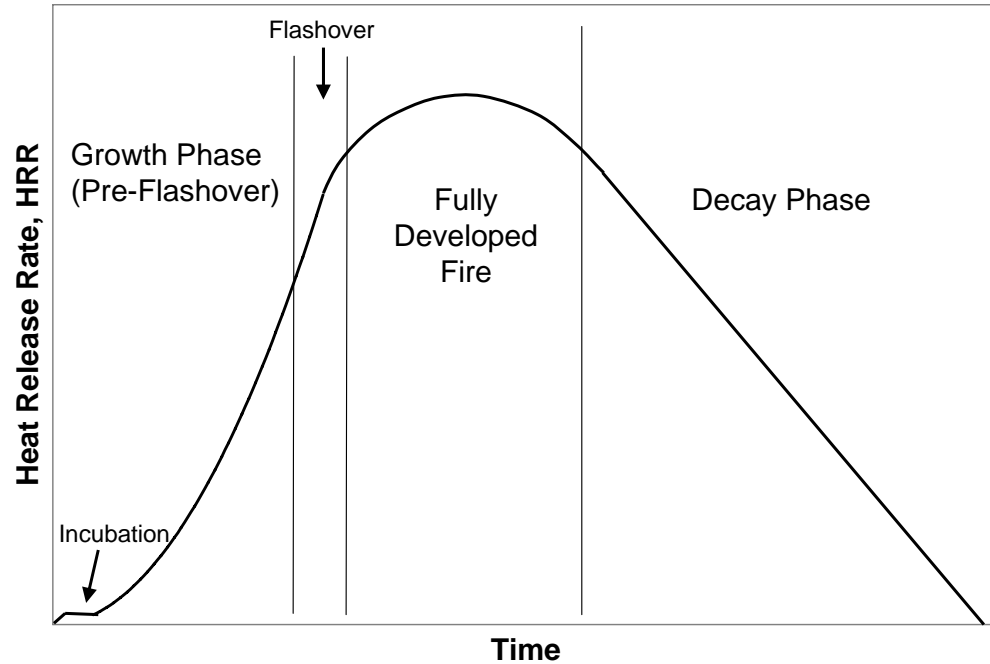


Figure 5 - 4: Theoretical Fire Heat Release Behaviour

For the purposes of this research project, an idealized fire heat release curve is assumed, shown in Figure 5 - 5 below. As mentioned above, the growth phase to flashover will only be considered, and not the fully-developed or decay regions of the curve. As discussed in Section 2.3, many of the growth phase HRR modeling methods do not predict the maximum or peak HRR for the fire. The maximum HRR assumed for the idealized HRR curve shown in Figure 5 - 5 will be investigated in Section 5.6.

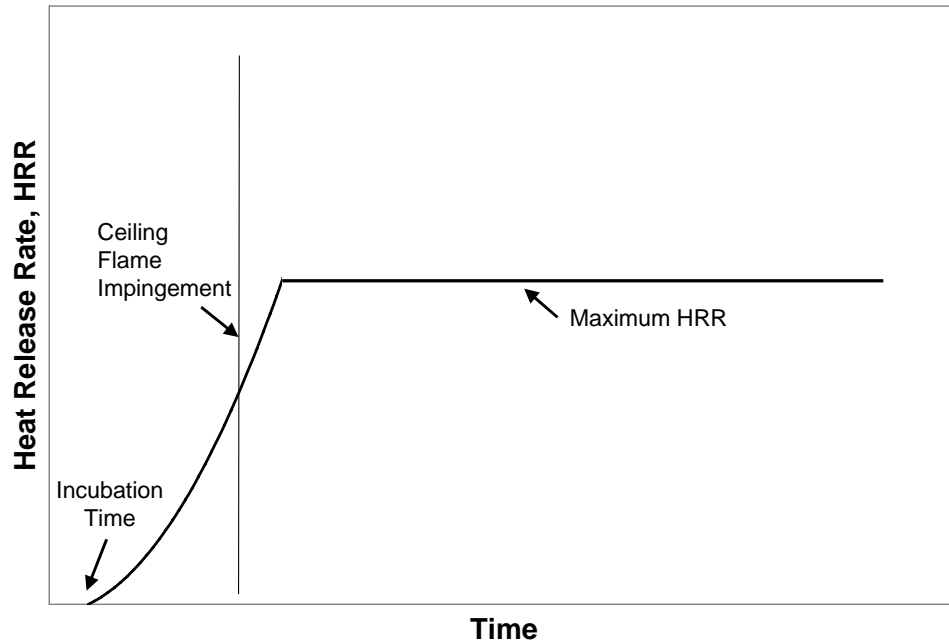


Figure 5 - 5: Idealized Fire Heat Release Rate Curve

Section 5.3 will discuss the incubation times for Mattress 1 and 2, followed by Section 5.4 which will discuss the methods used for the growth phase HRR modeling.

Section 5.5 will then discuss the methods used for predicting the maximum HRR. The idealized HRR curve will then be used to predict the temperatures in the mattress fires, which will then be compared to experimental results in Section 5.7.

5.3 Edmonton II Incubation Time

Determining the incubation time is important in order to identify the beginning of the fire growth phase. Determining the incubation time is accomplished using two methods: examining the temperature measurements and identifying the time associated with significant temperature increase and through experimental observations made during testing. A combination of these two methods was used to determine the incubation

times for Mattress 1 and Mattress 2. The incubation times for Mattress 1 and Mattress 2 were found to be 60 s (1 min) and 300 s (5 min) respectively, and can be seen in Figure 5 - 6, showing the complete data obtained for the Thermocouple 5 location during the Mattress 1 and Mattress 2 tests.

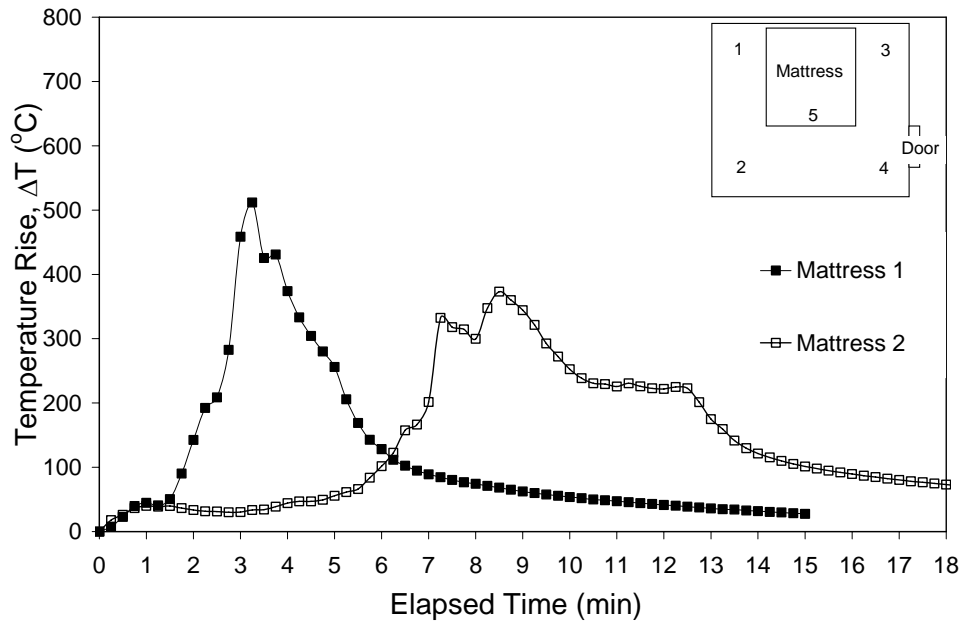


Figure 5 - 6: Comparison of Ceiling Thermocouple Location 5 Results (Complete Results Showing Incubation Phase)

5.4 Edmonton II Fire Growth Phase HRR Modeling

Each of the heat release rate modeling techniques discussed in Chapter 2 is investigated with respect modeling the Edmonton II mattress burns. This section presents each of the methods and discusses their practicality and their relevancy with respect to the Edmonton II mattress field tests. The predicted temperatures, based on using these HRR models combined with the Alpert ceiling temperature correlation will be presented in Section 5.7.1 and compared to experimental results.

5.4.1 Combustion Science Theoretical Rate of Heat Release

The theoretical rate of heat released from any burning fuel is shown below in Equation 5.1. This method is difficult to implement in practice, as it involves several variables which are challenging to obtain through experimentation as discussed in Section 2.3.1.

$$\dot{Q} = \dot{m}x\Delta H_c \quad (5.1)$$

where:

$$\begin{aligned} \dot{Q} &= \text{Heat Release Rate [kW]} \\ \dot{m} &= \text{Rate of Mass Loss [g/s]} \\ x &= \text{Efficiency Factor} \\ \Delta H_c &= \text{Heat of Combustion [kJ/g]}. \end{aligned}$$

Both the mass burning rate (which can be converted to an area burning rate multiplied by the area density) and the combustion efficiency factor in Equation 5.1 are very difficult to estimate from full-scale tests such as the Edmonton II set of experiments.

Measuring the area burning rate is complicated even further for a composite sample, or a thick material, as the burning rate may also become a function of the depth within the sample. The infrared video taken during the second mattress burn test was examined and an area burning rate estimated based on the area of the mattress involved in the fire as a function of time. Measurements of the combustible material density and cone calorimeter measurements of the heat of combustion of the mattress samples were used to estimate a theoretical heat release rate, assuming an efficiency factor of 65 percent, which is typically done in the literature [5]. The combustible material density was estimated on a per unit surface area basis by weighing a composite sample of the mattress (not including the steel springs). The average heat of combustion was measured during cone calorimeter small-scale testing and was found to be 16.4 MJ/kg, which is supported by examining published data [12,27] for similar materials.

Figure 5 - 7 below, shows the heat release predicted using this theoretical approach for the Edmonton II experiment for the second mattress test. A detailed sample calculation using this HRR model is located in Appendix B. The video captured during the first and third mattress burns did not allow predictions of the burning area rate, and therefore heat release rate, to be estimated.

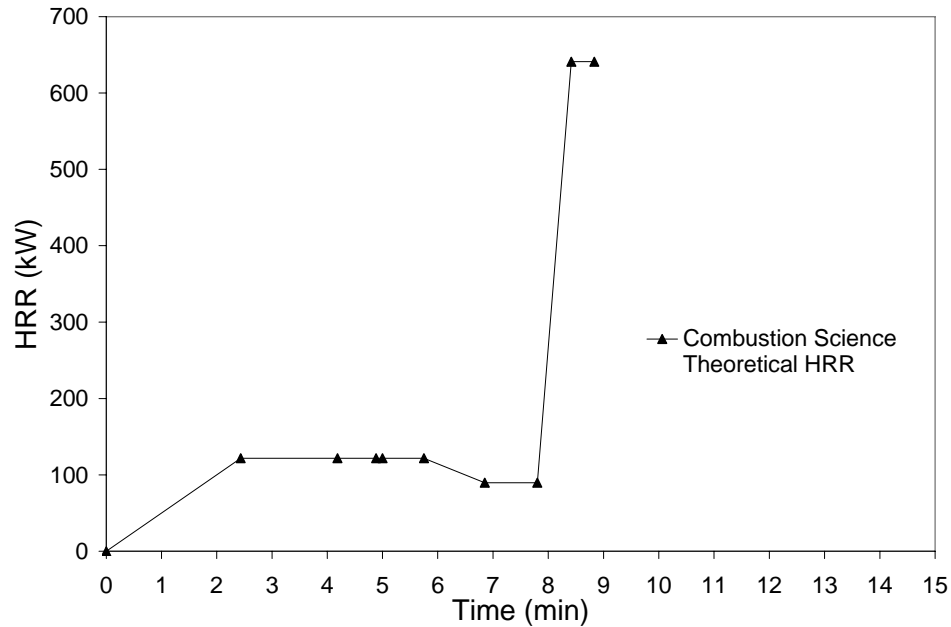


Figure 5 - 7: HRR Predicted Using Combustion Science Theoretical HRR

There are several reasons why the theoretical results are difficult to implement in practice. The most obvious of these are the large assumptions of the combustion efficiency factor and the difficulty in obtaining the area burning rates from the video of the experiments, which were obtained by the inaccurate means of video estimation with only one camera angle in the Edmonton II experiments. Both of these values are approximated, and likely do not reflect the actual quantities with much accuracy. This method of heat release rate prediction requires several variables to be known, which are difficult to experimentally quantify. It does not provide an accurate and user-friendly method of determining the heat release from fires, as video evidence from full-scale tests is required. This method would not allow prediction of the heat release rate without performing experiments to obtain the input quantities, and therefore would not be of much use to engineers in estimating fire behaviour in enclosures where full-scale

experimental information was not available. Therefore, it was determined that this method would not be used in the rest of this project based on practicality issues.

5.4.2 Semi-Universal Heat Release Model

The semi-universal heat release model, presented in Chapter 2, was also investigated as a method of modeling the heat release from the mattress burned in the Edmonton II set of experiments. This modeling technique assumes the heat release rate can be modeled by a piece-wise correlation based on experimentally determined constants and only requires time as an input variable as seen below.

$$\dot{Q} = \left\{ \begin{array}{ll} 10 \exp(0.025t) & 0 \leq t \leq 147.6s \\ 400 \exp(0.01(t-145.6)) & 147.6s \leq t \leq 349s \\ 300 \exp(0.005(t-349)) & 349s \leq t \end{array} \right\} \quad (5.2)$$

where:

$$\begin{aligned} \dot{Q} &= \text{Fire HRR [kW]} \\ t &= \text{Time [s]}. \end{aligned}$$

The predicted heat release rate history obtained from the semi-universal heat release model during the fire growth phase is shown in Figure 5 - 8 below. Appendix B contains a detailed sample calculation of this HRR model.

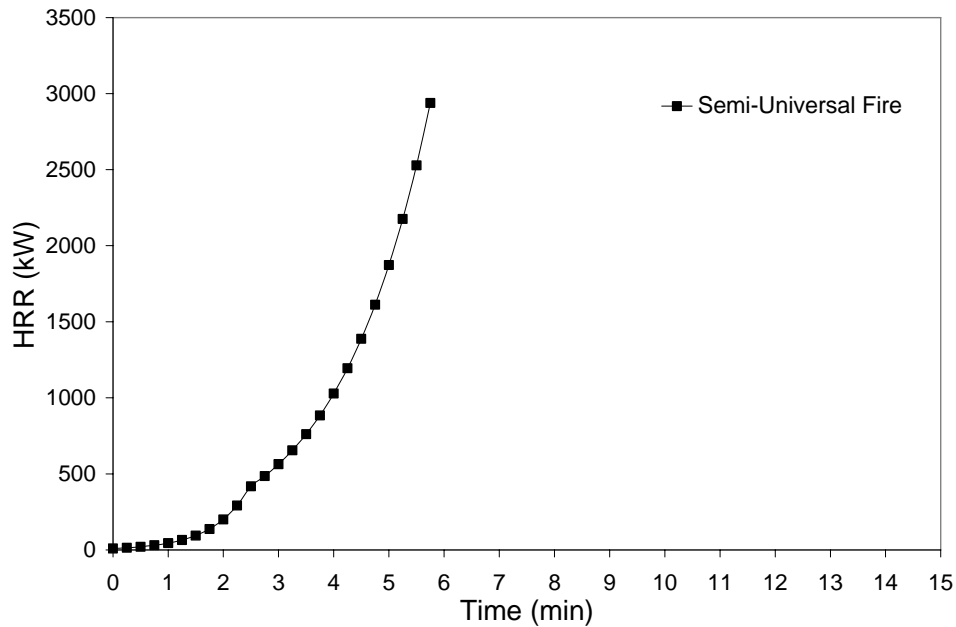


Figure 5 - 8: HRR Predicted Using Semi-Universal Fire

One of the downfalls of the semi-universal HRR model is that it cannot distinguish material or burning characteristic differences between the mattresses burned in this research work. The literature is not detailed in the explanation of the development of the semi-universal heat release model and does not thoroughly explain the development of the model or the situations where it should be applied. While the semi-universal heat release model is very simple and easy to implement, it does not provide an accurate means of predicting the heat released from the mattress experiments, as it does not allow for any type of material property inputs. Therefore, the model is not considered suitable for this research work, as it does not account for differences in the fuel being burned. However, for completeness, the ceiling temperatures at one thermocouple location using the HRR curve in Figure 5 - 8 will be compared to experimental results in Section 5.7.

5.4.3 Generic Upholstered Furniture Fire Growth Model

The upholstered furniture fire growth model proposed by Babrauskas [12] was also investigated. It was assumed during this investigation that a mattress would behave similarly to an upholstered furniture item due to similarities in materials and construction methods. This method is based on experimental evidence and the classification of the burning item by a series of dimensionless factors. The dimensionless factors, shown below with suggested values, account for differences in the upholstered furniture such as the type of fabric, foam, frame and the style of the item. This model assumes a triangular shaped heat release rate curve with the maximum heat release rate and total time calculated from equations 5.3 and 5.4 below.

$$\dot{Q}_{\max} = 210(FF)(PF)(CM)(SF)(FC) \quad (5.3)$$

$$t_b = \frac{(FM)(CM)\Delta h_{c,\text{net}}}{\dot{Q}_{\max}} \quad (5.4)$$

where:

\dot{Q}_{\max} =Maximum Heat Release Rate [kW]

FF =Fabric Factor

PF =Padding Factor

CM =Combustion Mass [kg]

SF =Style Factor

FC =Frame Combustibility Factor.

t_b =Burn Time [s]

FM =Frame Material Factor

ΔH_c =Effective Heat of Combustion [kJ/kg].

The following table shows suggested values for the factors in the above equations presented in the literature [12]. The values used for this analysis are shown in bold.

Table 5 - 1: Suggested Factors for Upholstered Furniture Fire Growth Model [12]

Factor	Description	Suggested Value in Literature*
Fabric (FF)	Thermoplastic Fabrics	1.00
	Cellulosic Fabrics	0.40
	PVC or Polyurethane Film Coverings	0.25
Padding (PF)	Polyurethane Foam or Latex Foam	1.00
	Cotton Batting	0.40
	Neoprene Foam	0.40
	Mixed Materials (i.e. both polyurethane and cotton)	1.00
Frame (FC)	Non-Combustible	1.66
	Melting Plastic	0.58
	Wood	0.30
	Charring Plastic	0.18
Style (SF)	Ornate, Convolute Shapes	1.50
	Intermediate Shapes	1.2-1.3
	Plain, Primarily Rectilinear Construction	1.00
Frame Material (FM)	Metal, Plastic	1.80
	Wood	1.30

*Note: Bold values indicate quantities chosen for this mattress analysis.

The fabric factor was chosen to be 0.40 representing cellulosic fabrics such as cotton.

The padding factor was assumed to be 1.0 representing mixed materials, chosen due to the combination of the covering fabric layer, foam and backing material. The mattress steel spring structure was assumed to be equivalent to the upholstery frame, and therefore a value of 1.66 was used for the frame factor representing a non-combustible frame and 1.80 was used for the frame material factor representing a metal frame material.

As with the theoretical combustion science heat release model, the heat of combustion was obtained from small-scale cone calorimeter tests of the mattress samples. A value of 16.4 MJ/kg, obtained from averaging the five cone calorimeter tests, was used for the heat of combustion in Equation 5.4 above in addition to the bolded factors shown in Table 5 - 1. Figure 5 - 9 below shows the heat release rate using the upholstered furniture fire growth model. A detailed sample calculation can be found in Appendix B.

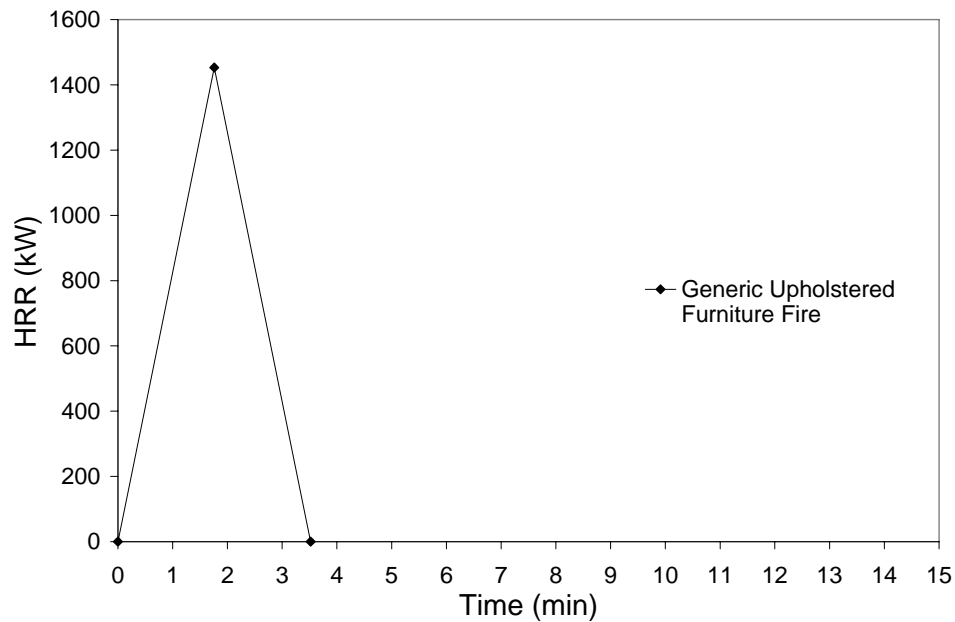


Figure 5 - 9: HRR Predicted Using Generic Upholstered Furniture Fire

The generic upholstered furniture fire modeling technique provides more information than the two techniques previously discussed in this section. The generic upholstered furniture fire growth model predicts a peak HRR of 1453 kW, and a time to peak HRR of 1.8 min.

The upholstered furniture fire growth model is obviously not an exact method of predicting the HRR from an upholstered furniture fire, but instead is only an approximation based on experimental evidence. It was developed as a simplified method of characterizing the fire hazard of upholstered furniture, and not necessarily mattresses. Considering that this model was developed using experimental results from upholstered chairs tested in a furniture calorimeter [12], the experimentally determined factors and constant in Equations 5.3 and 5.4 are likely different for the mattresses tested in this research project, although it is impossible to quantify these differences without further experimental testing. The upholstered furniture fire growth model was not considered an acceptable method of modeling the fire growth of the mattresses burned in the Edmonton II set of experiments. This is due to the ambiguous nature of the input factors which describe the upholstered item, and the fact that it was developed specifically for upholstered furniture and is not valid for a more general fire including other combustible materials. Predicted temperatures using this HRR model will be compared in 5.7, however, for completeness.

5.4.4 t-Squared Heat Release Rate Model

As discussed in Chapter 2, the t-squared fire model is a very popular and well-documented method of predicting the heat released from a fire [29,32]. Using this method, fires involving different materials have been classified into slow, medium, fast and ultra-fast t-squared fires representing increasing fire growth rates. As seen in Table 2-1, traditional mattresses and upholstered furniture typically fall in the medium t-squared classification, whereas polyurethane foam mattresses have been found to behave

as a fast t-squared fire. Following these guidelines, the mattress tests conducted in Edmonton are expected to be either a medium or fast t-squared fire.

The focus of this work is to predict the full-scale behaviour of the mattresses either through simple correlations alone or correlations that involve small-scale data collected using the cone calorimeter. The other methods discussed in the previous sections indicate that other researchers have found it quite difficult to develop upholstered furniture and mattress heat release rate empirical correlations that apply to a broad range of furniture items and predict the full-scale heat release rate with accuracy. The challenges of directly predicting full-scale heat release rates from cone calorimeter small-scale measurements were discussed in Chapter 1.

The approach that was taken for modeling the mattress burns as a t-squared fire was one similar to that of a fire protection engineer, who would not necessarily have any small-scale or full-scale information to use. If a fire protection engineer was to try and model the heat release rate of mattresses, they would consult the suggested t-squared classifications in an engineering handbook such as the SFPE handbook [29].

Considering the Edmonton II set of experiments, this would lead the fire protection engineer to choose a fast t-squared fire for Mattresses 1 and 2 (polyurethane foam) and a medium t-squared fire for Mattress 3 (traditional mattress).

In addition to the suggested t-squared classification of a mattress fire given in the literature, in this study the cone calorimeter was also available to provide small-scale results which could be used as another tool in classifying the mattress fires. The data

obtained during cone calorimeter testing of the mattress samples was discussed in Chapter 3 and is summarized in Table 5 - 2 below. This information shows a definite trend of decreasing fire hazard posed by Mattresses 1, 2 and 3, respectively, when examining all of the following three parameters: peak cone calorimeter HRR, three-minute average HRR and total heat released (THR). This trend is supported by examining the full-scale experimental results presented in Chapter 4, where the maximum temperatures in the room were 580°C for Mattress 1, 413°C for Mattress 2 and approximately 65°C for Mattress 3.

Table 5 - 2: Average Cone Calorimeter Mattress Sample Results (Incident Heat Flux of 35 kW/m²)

Material	Cone Calorimeter Results		
	Peak HRR (kW/m ²)	180s Average HRR (kW/m ²)	THR* @180s (MJ/m ²)
Mattress 1	290.9	190.0	29.1
Mattress 2	225.7	126.4	23.2
Mattress 3	114.6	61.2	11.6

*Note: THR = Total Heat Released

There is a limited amount of full-scale and cone calorimeter mattress test data that has been published in the literature. This is likely due to the fact that little testing has been done specifically on mattresses with the exception of a few major projects such as the NIST/CBHF [27] and the CBUF [42] projects, and the fact that many of the tests that have been done are done for industry groups and are therefore not published in academic sources. Several researchers have published cone calorimeter test data on polyurethane foam (e.g. [12]), however few have done so for mattress composite samples consisting of a top fabric, foam layer and a backing material. An article by Fritz et al. [55], presents test data for a series of cone calorimeter composite sample mattress burns. This

article indicates that the tests (using a similar sample preparation and test method as that described in Chapter 3) give a broad range of HRR and THR results based on both the laboratory doing the testing and on the type of materials used in the mattress as seen in Table 5 - 3 below.

Table 5 - 3: Typical Cone Calorimeter Mattress & Polyurethane Foam Results

Sample Material*	Minimum			Maximum			Source
	Pk HRR (kW/m ²)	180s Avg HRR (kW/m ²)	THR (MJ/m ²)	Pk HRR (kW/m ²)	180s Avg HRR (kW/m ²)	THR (MJ/m ²)	
Mattress Composite Normal	216	116	22.7	328	172	33.9	[55]
PU California	n/a	170	n/a	n/a	194	n/a	[12]
117 PU	n/a	n/a	n/a	n/a	162	n/a	[12]

*Note: PU = Polyurethane Foam

An extensive literature search indicated a lack of cone calorimeter and full-scale mattress burn information. Curves of both the small-scale mattress composite cone calorimeter results and the full-scale test results of the same mattress are not readily available. Besides the guidelines printed in engineering handbooks, Table 5 - 4 presents data from several researchers that have found that polyurethane foam mattresses behave like fast t-squared fires.

Table 5 - 4: t-Squared Fire Mattress Classification Based on the Literature

Description	Source	t-Squared Fire Classification
Traditional Mattress	[29]	Medium
Polyurethane Foam Mattress	[29]	Fast
Polyurethane Foam Mattress (Centre Burn)	[64]	Fast to Ultra-Fast
Polyurethane Foam Mattress (Corner Burn)	[65]	Fast
Polyurethane Foam Sofa	[32]	Fast

Figure 5 - 10 below shows some data obtained by NIST during two full-scale mattress burns [64,65] (shown in Table 5 - 4). The centre burn figure was obtained during a full-scale fire test in a furniture calorimeter where the mattress was ignited in the centre, and demonstrates fast to ultra-fast fire growth behaviour because the flame is able to spread in all directions. The corner burn data was obtained during a test with the mattress ignited at one of the corners, and indicates a slower fire growth behaviour (fast t-squared) as the flame spread was limited to spread in only two directions. Considering that the Edmonton II mattresses were all started on the end, they would be expected to behave more like the NIST corner burn test than the NIST centre burn test and would likely demonstrate more of a fast fire growth than an ultra fast growth.

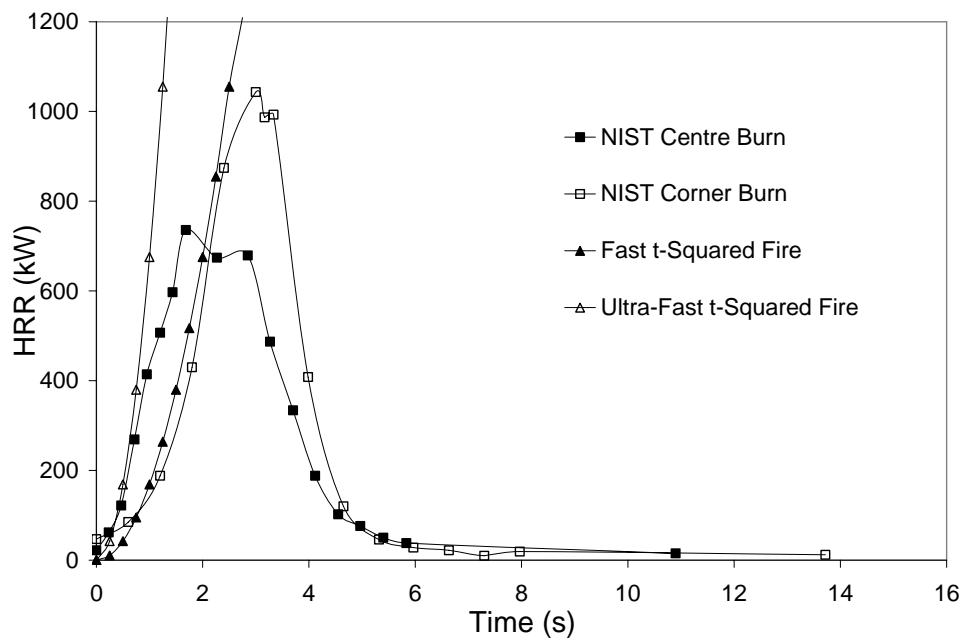


Figure 5 - 10: NIST Full-Scale Mattress Burns [64;65]

Considering all of the information contained in Table 5 - 2, Table 5 - 3 and Table 5 - 4, it was estimated that the first Edmonton II mattress would behave like a fast t-squared

fire. This is largely based on the fact that the Mattress 1 small-scale cone calorimeter results approximately fall in the average range of published small-scale results for similar polyurethane foam mattress materials and it is known that most polyurethane foam mattresses behave like fast t-squared fires in full-scale tests. It was also estimated that Mattress 2 would fall between a medium and a fast t-squared fire. A relative ranking of the fire hazard posed by the three mattresses (shown in Table 5 - 2) qualitatively shows that Mattress 2 has a significantly lower fire hazard than Mattress 1 (and Mattress 1 should behave like a fast t-squared fire.)

Finally, it was estimated that Mattress 3 should behave like a medium or slow t-squared fire. Unfortunately, as discussed in Chapter 4, no significant temperature data was obtained for the third mattress. This is consistent with the thought that the third mattress was expected to be non-propagating as will be shown in Section 5.5.2. Since there is no significant temperature increases to compare the ceiling temperature predictions with, for Mattress 3, this chapter will focus on Mattresses 1 and 2.

While the other HRR models were rejected earlier in this chapter for reasons of practicality, the HRR results predicted using the four modeling techniques presented are compared in Figure 5 - 11. As described above, the t-squared fire modeling technique will be used for the remainder of the analysis. Figure 5 - 11 indicates that a fast t-squared fire falls between the semi-universal HRR model and the generic upholstered furniture fire growth model, further supporting the choice of this model. A detailed sample calculation of the t-squared HRR model can be found in Appendix B.

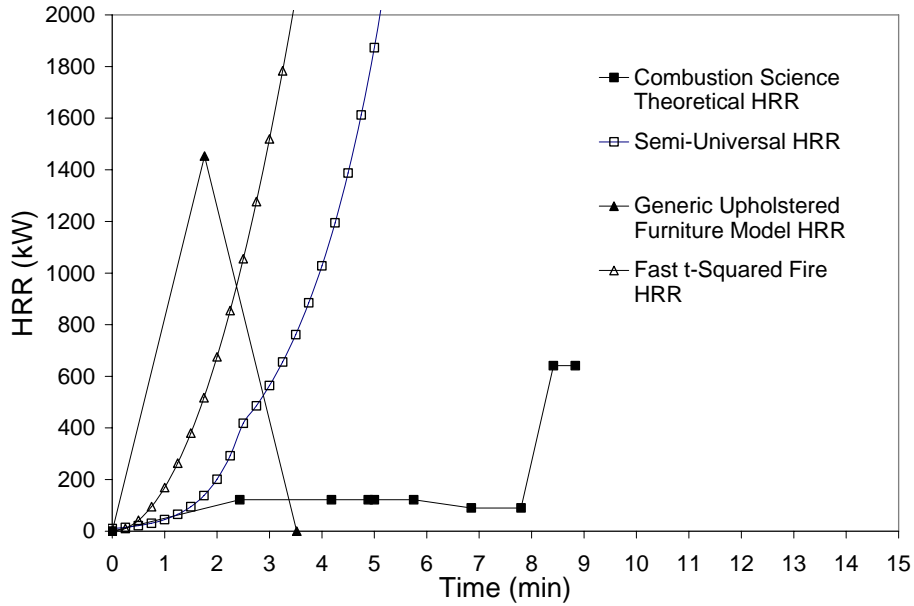


Figure 5 - 11: Comparison of Mattress HRR Modeling Techniques

5.4.5 Fuel/Ventilation-Controlled Fire

The transition from fuel to ventilation controlled fire behaviour can significantly affect the fire growth and burning characteristics of an enclosure fire. This transition can limit the HRR of the fire, as the fire becomes starved of oxygen. A simple correlation has been developed for predicting the HRR required for this transition.

$$\begin{aligned} \dot{Q}_{vc} &= 3000 \cdot \dot{m}_a \quad [\text{kW}] \\ \dot{m}_a &= 0.5A_o H^{1/2} \quad [\text{kg/s}] \end{aligned} \quad (5.5)$$

where:

$$\begin{aligned} \dot{Q}_{vc} &= \text{HRR Required for Onset of Ventilation-Controlled Fire [kW]} \\ \dot{m}_a &= \text{Mass Flowrate of Air [kg/s]} \\ A_o &= \text{Area of Ventilation Openings [m}^2\text{]} \\ H_o &= \text{Height of Ventilation Openings [m].} \end{aligned}$$

The correlation for predicting the transition from fuel to ventilation-controlled behaviour uses only the geometric properties of the openings, as this governs the amount of oxygen the enclosure fire will receive. The maximum HRR required for transition to ventilation-controlled behaviour is predicted to be 3373 kW for the Edmonton II enclosure used for the mattress burns, as shown in Appendix B. This transition HRR, which is significantly higher than the expected heat released from the mattress fires (and is higher than that required for flashover in the enclosure as explained in Section 5.6) indicates that all three mattress fires will certainly be fuel-controlled and will not be oxygen-deprived.

5.5 Edmonton II Maximum HRR Modeling

The ability to predict the point of flashover is extremely important as it marks the transition between localized burning and a fully-developed enclosure fire where all combustible items are involved. The HRR required for flashover will be estimated and the maximum fire HRR will be investigated.

5.5.1 Edmonton II McCaffrey Prediction of Flashover

Using the empirical correlation presented in Chapter 2, also shown below as Equation 5.6, the heat release rate required to produce flashover can be predicted. The point of flashover for an enclosure is easily detectable by visual observation, or by other methods such as a 550°C to 600°C temperature rise at the ceiling [5] as discussed in Section 1.4.2. In a small room such as the one used for the Edmonton II set of experiments, the point of flashover is indicated by flames engulfing the entire room (as the hot gas layer is

ignited) and flames typically project out from the openings. Visual observations of the Edmonton II set of experiments indicate that flashover did not occur for any of the three mattress tests.

$$\dot{Q}_{FO} = 610(h_k A_T A_o H^{1/2})^{1/2} \quad (5.6)$$

where:

\dot{Q}_{FO} = HRR Required for Flashover [kW]

h_k = Enclosure Conductance (defined below) [kW/m²/K]

A_T = Internal Enclosure Area Excluding Openings [m²]

A_o = Area of Ventilation Openings [m²]

H_o = Height of Ventilation Opening [m].

The heat release rate required for flashover, using the above correlation, was calculated to be 1341 kW/m², as shown in Appendix B. This value was determined using the geometric properties of the enclosure, assuming that flashover would occur at a time greater than the thermal penetration time, t_p (calculated to be 161 sec after the incubation period as seen in Appendix B) and assuming that all walls were constructed of 0.016 m (5/8 in.) thick drywall with a thermal conductivity of 0.48×10^{-3} kW/m⁰·C. The time to reach flashover for a fast t-squared fire is calculated to be approximately 170 s after the incubation time (using the method shown in Appendix B), which supports the assumption that flashover will occur at a time greater than the thermal penetration time.

5.5.2 NIST/CBHF Upholstered Furniture and Mattress HRR Correlation

There has been a considerable amount of research aimed at trying to characterize the full-scale burning behaviour of upholstered furniture and mattresses by NIST and the

California Bureau of Home Furnishings (CBHF). The findings of the NIST/CBHF research relevant to this project, presented in Chapter 2 and also below in Figure 5 - 12, are concerned with trying to predict full-scale HRR behaviour from cone calorimeter results of upholstered furniture and have been published by several authors (e.g. [12,27,48].) The NIST/CBHF research work demonstrates that the cone calorimeter can successfully be used as a tool for determining the degree of full-scale fire hazard of upholstered furniture.

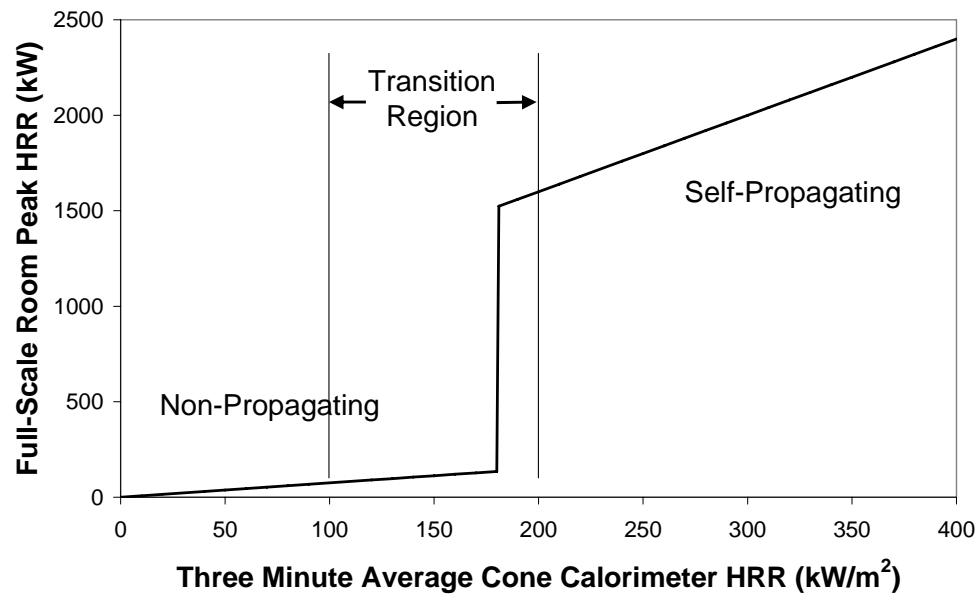


Figure 5 - 12: NIST/CBHF Upholstered Furniture and Mattress HRR Correlation

The NIST/CBHF findings indicate that materials producing a cone calorimeter three-minute average HRR, in tests with an incident heat flux of 35 kW/m², less than approximately 100-150 kW/m² would produce a non-propagating full-scale fire. Conversely, materials giving a cone calorimeter three-minute average HRR greater than approximately 150-200 kW/m² would produce a self-propagating full-scale fire. The behaviour of the third Edmonton II mattress test, where there was no significant

temperature increase in the room, can be explained by looking at the cone calorimeter results of the mattress samples as presented in Chapter 3, also shown in Table 5 - 2.

The third mattress falls in the non-propagating fire scenario. The Mattress 3 180 s average cone calorimeter HRR was 61.2 kW/m^2 , which is less than the 100 kW/m^2 threshold for a self-propagating fire. As a result, Mattress 3 would not be expected to release significant energy resulting in a low temperature rise at the ceiling. This predicted behaviour is supported by examining the video of the third mattress burn. The video indicates that the fire does not significantly grow in time, but instead, is subject to smouldering combustion, indicative of a non-propagating fire. The first and second mattresses, however, did exhibit self-propagating behaviour in the full-scale experimental tests. Mattress 1 is very close to the lower boundary of the self-propagating fire behaviour presented by the NIST/CBHF findings; although these findings indicate that there is a large transition region corresponding to cone calorimeter HRR values of $100\text{-}200 \text{ kW/m}^2$ where the non-propagating/self-propagating behaviour cannot be accurately predicted.

Using the NIST/CBHF correlations presented in Chapter 2, also shown below in Equation 5.5, combined with the average hot gas temperature correlation, the peak experimental HRR was predicted for the Edmonton II set of experiments for all three mattress burn tests. These results are summarized in Table 5 - 5 below. Mattresses 1 and 2 both fall into the transition region, where the full-scale behaviour was found to be either non-propagating or self-propagating. The peak HRR was predicted for both regimes as seen in the table. A detailed sample calculation can be found in Appendix B.

$$\dot{Q}_{FullScalePk} = \begin{cases} 0.75\dot{Q}_{3MinCone}'' & \text{Non-Propagating} \\ 4\dot{Q}_{3MinCone}'' + 800 & \text{Self-Propagating} \end{cases} \quad (5.7)$$

where:

$\dot{Q}_{FullScalePk}$ = Full-Scale Peak Heat Release Rate [kW]

$\dot{Q}_{3MinCone}''$ = 180 second Average Cone Calorimeter HRR [kW/m²].

Table 5 - 5: NIST/CBHF Peak HRR Predictions

Material	NIST/CBHF Predicted Regime	Predicted Full-Scale Pk HRR (kW)	
		Non-Propagating	Propagating
Matt 1	Transition	142.5	1560.0
Matt 2	Transition	94.8	1305.5
Matt 3	Non-Propagating	45.9	n/a

One of the downfalls of this method is that it does not allow an engineer to estimate the HRR-time history or the time to peak heat release rate, which would be important for estimating fire detector response times as well as rates of fire spread within an enclosure. The predicted peak HRR, however, can be combined with another method such as a t-squared fire HRR growth curve to develop a complete HRR history. Another downfall is the large transition region in the correlation between three-minute average cone calorimeter HRR of approximately 100 to 200 kW/m² (corresponding to the results from Mattress 1 and 2). If full-scale experiments were not performed on Mattresses 1 and 2 an engineer would draw on their experience and judgement and would predict that they would be propagating fires, considering they were polyurethane foam. An engineer would ultimately adopt the worst-case scenario and assume that they were self-propagating fires, which would lead them to use the predicted HRR for self-propagating fires shown in Table 5 - 5 above.

This method of predicting full-scale fire behaviour definitely shows some promise, especially for predicting peak heat release rate. Unfortunately, on its own, it does not give any indication as to the time to peak heat release rate or the heat release rate-time history, and therefore is limited in its usefulness. Combined with another fire growth phase HRR model, however, an entire HRR-time history can be obtained. It provides a good correlation for predicting non-propagating versus self-propagating full-scale fire behaviour based on cone calorimeter results. This correlation is supported by qualitative video evidence from the experiments in that Mattress 3, falling in the non-propagating fire scenario, was in fact a non-propagating fire.

5.6 Summary of Edmonton II Mattress HRR Model

As discussed in Section 5.4, the combustion science theoretical HRR prediction, the semi-universal HRR model and the generic upholstered furniture fire growth HRR can be eliminated based on their practicality. However, temperatures predicted using the semi-universal HRR and generic upholstered furniture fire growth models will be compared in Section 5.7.2. The t-squared fire model is the most versatile and popular of these simplified HRR modeling techniques and was chosen for this analysis.

The HRR required for flashover predicted by the McCaffrey correlation (1341 kW) and the maximum HRR predicted using the NIST/CBHF correlation (1560 kW for Mattress 1 and 1306 kW for Mattress 2) are close to one another. The NIST/CBHF correlation will be used to approximate the maximum bound for the t-squared fire growth HRR model as it allows for differences between the fuel being burned, based on cone calorimeter results. The McCaffrey flashover correlation is a more general approximation and makes assumptions based on the geometry and wall material properties. In addition, the walls were conservatively assumed to be constructed entirely of drywall for the McCaffrey flashover HRR calculation, whereas in the actual Edmonton II enclosure, two of the walls were constructed of insulated metal. The thermal conductivity of the metal would be greater than that of the drywall, and therefore would require a greater fire HRR for flashover as there would have been greater heat losses through the walls.

The predicted Mattress 1 and Mattress 2 HRR histories are shown below in Figure 5 - 13 and Figure 5 - 14. These predictions assume a fast and medium to fast t-squared fire for Mattresses 1 and 2, respectively, as discussed in Section 5.4.4 on the t-squared fire growth model. Figure 5 - 13 and Figure 5 - 14 also assume that the fire will grow until it reaches a maximum heat release rate predicted by the NIST/CBHF correlation, which was found to be 1560 kW and 1306 kW for Mattress 1 and 2, respectively. This research project did not focus on the fire decay stage or the fully-developed fire stage, and conservatively assumes that the fire will reach the maximum HRR and remain constant until the fuel is consumed.

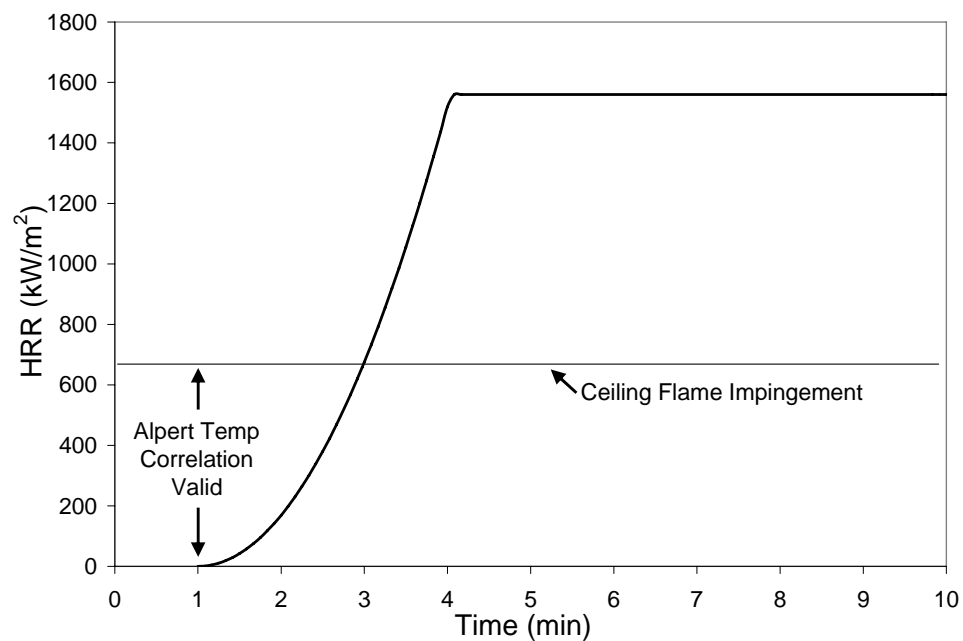


Figure 5 - 13: Mattress 1 Predicted HRR Showing Point of Ceiling Flame Impingement and Temperature Correlations Used in Analysis

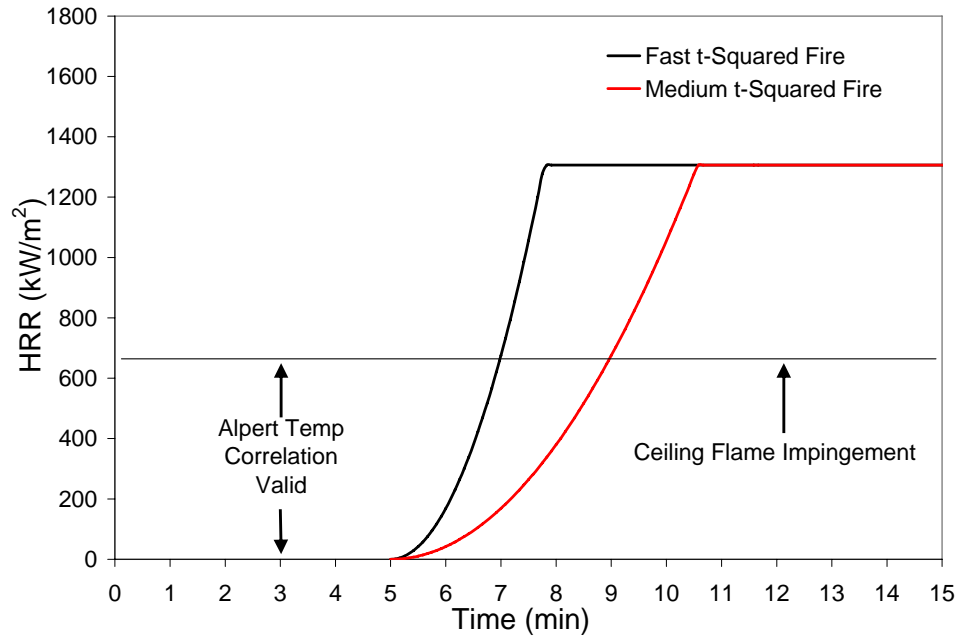


Figure 5 - 14: Mattress 2 Predicted HRR Showing Point of Ceiling Flame Impingement and Temperature Correlations Used in Analysis

5.7 Edmonton II Temperature Predictions

As discussed in Chapter 2, the ability of engineers to predict enclosure temperatures during a fire is important for several reasons including the analysis associated with fire sprinkler activation time and the effect of the fire on building structural components.

The Alpert ceiling temperature correlations and the hot gas layer temperature correlation, which were used in this work, are very common and well accepted correlations that are often included in fire protection engineering handbooks [29,38].

While it is clear that the fire HRR is the most important variable, the HRR could not be measured in the Edmonton II experiments. Therefore, temperature predictions using the HRR models discussed in Section 5.4, and specifically the t-squared HRR model were compared to experimental results in order to assess the various HRR models. For

purposes of completeness, temperature predictions using the HRR curves generated by the semi-infinite and the generic upholstered furniture fire growth model, which were rejected primarily for reasons of practicality, are also presented and compared to experimental results.

5.7.1 Comparison of Predicted Ceiling Temperatures and Experimental Results

The Alpert ceiling temperature correlation, presented in Chapter 2, which is well accepted as a reasonable approximation of enclosure temperature during early fire stages [39], is assumed to be valid during the early stages of the fire. As discussed in Chapter 2, the Alpert ceiling temperature correlations are known to be valid only when there is not a “significant” build-up of hot gases at the ceiling. It is difficult to pinpoint an exact point where the hot gas layer has become significant; however, video evidence from the Edmonton II set of experiments indicates that there is not a significant build-up of hot gases at the point of flame impingement at the ceiling. For the purposes of this research work, it is assumed that the Alpert ceiling temperature correlations are therefore valid until the flames impinge on the ceiling of the enclosure, shown in the idealized HRR curve in Figure 5 - 5. The flame height can be estimated by the simple correlations presented in Chapter 2, also seen below.

$$H_f(t) = 0.1743(k\dot{Q}(t))^{0.4} \quad (5.8)$$

where:

H_f = Flame Height [m]

k = Configuration Factor (Previously Defined)

\dot{Q} = Fire HRR [kW].

This correlation can be used to estimate the heat release rate required for flame impingement on the ceiling, and therefore determining the length of time that the Alpert ceiling temperature correlations are valid. Equation 5.8 above, combined with the geometry of the enclosure, indicates that flames will impinge on the enclosure ceiling for a fire heat release rate of 658 kW, as shown in Appendix B. Therefore, the Alpert ceiling temperature correlation is assumed to be valid until a HRR of 658 kW is reached. For heat release rates larger than 658 kW, the average hot gas temperature correlation presented in Chapter 2 will be used for comparison to experimental results.

Figure 5 - 16 to Figure 5 - 20, which follow, show the ceiling temperatures for the five Edmonton II thermocouple locations (as described in Chapter 4) predicted using a fast and medium to fast t-squared fire for Mattresses 1 and 2, respectively, until flame impingement. Using a t-squared HRR model, the HRR required for flame impingement on the ceiling corresponds to predicted ceiling temperatures of 161°C, 98°C, 219°C, 103°C and 193°C for thermocouple locations 1 through 5, respectively, as seen below. A sample calculation of predicted temperature using the Alpert ceiling temperature correlation can be found in Appendix C.

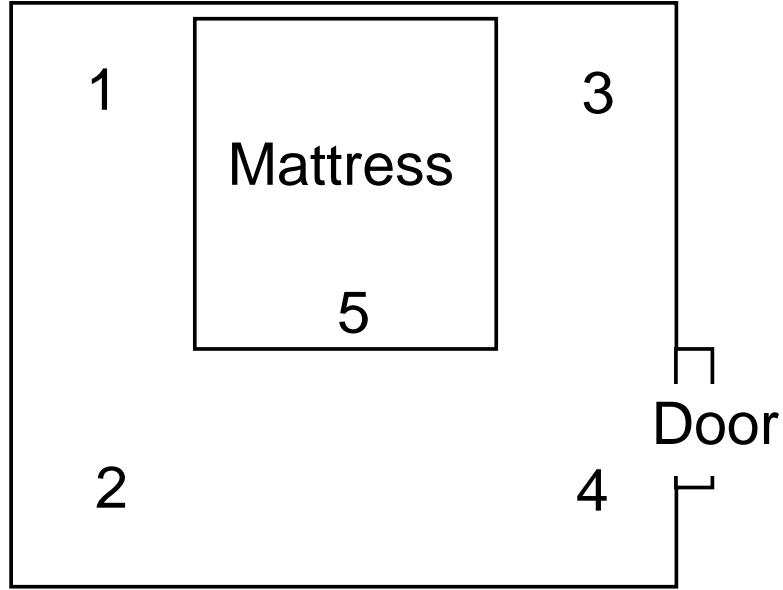


Figure 5 - 15: Schematic of Enclosure Showing Thermocouple Locations 1 to 5 Relative to Mattress

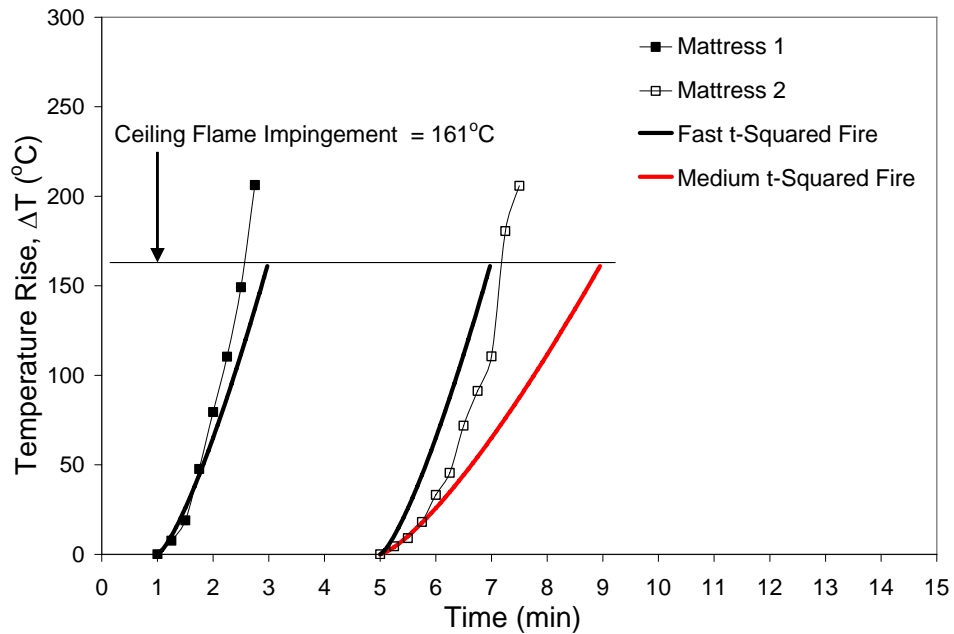


Figure 5 - 16: Thermocouple 1 Location Predicted and Measured Temperatures

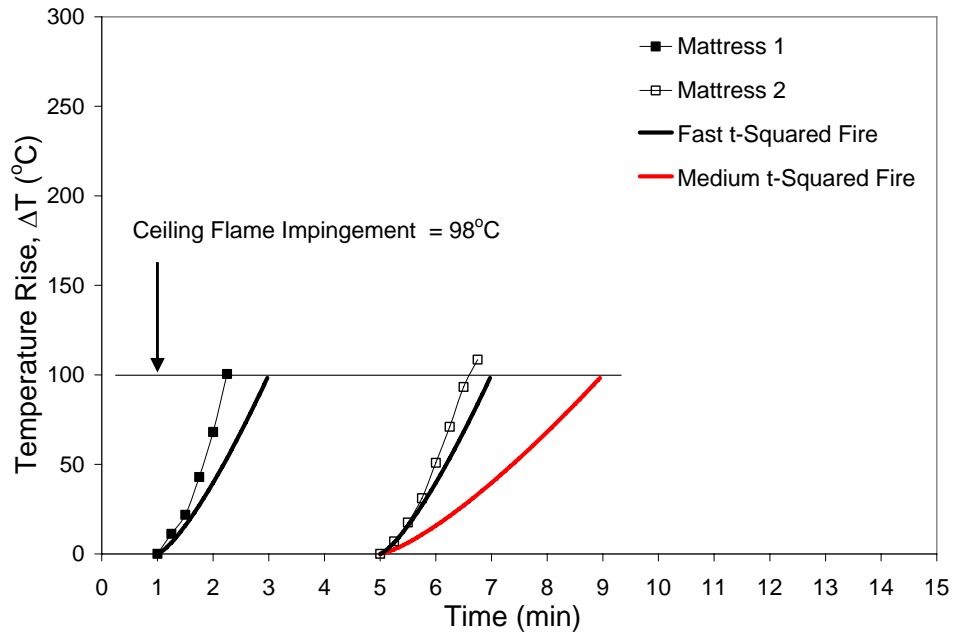


Figure 5 - 17: Thermocouple 2 Location Predicted and Measured Temperatures

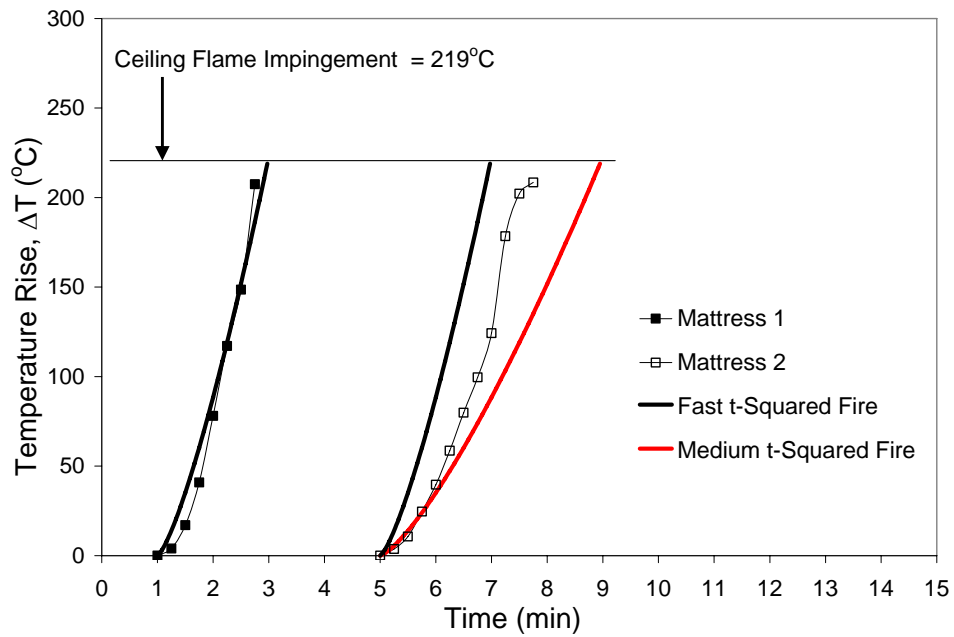


Figure 5 - 18: Thermocouple 3 Location Predicted and Measured Temperatures

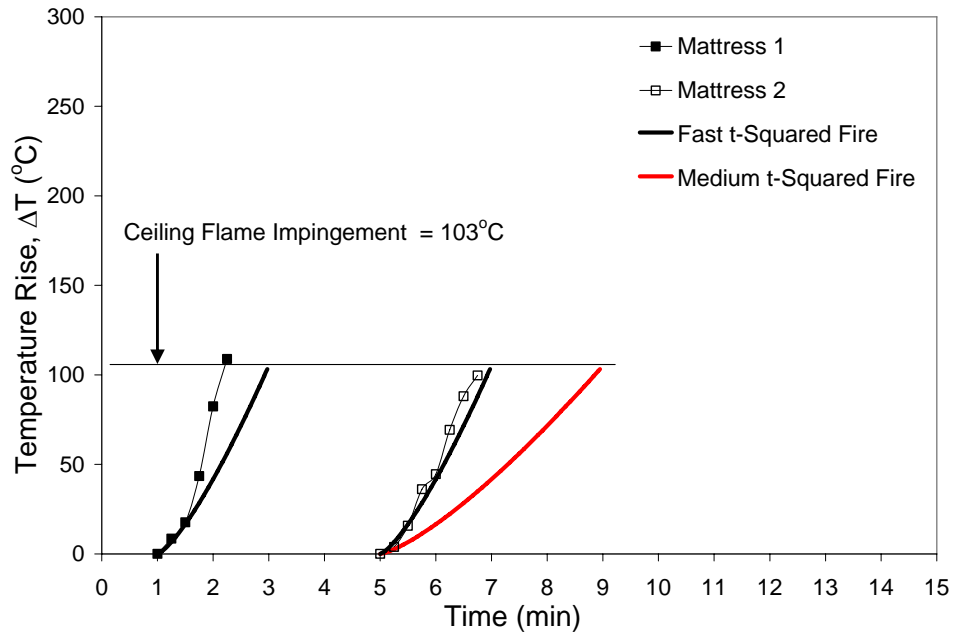


Figure 5 - 19: Thermocouple 4 Location Predicted and Measured Temperatures

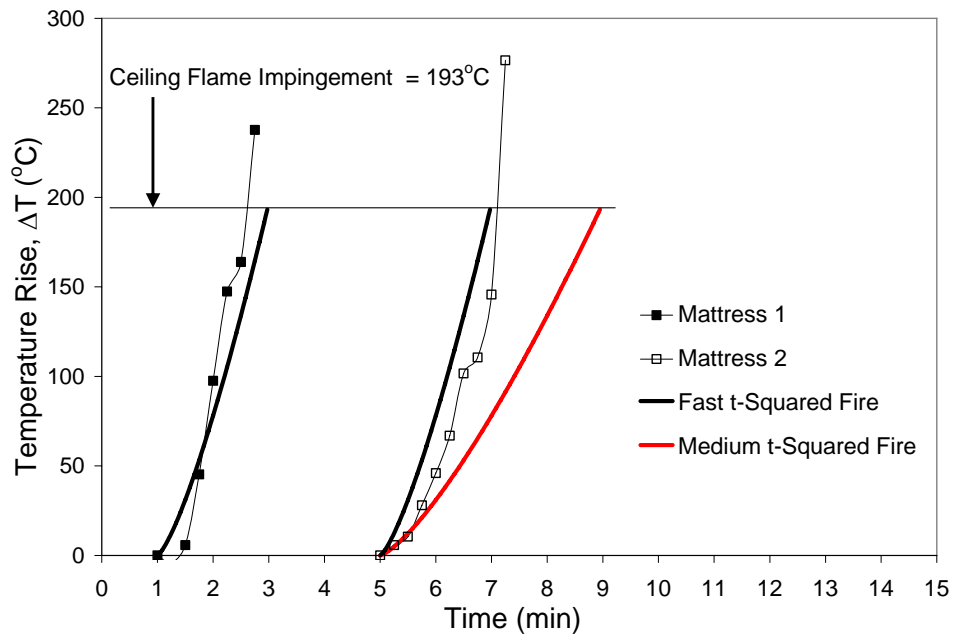


Figure 5 - 20: Thermocouple 5 Location Predicted and Measured Temperatures

The predicted temperatures were reasonably close, within the context of fire temperature modeling, to the experimentally measured temperatures at all five thermocouple locations for Mattress 1, as the temperatures were within approximately 30% for the majority of the tests. The reasonable agreement supports the assumption of a fast t-squared fire. The above figures also indicate that the predicted temperatures for Mattress 2 are reasonably close to those measured in the Edmonton II set of experiments, as they are also within approximately 30% for the majority of the tests. A fast t-squared fire seems to characterize the Mattress 2 experiment better than a medium t-squared fire.

During the fire growth phase to ceiling flame impingement, one of the sources of difference between predicted and experimental results is the assumption that the fire was centred at the centre of the mattress and the radial distance between the fire centre axis and the ceiling thermocouples did not vary with time. During the duration of the fire tests, the flames spread from the foot of the bed, where it was started, to the head of the bed, causing the radial distance between the fire centre and ceiling thermocouples to be a function of time. Figure 5 - 21 shows the sensitivity of predicted temperature to the radial distance from the fire centre at the ceiling location of Thermocouple 1 during the Mattress 1 burn.

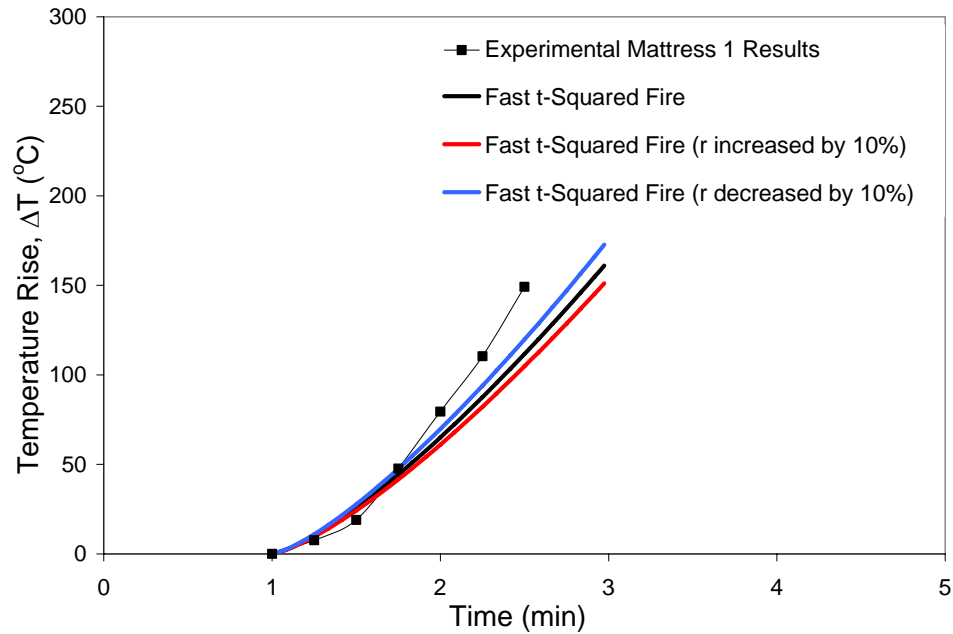


Figure 5 - 21: Model Sensitivity to Radial Distance, R, During Fire Growth to Flame Impingement

As seen in the above figure, when the radial distance is varied by 20% (from -10% to +10%), the predicted temperatures change by 14.4% at the point of ceiling flame impingement. Therefore, it is evident that the Alpert ceiling temperature correlation is not highly sensitive to the radial distance, supporting the assumption of a constant radial distance throughout the tests.

Figure 5 - 22 shows the sensitivity of predicted temperature to the HRR during the Mattress 1 burn.

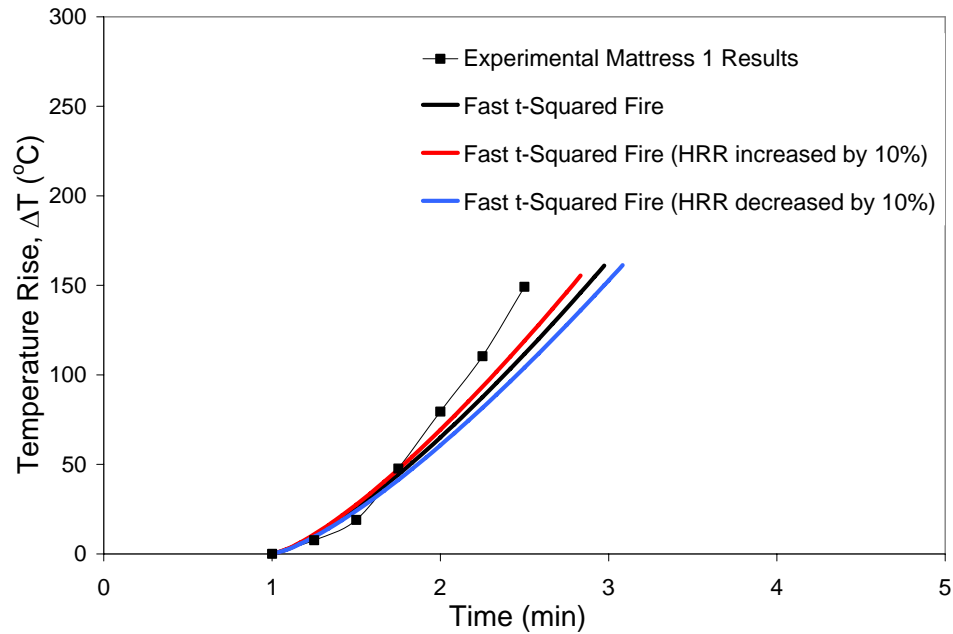


Figure 5 - 22: Model Sensitivity to Fire HRR, Q, During Fire Growth to Flame Impingement

Figure 5 - 22 shows that when the HRR value is changed by 20% (-10% to +10%), the predicted temperatures only change by approximately 14.3% at approximately 2.8 min. Therefore, it is evident that the Alpert ceiling temperature correlation is not highly sensitive to the HRR either, demonstrating that extremely high accuracy in the HRR modeling may not be required.

Figure 5 - 23 shows the ceiling temperatures predicted using the Alpert ceiling temperature correlation combined with the HRR predicted using the generic upholstered furniture model and the semi-universal HRR model for one thermocouple location.

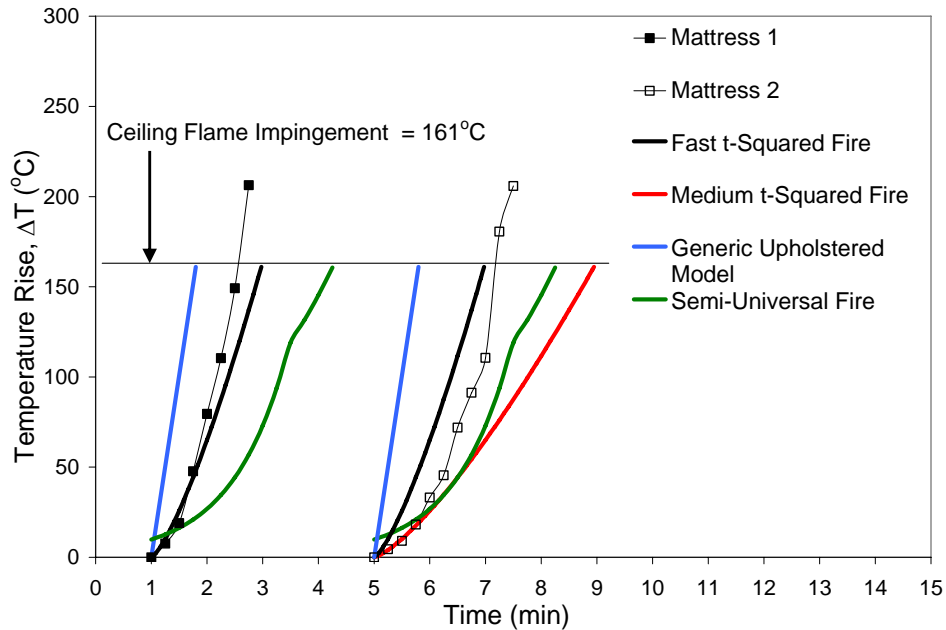


Figure 5 - 23: Comparison of Other HRR Models Combined With the Alpert Ceiling Temperature Correlation to Experimental Results for Thermocouple 1

Figure 5 - 23 shows typical results for one of the ceiling thermocouple locations. Overall, the t-squared HRR model, combined with the Alpert ceiling temperature correlation, does the best job of predicting the experimental results. The generic upholstered furniture model combined with the Alpert ceiling temperature correlation overestimates the temperatures reached at the ceiling. As Figure 5 - 23 indicates, the semi-universal furniture HRR model, combined with the Alpert ceiling temperature correlation underestimates the experimental temperatures measured in the field. Both the generic upholstered furniture model and the semi-universal model are rejected primarily based on their practicality, but also on their inability to accurately predict the enclosure temperatures when combined with the Alpert ceiling temperature correlation as seen in Figure 5 - 23.

5.7.2 Edmonton II Average Hot Gas Layer Temperature Predictions

As shown in Figure 5 - 13 and Figure 5 - 14 above, the average hot gas temperature correlation is used to predict the temperature in the enclosure. The predicted maximum HRR is assumed to be 1560 kW and 1306 kW, corresponding to maximum average hot gas layer temperatures of 546°C and 485°C for Mattress 1 and 2 respectively as discussed in Section 5.5 and Section 5.6.

Figure 5 - 24 and Figure 5 - 25, below, show the predicted average hot gas layer temperature compared to the experimentally measured thermocouple tree measurements. Appendix C contains a detailed calculation using the average hot gas layer temperature correlation.

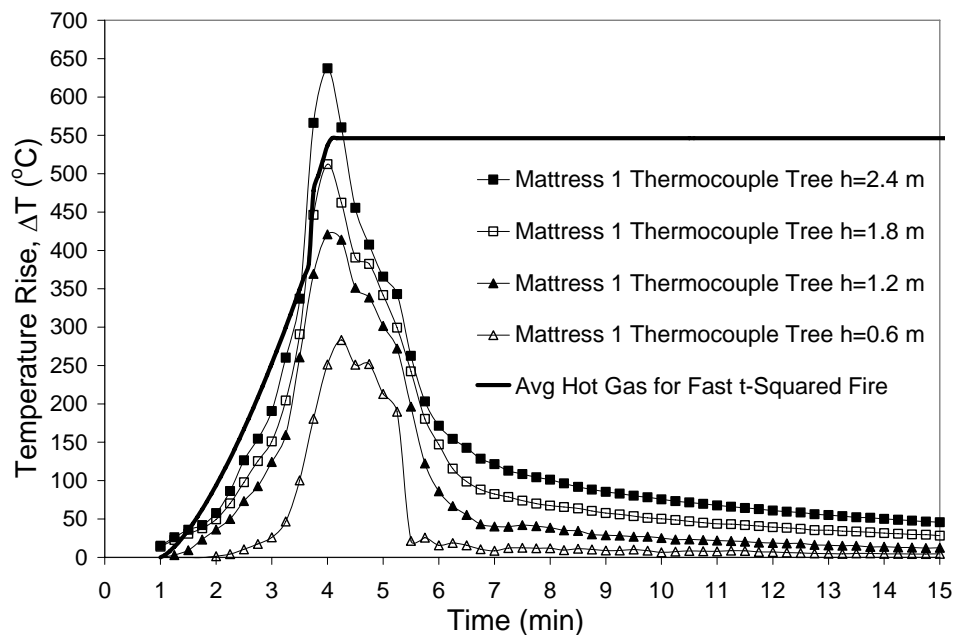


Figure 5 - 24: Average Hot Gas Layer Temperature Compared to Edmonton II Experimental Thermocouple Tree Results for Mattress 1

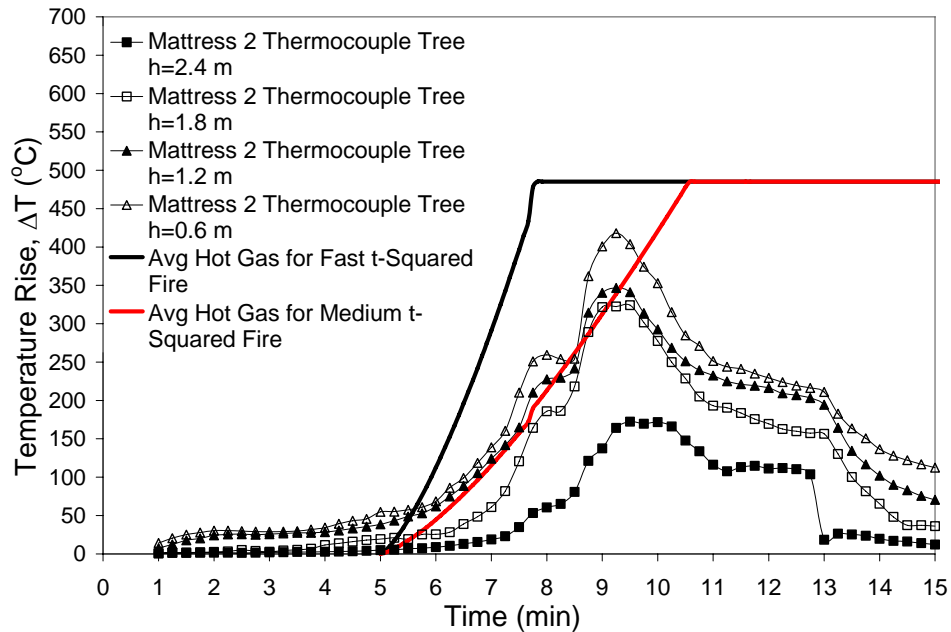


Figure 5 - 25: Average Hot Gas Layer Temperature Compared to Edmonton II Experimental Thermocouple Tree Results for Mattress 2

As seen in Figure 5 - 24, the peak experimental temperature exceeded the predicted temperature for Mattress 1 by approximately 90°C at the thermocouple located 2.4 m above the ground. Figure 5 - 25 indicates that the maximum experimental temperature for Mattress 2, recorded at a distance of 2.4 m above the floor, was approximately 60°C lower than the predicted temperature for Mattress 2. The average upper hot gas layer temperature correlation predicts maximum temperatures to within approximately 17%, which is considered reasonably good in the context of fire temperature prediction, for both Mattresses 1 and 2 when combined with the t-squared HRR model.

For purposes of completeness, it should be noted that the semi-universal HRR model will give the same difference between the maximum experimental temperature and predicted temperature as the t-squared HRR model. This is because the maximum HRR

of the semi-universal curve is assumed to be the HRR given by the NIST/CBHF correlation, which was also assumed to be the maximum for the t-squared HRR curve. The generic upholstered furniture fire growth model, however, is able to predict the maximum HRR, which was found to be 1453 kW. Comparing the temperatures predicted using the generic upholstered furniture model maximum HRR in the average hot gas layer temperature correlation to the experimental temperature results, differences of 53% and 25% were observed for Mattresses 1 and 2 respectively. The generic upholstered furniture fire growth model predicts the same maximum HRR for Mattress 1 and 2 of 1453 kW, however, the enclosure conductance quantity is different for the mattresses, resulting in different maximum temperatures. The t-squared HRR model, therefore, is preferred over the generic upholstered furniture model on the basis of comparison between predicted temperatures using the hot gas layer correlation and experimentally measured temperatures as well as on the basis of practicality.

5.8 Summary

Several methods of modeling the heat release rate from the mattress burn tests were investigated with varying degrees of success. The most successful correlations that were examined with respect to this research work were the NIST/CBHF correlation, which predicts the peak HRR based on cone calorimeter results, and the t-squared fire growth model. The NIST/CBHF correlation provides a useful, relatively accurate and easily implemented prediction of non-propagating and self-propagating fire behaviour. The t-squared fire growth model, combined with the Alpert ceiling temperature correlation, predicts full-scale fire temperatures to within approximately 30% for the majority of the tests, which is considered reasonable given the context of fire temperature modeling. Predicted results within approximately 17% of the measured temperatures were obtained when the t-squared HRR model was combined with the average hot gas layer correlation. The challenge with the t-squared fire growth model is predicting what the fire growth coefficient, or which classification of fire growth to use for a specific fuel load. The fast t-squared fire growth coefficient for a polyurethane foam mattress, which is suggested in engineering handbooks and the literature for polyurethane foam, does in fact reasonably estimate the full-scale burning behaviour of the mattresses burned in the Edmonton II set of experiments.

This work supports similar research [32] indicating that a t-squared fire growth modeling approach can be used to estimate fire growth behaviour. Many fire parameters such as temperature, flame height, flashover and flamespread depend on the HRR, and therefore this research work highlights the extremely important requirement of an

accurate model of this quantity. One of the challenges of using CFD modeling packages is determining what fire growth HRR-time history should be input into the program.

Bounagui et al. [32] performed several full-scale fire tests on upholstered furniture and found that a fast t-squared fire more accurately modeled the HRR than the sophisticated FDS field modeling software package.

Results from this research indicate that mattresses, and similar upholstered furniture products are difficult fuels to accurately model. It is difficult to quantify effects such as the flame spread across the mattress layers and subsequently the radial distance in the Alpert ceiling temperature correlations. There are also a wide range of polyurethane foams used in mattresses, adding to the complexity of accurate modeling. Perhaps a more uniform and repeatable fuel should have been used for this investigation. A more uniform fuel, giving more repeatable burning characteristics, such as wood crib structure [34] or a liquid pool fire would likely have been easier to model. The fire diameter and location of fuel loads such as these would remain approximately constant during the fire duration. In addition, it would be easier to perform small-scale testing to determine fire characteristics on materials such as wood or a liquid fuel. Wood, for example, is much easier to test in the cone calorimeter as it does not have the added complication of sample compressibility effects and multi-layer composite sample effects.

CHAPTER 6: CONCLUSIONS & FUTURE WORK

The focus of this thesis was to investigate several relatively simple heat release rate modeling techniques and temperature prediction correlations as well as to examine the current building spatial separation requirements in the National Building Code of Canada. Full-scale experimental temperature data was obtained by conducting a set of three field fire tests on mattresses which were used for comparison with theoretical temperature predictions obtained using several different modeling techniques. In addition, radiant heat flux results were obtained from a full-scale building fire and were used for comparison with the theoretical prediction of radiation heat flux emitted by a burning building according to the National Building Code of Canada. Conclusions and recommendations for future work are presented below.

6.1 Conclusions

- The results from this research suggest that the current building spatial separation requirements in the Canadian National Building Code slightly underestimate the radiant heat flux emitted by a burning building. A peak radiant heat flux during the initial 10 min of the full-house burn of approximately 19 kW/m^2 was measured, compared to the spatial separation peak heat flux estimate of approximately 15 kW/m^2 . The main reason for the difference between the predicted and measured heat fluxes is the assumption of a constant view factor from the building unprotected openings to an adjacent structure. Experimental

observations indicate, however, that the view factor will increase with time as the fire spreads from the unprotected openings to the exterior of the building, therefore increasing the heat transferred by radiation to the surroundings.

- The results from this research work indicate that using a t-squared fire growth model to predict the burning behaviour of the mattresses results in a very good approximation to the full-scale behaviour as suggested in many fire protection engineering handbooks. In addition to the t-squared fire model, the combustion science HRR model, semi-universal HRR model and generic upholstered furniture fire growth model were examined. On the basis of both practicality and on comparison with experimental temperature results when combined with the Alpert and hot gas layer temperature correlations, all but the t-squared HRR model were eliminated. A fast t-squared fire was the best choice for classifying the polyurethane foam mattresses burned in the Edmonton II experiments, based on a review of the literature and on the experimental results obtained during this research work.
- As HRR could not be experimentally measured in the field, temperature was used for means of comparison between fire models. It was found that the Alpert ceiling temperature correlation combined with a fast t-squared fire growth model predicted the enclosure temperatures, up to the point of flame impingement on the ceiling, to within approximately 30% for the majority of experimental test results at five different ceiling locations. It was also found that the

average hot gas layer temperature correlation combined with a fast t-squared fire growth model predicted maximum enclosure temperatures to within approximately 17% of the experimental results.

- It was found that small-scale cone calorimeter testing of composite samples comprised of several materials can be difficult due to complications regarding the choice of a representative sample. This research indicated, however, that repeatability within approximately 20% was obtained during cone calorimeter testing of mattress composites, which is considered reasonable for the purposes of this research project.
- The cone calorimeter was used to obtain results that could be input into the NIST/CBHF correlation to predict whether a mattress will be non-propagating or self-propagating, severely affecting enclosure heat release rate hazard predictions. Combining the NIST/CBHF correlation, the cone calorimeter results from three different mattresses and limited fire test experience, the propagating versus non-propagating fire behaviour was successfully predicted for all three mattresses.

6.2 Recommendations for Future Work

The recommendations for future work are included below. These recommendations are based on performing more detailed full-scale fire tests aimed at examining enclosure fire behaviour, specifically with respect to mattresses.

- A more uniform, homogeneous fuel such as wood or a liquid combustible fuel would allow for easier characterization of both the small-scale experimental heat

release rate obtained through cone calorimeter testing and the full-scale burning geometry.

- Perform full-scale room and furniture calorimeter experiments in a dedicated experimental test facility in order to obtain full-scale heat release rates. This would allow for easier comparison with the heat release rate models, as it is the prime variable of interest in modeling fire behaviour.
- Acquire infrared and regular video footage of the fire allowing a more accurate post-fire reconstruction of events and estimation of flame-spread rates.
- Use sensors or video footage to estimate the growth of the hot gas/smoke layer in the enclosure for more accurate assessment of the validity of the Alpert ceiling temperature correlation.
- Investigate methods of predicting the heat release rate during the fire decay period allowing for a more complete characterization of the fire.
- Investigate a method of correcting the skin simulant sensor heat flux data, as this research indicated that measurement errors become significant when the skin simulant sensors are exposed to high heat fluxes for extended periods of time.
- Obtain more detailed photos and video observations of flame projection and exterior building fire spread during building fires, in order to try and quantify the increase in the radiation view factor as the fire progresses.
- Further investigate the differences between the radiation heat flux results predicted using the spatial separation guidelines in the National Building Code of Canada and the measured radiation heat flux by the sensors in the Edmonton I investigation. The results should be studied further and more experimental

results obtained to determine if differences in modern building practices and materials have impacted the spatial separation requirements in the current building code.

REFERENCES

1. Council of Canadian Fire Marshals and Fire Commissioners. Fire losses in Canada: annual report 2000. 2002. Ottawa, ON, Human Resources Development Canada.
2. Hall JR, Cote AE. An overview of the fire problem and fire protection. In: Cote AE, Hall JR, Powell PA, Grant CC, eds. Fire protection handbook. Quincy, Massachusetts: National Fire Protection Association; 2003. Vol. 1, pp 2-5-2-36.
3. Gottschalk J. Firefighting. New York: DK Publishing Inc.; 2002.
4. Budnick EK. Quantitative fire hazards analysis - an overview of needs, methods and limitations. Fire Safety Journal 1986; 11: 3-14.
5. Drysdale D. An introduction to fire dynamics. West Sussex, England: John Wiley & Sons; 1998.
6. Babrauskas V, Peacock RD. Heat release rate: the single most important variable in fire hazard. Fire Safety Journal 1992; 18: 255-272.
7. Hirschler, M. M. Use of heat release measurements and/or fire hazard assessment in codes and standards in the USA. 2000. National Fire Protection Research Foundation. Fire Risk & Hazard Assessment Symposium. June 6, 2000.
8. Bounagui, A. and Benichou, N. Literature review on the modeling of fire growth and smoke movement. August 28, 2003. National Research Council Canada. Institute for Research in Construction.
9. Lawson JR, Quintiere JG. Slide rule estimates of fire growth. Fire Technology 1985; 21: 267-291.
10. Gann RG, Babrauskas V, Peacock RD. Fire conditions for smoke toxicity measurement. Fire and Materials 1994; 18: 193-199.
11. Loughheed, G. D. Basic principles of smoke management for atriums. 47. 2000. Ottawa, ON, National Research Council of Canada, Institute for Research in Construction. Construction technology update.
12. Krasny JF, Parker WJ, Babrauskas V. Fire behaviour of upholstered furniture and mattresses. Norwich, NY: Noyes Publications; 2001.
13. ASTM E 1321, standard test method for determining material ignition and flame spread properties. West Conshohocken, PA: American Society of Testing and Materials; 2002.

14. An analysis to establish a nightclub sprinkler threshold. 1-15. April 9, 2003. St. Louis, Missouri, Code Consultants, Inc. National Fire Protection Association Technical Committee on Assembly Occupancies.
15. NIST and the world trade center. <http://wtc.nist.gov> . 2005. Accessed July 24, 2005.
16. Canadian Commission on Building and Fire Codes. National building code of Canada. Ottawa, ON: National Research Council of Canada; 1995.
17. Puchovsky MT. Performance-based codes and standards for fire safety. In: Cote AE, Hall JR, Powell PA, Grant CC, eds. Fire protection handbook. Quincy, Massachusetts: National Fire Protection Association; 2003. Vol. 1, pp 3-181-3-195.
18. National building and fire codes. <http://www.nationalcodes.ca>. 2005. Accessed July 24, 2005.
19. ASTM E 2067, standard practice for full-scale oxygen consumption calorimetry fire tests. West Conshohocken, PA: American Society of Testing and Materials; 2003.
20. ISO 9705. Room fire test is full scale for surface products. ISO 9705, International Organization for Standardization, Geneva, Switzerland 1990.
21. Babrauskas V, Grayson SJ. Heat release in fires. Chapman & Hall; 1996.
22. Shorter GW, McGuire JH, Hutcheon NB, Legget RF. The St. Lawrence burns. Quarterly of the National Fire Protection Association 1960; 53: 300-316.
23. McGuire JH. Fire and the spatial separation of buildings. Fire Technology 1965; 1: 278-287.
24. ASTM E 1354, standard test for heat and visible smoke release rates for materials and products using an oxygen consumption calorimeter. West Conshohocken, PA: American Society for Testing and Materials; 2004.
25. Babrauskas, V. Ten years of heat release research with the cone calorimeter. Tsukuba, Japan, Tsukuba Building Test Laboratory, Centre for Better Living. Japan Symposium on Heat Release and Fire Hazard, First Proceedings. May 10, 1993.
26. Kim A. Fire properties of room lining materials measured by the cone calorimeter, OSU, IMO, and full-scale room/corner tests. Fire and Flammability of Furnishings and Contents of Buildings, ASTM STP 1233 1994; 186-200.
27. Hirschler MM. Use of heat release rate to predict whether individual furnishings would cause self propagating fires. Fire Safety Journal 1999; 32: 273-296.

28. Babrauskas V, Baroudi D, Myllymaki J, Kokkala M. The cone calorimeter used for predictions of full-scale burning behaviour of upholstered furniture. *Fire and Materials* 1997; 21: 95-105.
29. DiNenno PJ, Beyler CL, Custer RLP, Walton WD, Watts JM, Drysdale D, Hall JR. *The SFPE handbook of fire protection engineering*. Society of Fire Protection Engineers; 1995.
30. Luo M, He Y, Beck V. Application of field model and two-zone model to flashover fires in a full-scale multi-room single level building. *Fire Safety Journal* 1997; 29: 1-25.
31. Peacock RD, Jones WW, Bukowski RW. Verification of a model of fire and smoke transport. *Fire Safety Journal* 1993; 21: 89-129.
32. Bounagui, A., Benichou, N., and Bwalya, A. Comparison of heat release rate from experiments against numerical predictions and evaluation of life safety in residential houses. 2005. National Research Council of Canada, Institute for Research in Construction.
33. Walton WD, Carpenter DJ, Wood CB. Deterministic computer fire models. In: Cote AE, Hall JR, Powell PA, Grant CC, eds. *Fire protection handbook*. Quincy, Massachusetts: National Fire Protection Association; 2003. Vol. 1, pp 3-83-3-96.
34. McGrattan, K. Fire dynamics simulator (version 4) technical reference guide. 1018. 2005. National Institute of Standards and Technology.
35. Hume, B. Fire models training manual for FSO's, Volume 3: Hazard-I. 7/98. 1998. Fire Research and Development Group.
36. Bukowski, R. W. Predicting the fire performance of buildings: establishing appropriate calculation methods for regulatory applications. Interscience Communications Limited. International Conference on Fire Science and Engineering. March 15, 1995.
37. Peacock, R. D., Forney, G. P., Reneke, P. A., Portier, R. M., and Jones, W. W. CFAST, the Consolidated Model of Fire Growth and Smoke Transport. NIST SP 1030. 2004. National Institute of Standards and Technology.
38. Budnick EK, Evans DD, Nelson HE. Simplified fire growth calculations. In: Cote AE, Hall JR, Powell PA, Grant CC, eds. *Fire protection handbook*. Quincy, Massachusetts: National Fire Protection Association; 2003. Vol. 1, pp 3-131-3-145.

39. Gott, J. E., Lowe, D. L., Notarianni, K. A., and Davis, W. D. Analysis of high bay hangar facilities for fire detector sensitivity and placement. NIST Technical Note 1423. 1997. National Institute of Standards and Technology, Building and Fire Research Laboratory.
40. Babrauskas V, Wetterlund I. Testing of furniture composites in the cone calorimeter: a new specimen preparation method and round robin results. *Fire Safety Journal* 1998; 30: 179-194.
41. Paul KT. CBUF conference - report and comments. *Fire Safety Journal* 1995; 25: 165-170.
42. Van Hees, P. Combustion behaviour of upholstered furniture - the CBUF project - major findings and applications. 2005. Swedish Research and Testing Institute.
43. Enright PA. CBUF model II applied to exemplary NZ furniture (NZ-CBUF). *Fire and Materials* 2001; 25: 105-115.
44. Threlfall, T. G, Torvi, D. A., and Thorpe, P. A. Exterior heat flux measurements during house burn and implications for building codes. 2004. Combustion Institute Canadian Section. Spring Technical Meeting. September 5, 2004.
45. Wickstrom U, Goransson U. Prediction of heat release rates of surface materials in large-scale fire tests based on cone calorimeter results. *Journal of Testing and Evaluation* 1987; 15: 364-370.
46. Bukowski RW. Fire hazard analysis. In: Cote AE, Hall JR, Powell PA, Grant CC, eds. *Fire protection handbook*. Quincy, Massachusetts: National Fire Protection Association; 2003. Vol. 1, pp 3-105-3-114.
47. NFPA 72, national fire alarm code. National Fire Protection Association; 2002.
48. Parker, W. J., Tu, K. M., Nurbakhsh, S., and Damant, G. H. Furniture flammability: an investigation of the California technical bulletin 133 test. Part III: full scale chair burns. NISTIR 4375. 1990. National Institute of Standards and Technology.
49. Alpert RL. Calculation of response time of ceiling-mounted fire detectors. *Fire Technology* 1972; 8: 181-195.
50. Beyler CL. Fire plumes and ceiling jets. *Fire Safety Journal* 1986; 11: 53-75.
51. Alpert RL, Ward EJ. Evaluation of unsprinklered fire hazards. *Fire Safety Journal* 1984; 7: 127-143.
52. Janssens M, Parker WJ. Oxygen consumption calorimetry. Heat release in fires. Chapman & Hall; 1996. pp 31-59.

53. Enright PA, Fleischmann CM. Uncertainty of heat release rate calculation of the ISO 5660 cone calorimeter standard test method. *Fire Technology* 1999; 35: 153-169.
54. ASTM E 1474-95, Standard Method for Determining the Heat Release Rate of Upholstered Furniture and Mattress Components or Composites Using a Bench Scale Oxygen Consumption Calorimeter. West Conshohocken, PA: American Society for Testing and Materials; 1995.
55. Fritz TW, Hunsburger PL. Testing of mattress composites in the cone calorimeter. *Fire and Materials* 1997; 21: 17-22.
56. ASTM E 1474-95, standard method for determining the heat release rate of upholstered furniture and mattress components or composites using a bench scale oxygen consumption calorimeter. West Conshohocken, PA: American Society for Testing and Materials; 1995.
57. Paul KT. Cone calorimeter: initial experiences of calibration and use. *Fire Safety Journal* 1994; 22: 67-87.
58. Enniful, E. K. and Torvi, D. A. Effects of moisture and incident heat flux on smoke production and heat release rates of vegetation. 2005. Halifax, NS. Combustion Institute Canadian Section Spring Technical Meeting. 15-5-2005.
59. ASTM E 1590-93, standard method for testing full scale mattresses. West Conshohocken, PA: American Society of Testing and Materials; 1993.
60. Diller TE. Advances in heat flux measurement. *Advances in Heat Transfer* 1993; 23: 279-368.
61. Dale, J. D., Crown, E. M., Ackerman, M. Y., Leung, E., and Rigakis, K. B. Instrumented mannequin evaluation of thermal protective clothing. McBriarty, J. P. and Henry, N. W. ASTM STP 1133, 717-733. 1992. West Conshohocken, PA, American Society for Testing and Materials.
62. Torvi, D. A. Heat transfer in thin fibrous materials under high heat flux conditions. 1997. University of Alberta. PhD Thesis.
63. Dale, J. D., Ackerman, M. Y., Torvi, D. A., Threlfall, T. G, and Thorpe, P. A. Interior temperature and heat flux measurements during a house burn. 2004. Canadian Institute Canadian Section. Spring Technical Meeting. 5-9-2004.

64. NIST. Centre mattress fire. <http://www.fire.nist.gov/fire/fires/matt1/mat1.html> .
2005. National Institute of Standards and Technology. Accessed July 24, 2005.
65. NIST. Corner mattress fire. <http://www.fire.nist.gov/fire/fires/matt2/mat2.html> .
2005. National Institute of Standards and Technology. Accessed July 24, 2005.

APPENDIX A: EDMONTON I SPATIAL SEPARATION CALCULATIONS AND ADDITIONAL INFORMATION

This appendix presents the details of the spatial separation calculations for the Edmonton I building. Both the spatial separation calculations will be presented as well as the experimental heat flux

A.1 Spatial Separation Sample Calculations

A schematic diagram of the building wall is seen below in Figure A - 1. The following sample calculation will be done assuming a “normal” fire hazard.

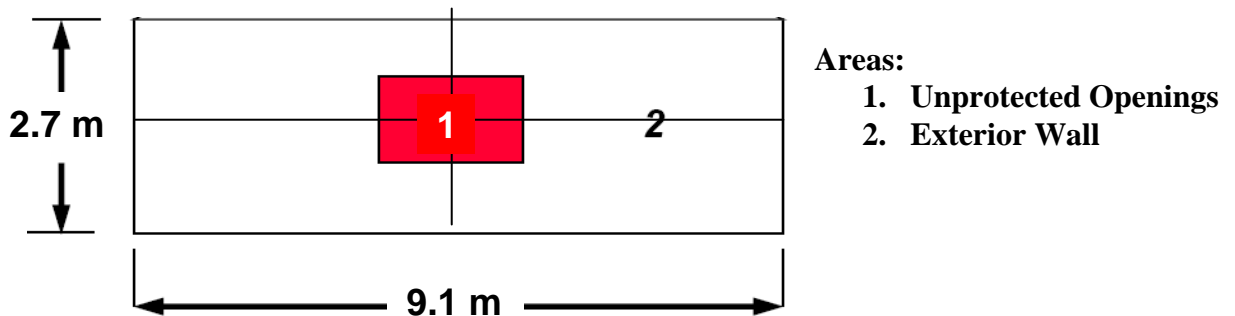


Figure A - 1: Schematic Diagram of Edmonton I House for Spatial Separation Calculations

The fraction of unprotected openings, u , will first be determined as follows:

$$u = \frac{\text{Area of Unprotected Openings}}{\text{Total Area of Building Face}}$$

$$u = \left(\frac{(1.8m)(1.2m) + (0.8m)(1.2m)}{(9.1m)(2.7m)} \right) \quad (\text{A.1})$$

$$u = 0.13$$

The building wall is then divided into 4 equal sized rectangles of size 4.5 m by 1.5 m for the view factor calculation. The critical view factor for the unprotected openings, F_u , to a point opposite the corner of the rectangle is found using the critical view factor for “normal” hazard by the following formula:

$$F_u = \frac{F_{cr}}{4u}$$

$$F_u = \frac{0.07}{4(0.13)} \quad (\text{A.2})$$

$$F_u = 0.14$$

where:

F_u = View Factor from Unprotected Openings to
Adjacent Building
 F_{cr} = Critical View Factor for Entire Wall
 = 0.07 for "normal" hazard
 = 0.035 for "severe" hazard.

Using view factor tables found in [5], the spatial separation distance can then be determined. The view factor tables commonly present tabulated results for the view factor as a function of S , the ratio of the rectangle length to width, and α , as defined below.

$$S = \frac{L_1}{L_2} \tag{A.3}$$

$$\alpha = \frac{(L_1)(L_2)}{d^2}$$

where:

L_1 = Width of Rectangle (1/2 of Wall Width) [m]

L_2 = Length of Rectangle (1/2 of Wall Height) [m]

D = Distance from Radiation Emitter to Receiver [m].

The value of S is found below:

$$S = \frac{L_1}{L_2}$$

$$S = \frac{1.4m}{4.6m}$$

$$S = 0.30$$

Using the critical view factor for unprotected openings calculated above and the value of S, α , is found from standard view factor tables to be 1.7, allowing the distance, d, to be calculated.

$$\alpha = 1.7 = \frac{(L_1)(L_2)}{d^2}$$

$$1.7 = \frac{(1.4m)(4.6m)}{d^2}$$

$$d = 2.0m$$

Including the flame projection, d_f , for a “normal” fire hazard of 1.5 m, the spatial separation distance is found to be 3.5 m as seen below:

$$\begin{aligned}d_a &= d + d_f \\d_a &= d + 1.5m \\d_a &= 2.0m + 1.5m \\d_a &= 3.5m\end{aligned}$$

Similarly, for a “severe” fire hazard, the spatial separation distance is found to be 6.3 m.

A.2 Theoretical Heat Flux At Sensor Location

The sensor tripod was located at a horizontal distance of 4.0 m and a vertical distance of 1.84 m as seen below in Figure A - 2. The window was located at a distance of 1.94 m from the ground and was 1.8 m wide by 1.2 m high. This calculation will assume the area radiating energy is only the window, and not the entire unprotected openings of the front face of the building. This was done because the fire was primarily located in the living room and significant fire growth could be seen through the front bay window.

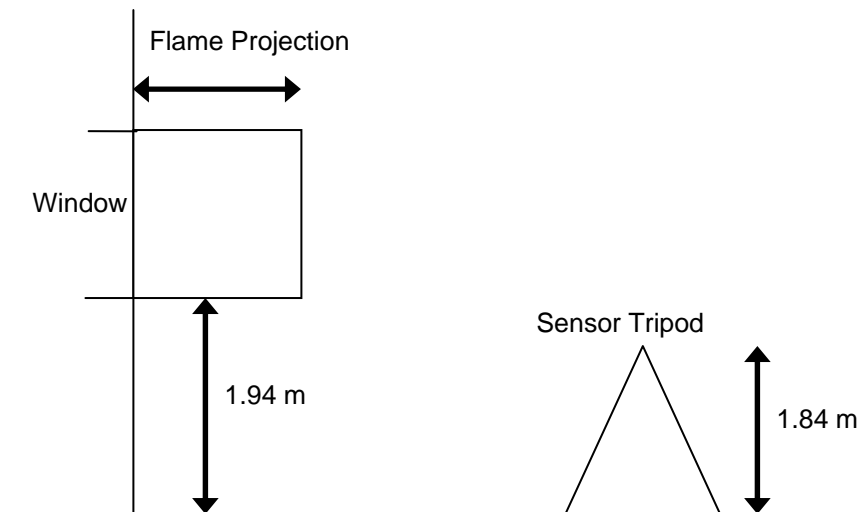


Figure A - 2: Schematic of Bay Window and Sensor Tripod Location

Assuming a flame projection for a normal hazard of 1.5 m, the view factor from the window to the sensor location is found due to the additive nature of view factors. Figure A - 3 below is used to determine the view factor from the window to the sensor location.

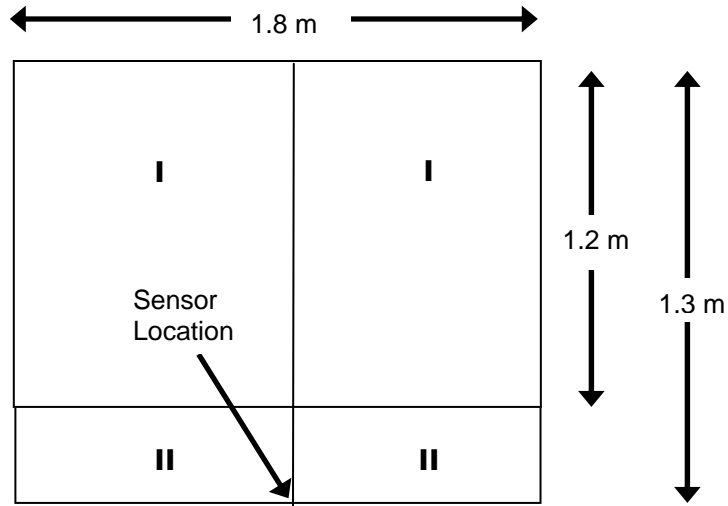


Figure A - 3: Schematic Diagram Used to Determine View Factor

The overall view factor is then found by the following formula:

$$F_{\text{window} \rightarrow \text{sensor}} = 2(F_{I\&II}) - 2(F_{II}) \quad (\text{A.4})$$

where:

$$\begin{aligned}
 F_{\text{window} \rightarrow \text{sensor}} &= \text{View Factor from Window to Sensor} \\
 F_{I\&II} &= \text{View Factor from Area I \& II to Sensor} \\
 F_{II} &= \text{View Factor from Area II to Sensor.}
 \end{aligned}$$

The view factors are determined for the rectangles labelled in Figure A - 3 using a similar method to that presented in Section A.1, found to be 0.047 for $F_{I\&II}$ and 0.004 for

F_{II} . Assuming a flame projection of 1.5 m, the following view factor was found:

$$\begin{aligned}
 F_{\text{window} \rightarrow \text{sensor}} &= 2(0.047) - 2(0.004) \\
 \boxed{F_{\text{window} \rightarrow \text{sensor}} &= 0.086}
 \end{aligned}$$

Assuming a normal hazard case, where a heat flux of 180 kW/m² is assumed at the unprotected opening, the heat flux received by the sensors can be calculated as follows:

$$q''_{\text{window} \rightarrow \text{sensor}} = F_{\text{window} \rightarrow \text{sensor}} q''_{\text{window}} \quad (\text{A.5})$$

where:

$q''_{\text{window} \rightarrow \text{sensor}}$ = Heat Flux Received at the Sensor

q''_{window} = Heat Flux Emitted at the Window

$F_{\text{window} \rightarrow \text{sensor}}$ = View Factor from the Window to the Sensor.

Therefore, the heat flux received at the sensor is found to be:

$$q''_{\text{window} \rightarrow \text{sensor}} = 0.086 \left(180 \frac{\text{kW}}{\text{m}^2} \right)$$

$$q''_{\text{window} \rightarrow \text{sensor}} = 15.4 \frac{\text{kW}}{\text{m}^2}$$

Similarly, for a “severe” fire hazard, the predicted heat flux received at the sensor is found to be 30.9 kW/m².

A.3 Edmonton I House Floor Plan Drawings

Figure A - 4 through Figure A - 7, below, present the floor plan for the house used in the Edmonton I set of experiments. The following symbols are used in the drawings:

q'' = Location of Skin Simulant Heat Flux Gauge
T/C Tree = Location of Thermocouple Tree.

The thermocouples on the tree are located at distances of 0.2 m, 1.4 m and 2.7 m from the floor.

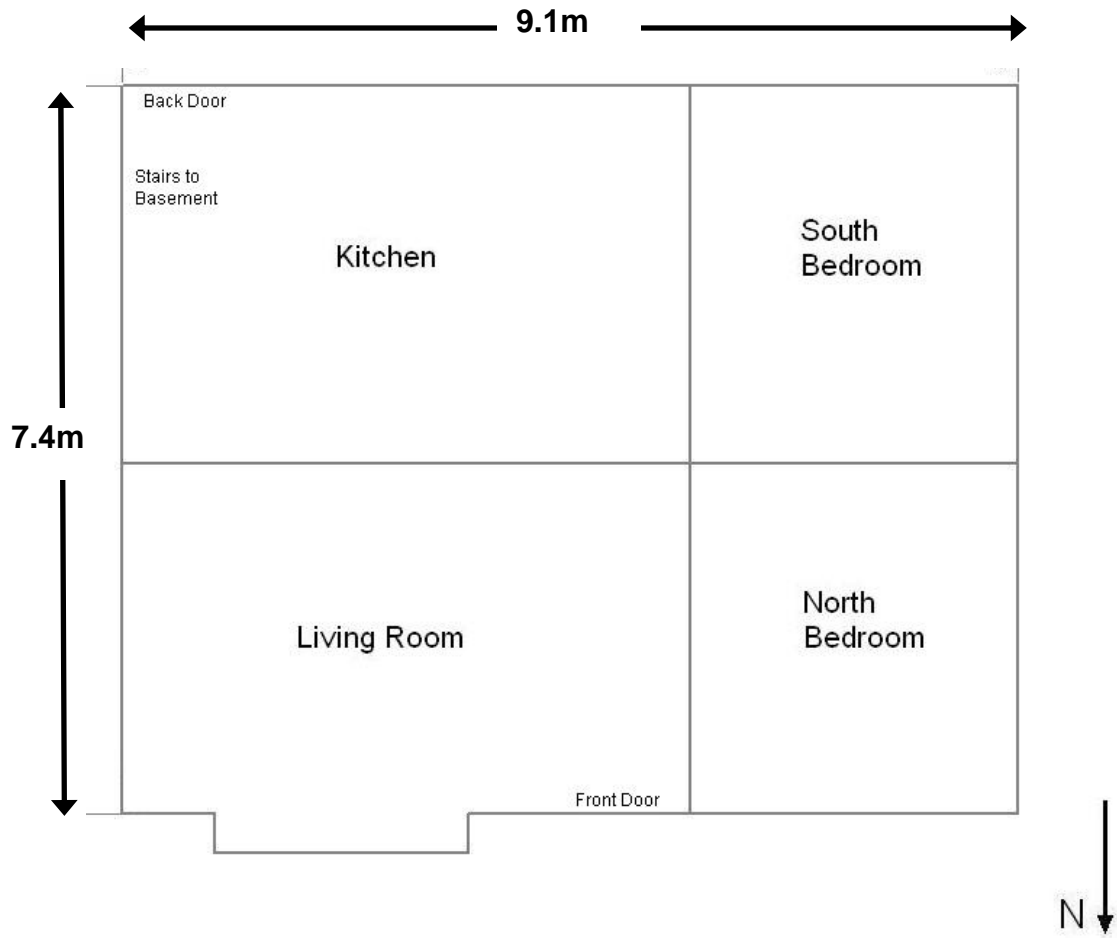


Figure A - 4: General Floor-Level Schematic of Edmonton I House

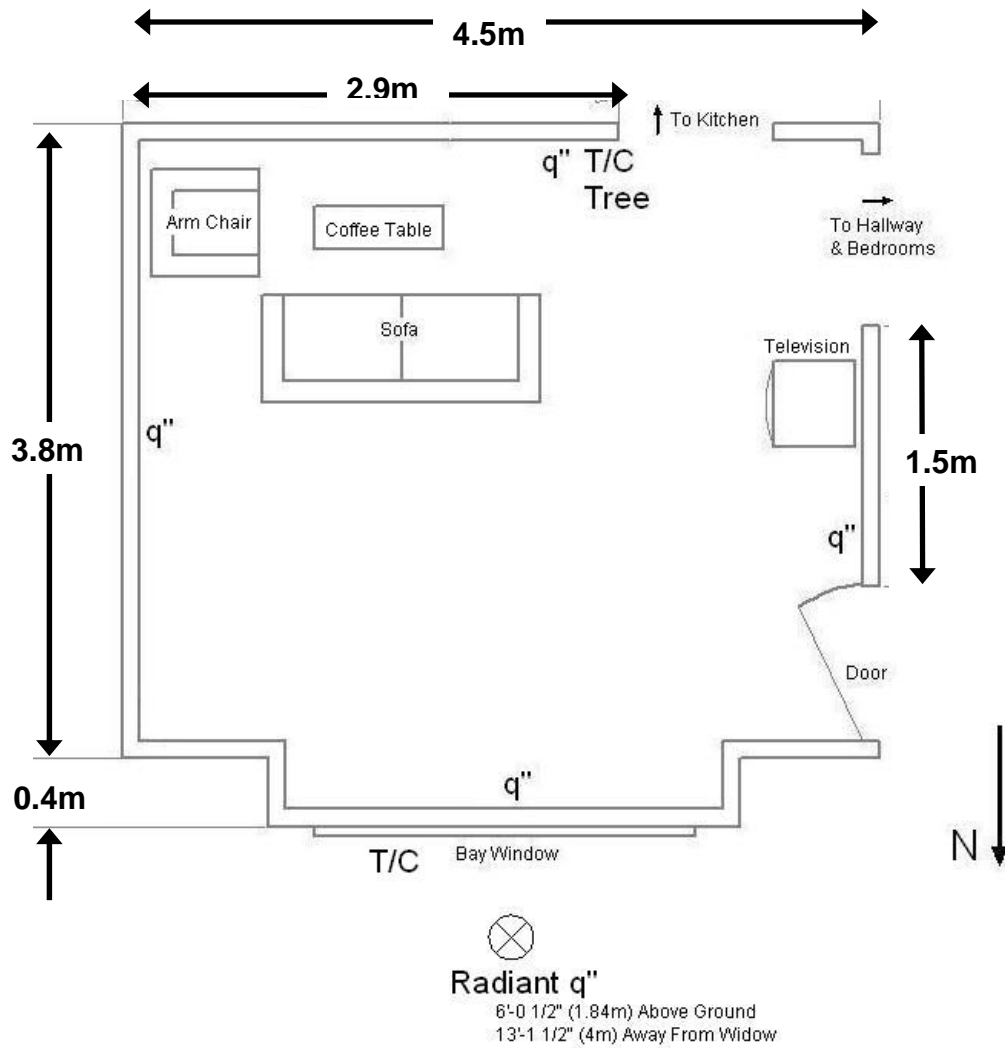


Figure A - 5: Living Room Floor Plan of Edmonton I House Showing Location of Sensors Used for Measuring Radiant Heat Flux Outside Window

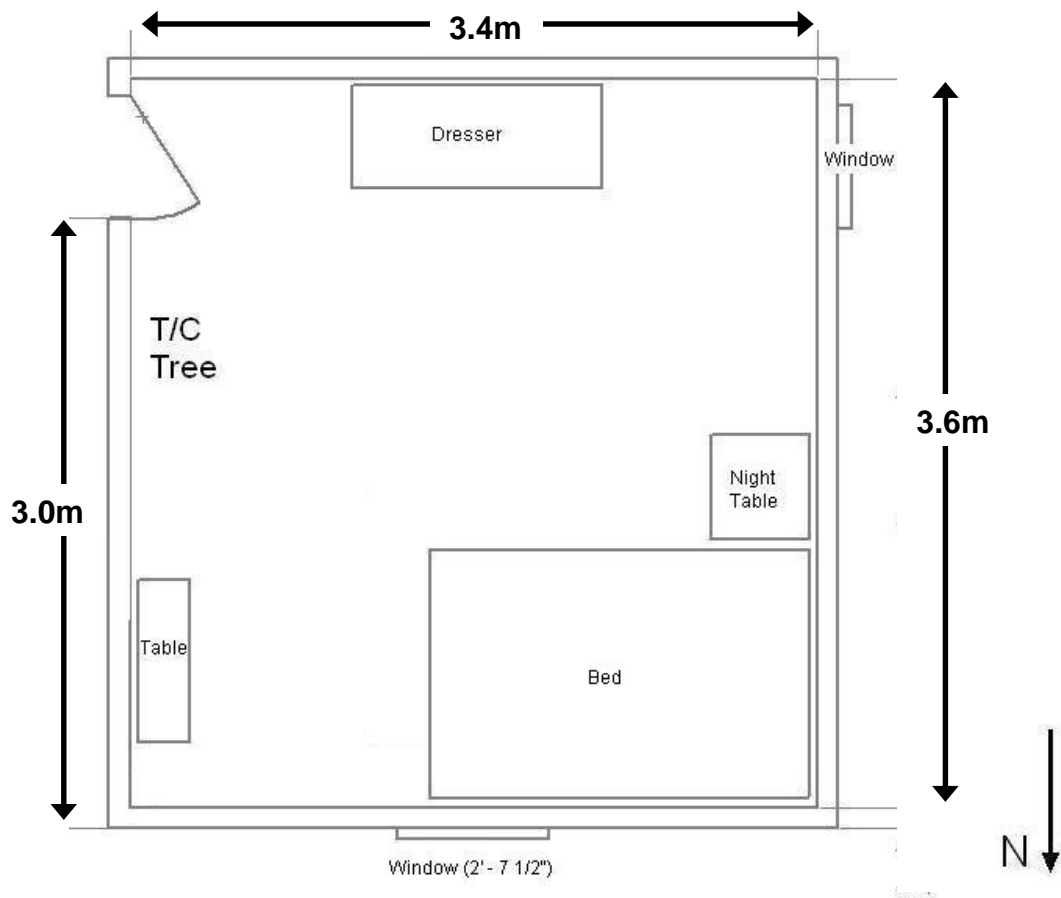


Figure A - 6: North Bedroom Floor Plan of Edmonton I House

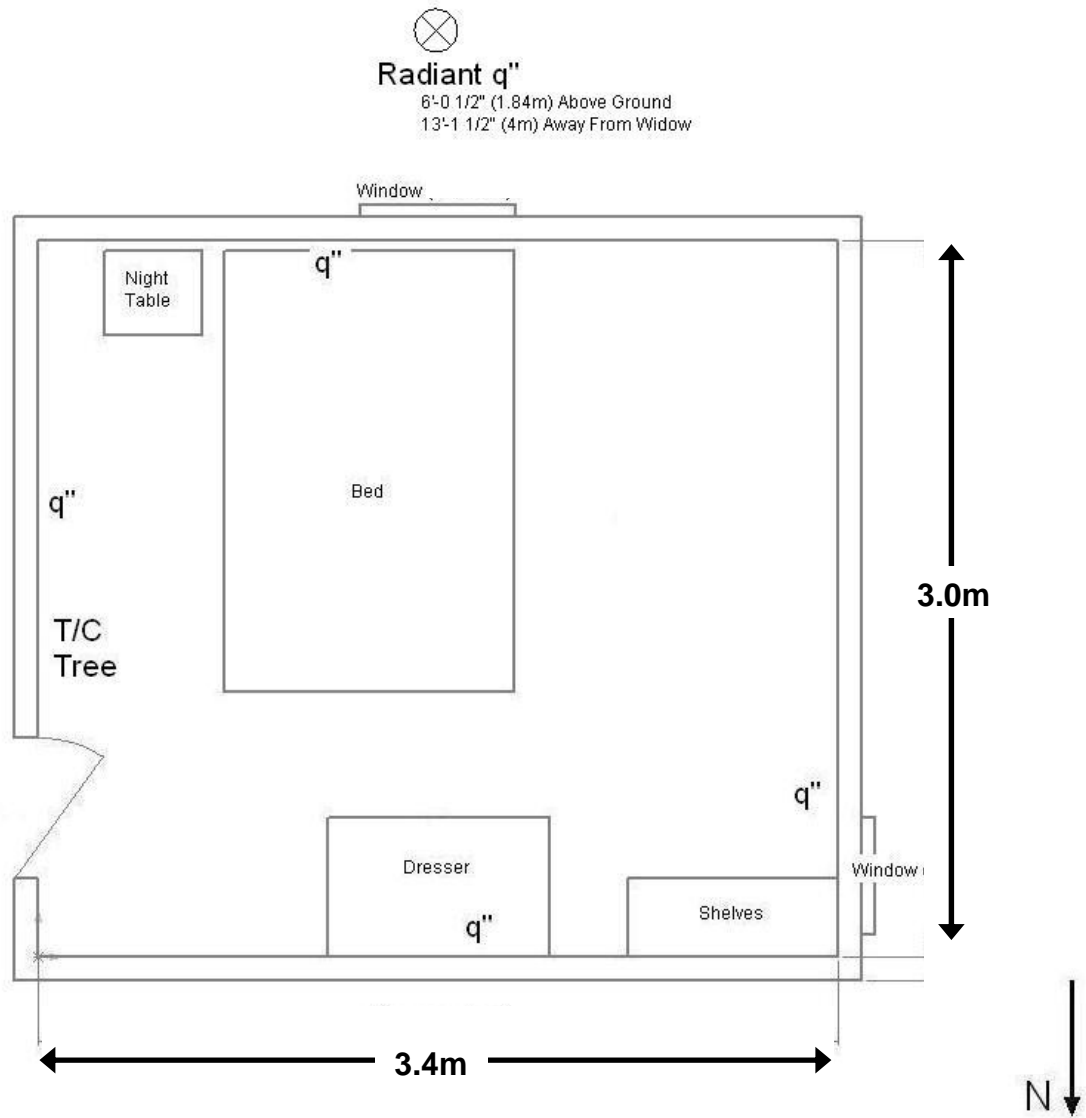


Figure A - 7: South Bedroom Floor Plan of Edmonton I House Showing Location of Sensors Used for Measuring Radiant Heat Flux Outside Window

A.4 Additional Edmonton I Temperature Results

In addition to the heat flux measurements obtained for the first and fourth burn tests (single room and entire house burn), temperature results were obtained for the four experiments, summarized below in Table A - 1.

Table A - 1: Summary of Edmonton I Set of Experiments

Test Burn	Room of Fire Origin	Details
1	South Bedroom	Extinguished by Edmonton Fire Department
2	Living Room	Extinguished by Edmonton Fire Department
3	Basement	Extinguished by Edmonton Fire Department
4	Living Room	Allowed to burn to the ground

The temperature results follow in Figure A - 8 through Figure A - 14.

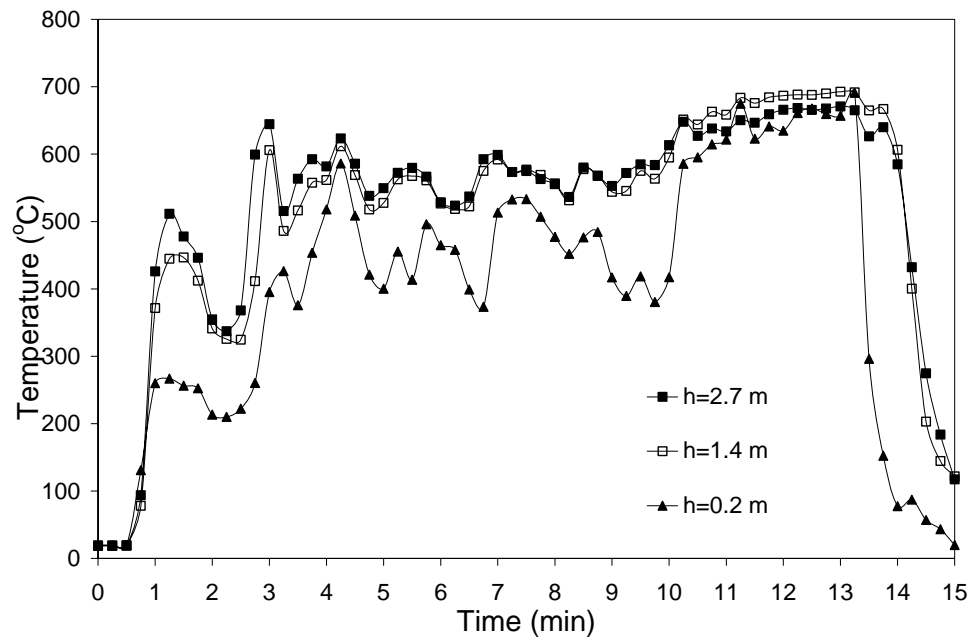


Figure A - 8: Burn Test 1 – South Bedroom Thermocouple Tree Temperature Results

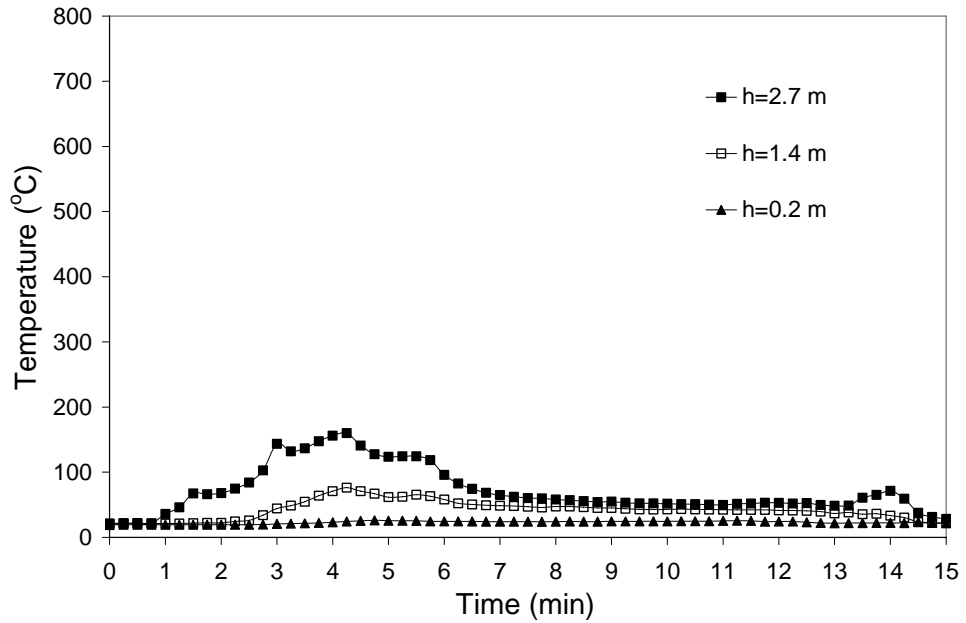


Figure A - 9: Burn Test 1 – Living Room Thermocouple Tree Temperature Results

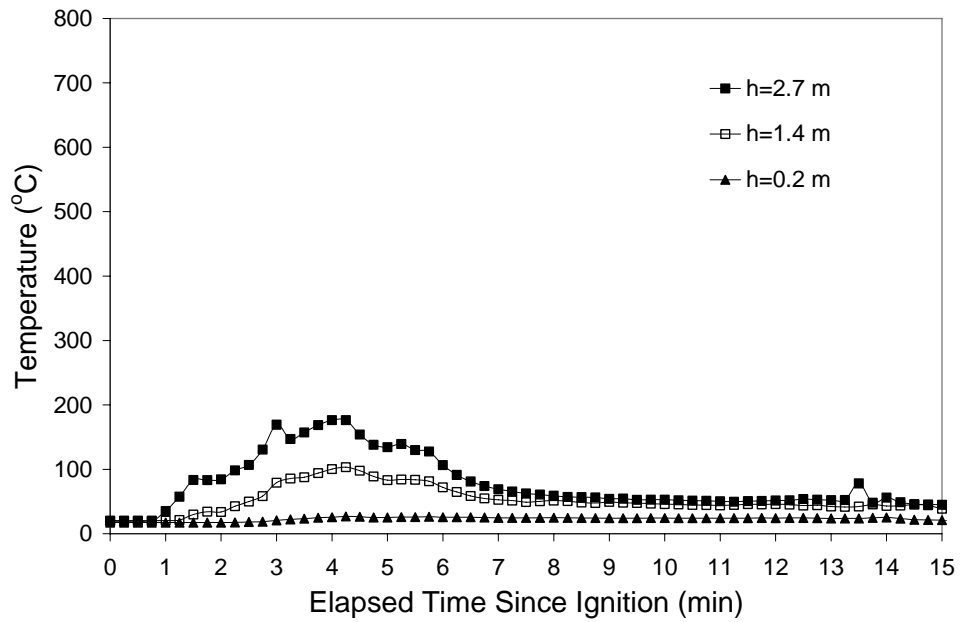


Figure A - 10: Burn Test 1 – North Bedroom Thermocouple Tree Temperature Results

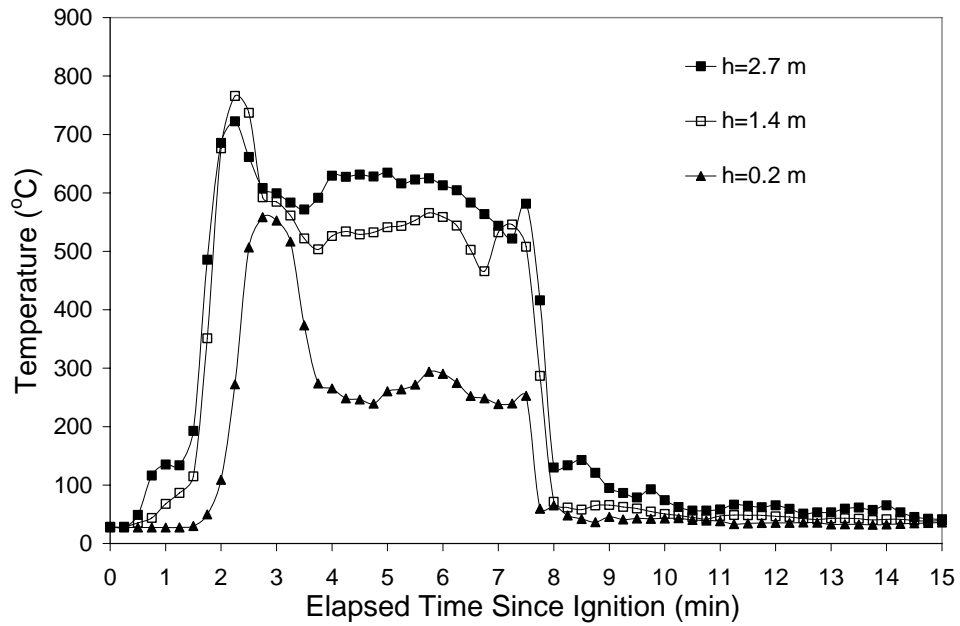


Figure A - 11: Burn Test 2 – Living Room Thermocouple Tree Temperature Results

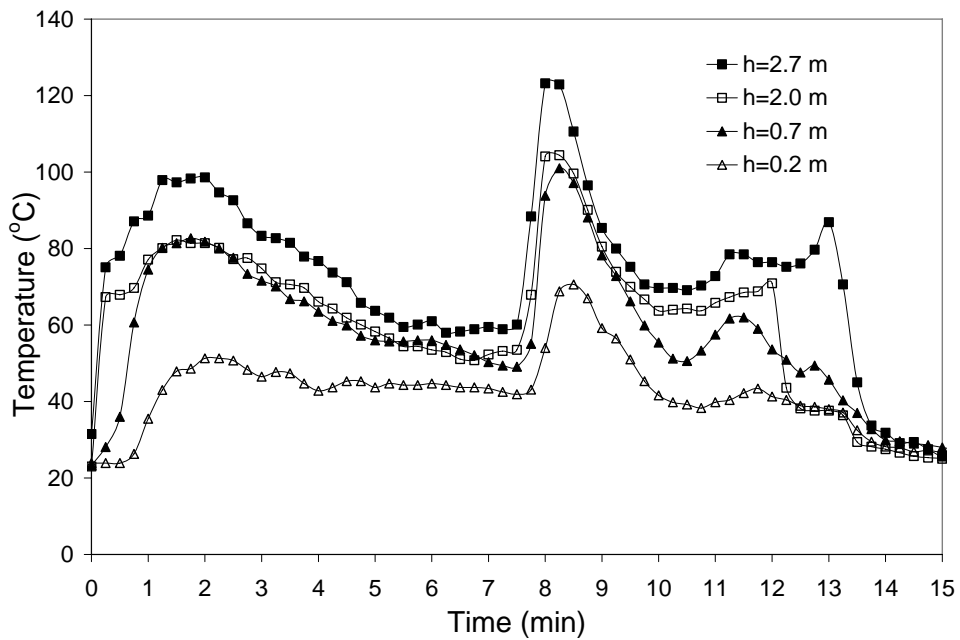


Figure A - 12: Burn Test 3 – Basement Thermocouple Tree Temperature Results

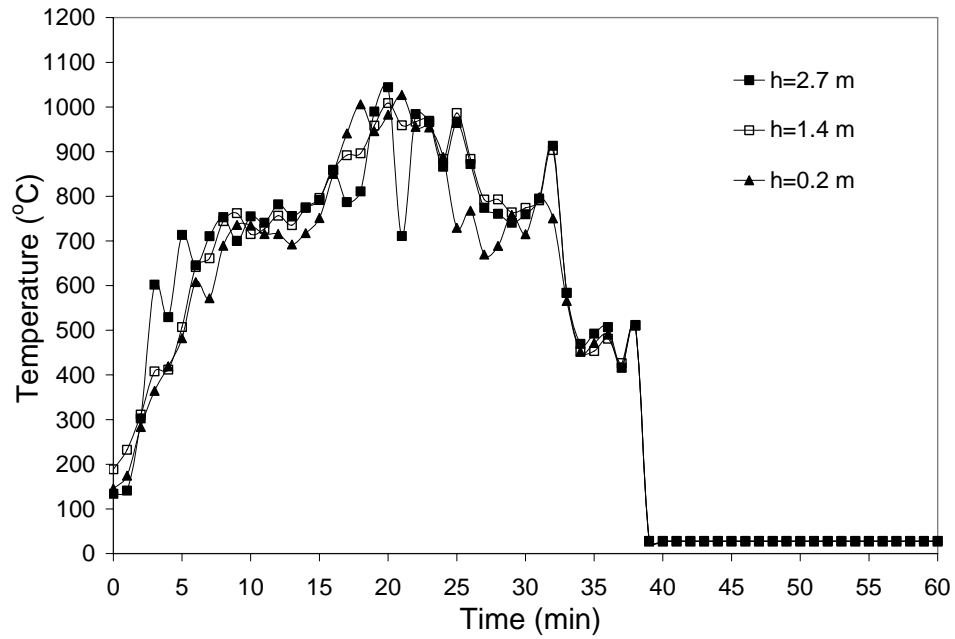


Figure A - 13: Burn Test 4 – Living Room Thermocouple Tree Temperature Results

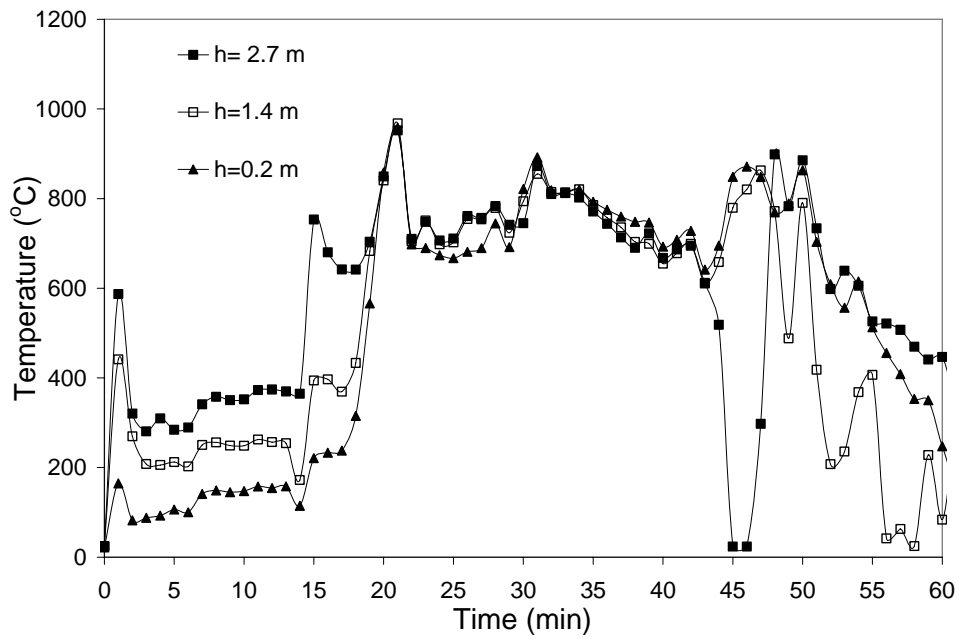


Figure A - 14: Burn Test 4 – North Bedroom Thermocouple Tree Temperature Results

APPENDIX B: HRR CALCULATIONS

Sample calculations for the heat release rate modeling will be presented in this appendix.

Sample calculations of the flame height, combustion science theoretical HRR, semi-universal HRR model, generic upholstered furniture fire growth HRR and t-squared HRR model follow. In addition, the HRR required for the onset of ventilation controlled fire behaviour, HRR required for flashover according to the McCaffrey equation and the NIST/CBHF peak full-scale HRR predictions are calculated.

B.1 Sample Flame Height Calculation

The point when flames impinge on the ceiling will be calculated for the Edmonton II set of experiments. The ceiling height of the enclosure was 2.74 m, and the fire was started on the top of the mattress, at a height of 0.41 m off the floor. For this analysis, it is assumed that the fire was started in the middle of the room, giving a configuration factor, k , of 1.

The formula for calculating flame height follows in Equation B.1.

$$H_f = 0.1743(k\dot{Q})^{0.4} \quad (\text{B.1})$$

where:

H_f = Flame Height [m]

k = Configuration Factor

= 1 if Fire in Centre of Room

= 2 if Fire Against Wall

= 4 if Fire in Corner

\dot{Q} = Heat Release Rate (HRR) [kW].

Assuming the flames touch the ceiling, the HRR required for ceiling flame impingement is calculated as:

$$(2.74 \text{ m} - 0.41 \text{ m}) = 0.1743(\dot{Q})^{0.4}$$

$$\boxed{\dot{Q} = 658.1 \text{ kW}}$$

B.2 Combustion Science Theoretical HRR Sample Calculation

The following sections will illustrate how the combustion science theoretical HRR modeling technique was used and will present sample calculations.

The burn rate was estimated from the video evidence and is shown in Table B - 1 below for the initial portion of the second mattress burn. Burn rate estimates could not be made from the video evidence obtained for Mattresses 1 and 3 due to incomplete video footage of the entire test and poor camera angles. The heat of combustion was obtained by an average of cone calorimeter small-scale tests for the Mattress 2 samples. The mass per unit area was obtained by sample mass measurements in the laboratory, as presented in Table 3 – 1 and was found to be approximately 4.0 kg/m² for Mattress 2, considering both the top and bottom surfaces of the mattress.

Table B - 1: Combustion Science Theoretical HRR

Mass/Unit Area, m" = 4.0 kg/m² *
 Efficiency Factor, x = 0.65
 Heat of Combustion, ΔHc = 16.364 MJ/kg

Time (s)	Burn Size		Burn Area (m ²)	Burn Rate (m ² /s)	HRR (kW)
	Length (m)	Width (m)			
0	0.00	0.00	0.00		0.0
146	0.46	0.91	0.42	0.00286	121.8
251	0.46	0.91	0.42	0.00000	121.8
293	0.46	0.91	0.42	0.00000	121.8
345	0.46	0.91	0.42	0.00000	121.8
411	0.61	0.91	0.56	0.00211	89.8
468	0.61	0.91	0.56	0.00000	89.8
505	1.22	0.91	1.11	0.01507	641.0
530	1.22	0.91	1.11	0.00000	641.0

*Note: This assumes the fire is burning on both the top and bottom surfaces.

B.2.1 Combustion Science Theoretical HRR Sample Calculations

The burn rate was calculated from the following formula:

$$\text{Burn Rate}_i = \frac{\Delta \text{Burn Area}_i}{\Delta \text{Time}_i} \quad (\text{B.2})$$

where:

Burn Rate_i = Burn Rate at Time i

$\Delta \text{Burn Area}_i$ = Change in Burn Area at Time i

ΔTime_i = Size of Time Step at Time i.

$$\dot{Q}_i = m'' \times \Delta H_c (\text{Burn Rate}_i)$$

where:

\dot{Q}_i = HRR at Time i

m'' = Combustible Mass per Unit Area

x = Efficiency Factor (Assumed to be 0.65)

ΔH_c = Heat of Combustion

Burn Rate_i = Burn Rate at Time i.

A sample calculation will be shown for 146 s, with reference to Table B - 1.

$$\text{Burn Rate}_i = \frac{\Delta \text{Burn Area}_i}{\Delta \text{Time}_i}$$
$$\text{Burn Rate}_i = \frac{\left(0.42 \frac{m^2}{s} - 0.00 \frac{m^2}{s} \right)}{(146s - 0s)}$$

$$\boxed{\text{Burn Rate}_i = 0.00286 \frac{m^2}{s}}$$

$$\dot{Q}_i = m'' \times \Delta H_c (\text{Burn Rate}_i)$$

$$\dot{Q}_i = 4 \frac{\text{kg}}{\text{m}^2} (0.65) \left(16.36 \frac{\text{MJ}}{\text{kg}} \right) \left(0.00286 \frac{\text{m}^2}{\text{s}} \right)$$

$$\boxed{\dot{Q}_i = 121.8 \text{ kW}}$$

B.3 Semi-Universal HRR Model

The following section presents details on the semi-universal HRR model.

B.3.1 Semi-Universal HRR Model Sample Calculations

The following formula was used for calculating the semi-universal HRR.

$$\dot{Q} = \left\{ \begin{array}{ll} 10 \exp(0.025t) & 0 \leq t \leq 147.6s \\ 400 \exp(0.01(t-145.6)) & 147.6s \leq t \leq 349s \\ 300 \exp(0.005(t-349)) & 349s \leq t \end{array} \right\} \quad (B.3)$$

where:

$$\dot{Q} = \text{HRR [kW]}$$

$$t = \text{Time (not including Incubation Time) [s].}$$

Sample calculations for the semi-universal HRR model are presented below for a time of 15 s (corresponding to 75 s including an incubation time of 60 s.)

$$\dot{Q} = 10 \exp(.025t) \quad \text{as } 15s < 147.6s$$

$$\dot{Q} = 10 \exp(.025 * 15s)$$

$$\boxed{\dot{Q} = 14.5kW}$$

Table B - 2, following, shows the initial portion of the semi-universal HRR model prediction for Mattress 1.

Table B - 2: Semi-Universal HRR Model Prediction Shown for Mattress One

Time (s)	Shifted Time to Include Incubation Time* (s)	Shifted Time to Include Incubation Time (min)	Semi-Universal HRR (kW)
0	60	1.00	10.0
15	75	1.25	14.5
30	90	1.50	21.2
45	105	1.75	30.8
60	120	2.00	44.8
75	135	2.25	65.2
90	150	2.50	94.9
105	165	2.75	138.0
120	180	3.00	200.9
135	195	3.25	292.2
150	210	3.50	418.0
165	225	3.75	485.6
180	240	4.00	564.2
195	255	4.25	655.5

*Note: Incubation time of 60 s corresponding to mattress one is used. An incubation time of 300 s is used for mattress two.

B.4 Generic Upholstered Furniture Fire Growth Model

The following section presents details on the generic upholstered furniture fire growth model.

B.4.1 Generic Upholstered Furniture Fire Growth Model Sample Calculations

The following formula was used for calculating the generic upholstered furniture HRR.

$$\begin{aligned}\dot{Q}_{\max} &= 210\{FF\}\{PF\}\{CM\}\{SF\}\{FC\} \\ CM &= m''A_{\text{mattress}} \\ t_b &= \frac{\{FM\}\{CM\}\Delta H_c}{\dot{Q}_{\max}}\end{aligned}\tag{B.3}$$

where:

- \dot{Q}_{\max} = Maximum HRR [kW]
- FF = Fabric Factor (defined below)
- PF = Padding Factor (defined below)
- FF = Fabric Factor (defined below)
- CM = Combustible Mass [kg]
- m'' = Combustible Mass Per Unit Area [kg/m²]
- A_{mattress} = Mattress Area [m²]
- SF = Style Factor (defined below)
- FC = Frame Factor (defined below)
- FM = Frame Material Factor (defined below)
- t_b = Triangular Base Time (Total Test Time) [s]
- ΔH_c = Heat of Combustion (16.36 MJ/kg).

The common values for the various factors are shown below in Table B - 3.

Table B - 3: Suggested Values for Factors

Factor	Description	Suggested Value in Literature*
Fabric (FF)	Thermoplastic Fabrics	1.00
	Cellulosic Fabrics	0.40
	PVC or Polyurethane Film Coverings	0.25
Padding (PF)	Polyurethane Foam or Latex Foam	1.00
	Cotton Batting	0.40
	Neoprene Foam	0.40
	Mixed Materials (i.e. both polyurethane and cotton)	1.00
Frame (FC)	Non-Combustible	1.66
	Melting Plastic	0.58
	Wood	0.30
	Charring Plastic	0.18
Style (SF)	Ornate, Convolute Shapes	1.50
	Intermediate Shapes	1.2-1.3
	Plain, Primarily Rectilinear Construction	1.00
Frame Material (FM)	Metal, Plastic	1.80
	Wood	1.30

*Note: Bold values indicate quantities chosen for this mattress analysis.

Sample calculations for the generic upholstered furniture fire growth HRR model are presented below, not including incubation times. The factors used in the calculations are shown in bold in Table B - 3 above. The combustible mass value was found by multiplying the mattress mass per unit area value of 4kg/m^2 (as discussed in B.2) by the mattress area (both sides) of 5.2m^2 .

$$CM = \left(2 \frac{kg}{m^2} \right) (5.211m^2)$$

$$CM = 10.4kg$$

$$\dot{Q}_{max} = 210(0.40)(1.0)(10.4kg)(1.0)(1.66)$$

$$\dot{Q}_{max} = 1453.2kW$$

$$t_b = \frac{(1.8)(10.4kg) \left(16,364 \frac{kJ}{kg} \right)}{1453.2kW}$$

$$t_b = 211.2s \text{ or } 3.52min$$

Table B - 4, following, shows the results for the generic upholstered furniture fire growth model predictions.

Table B - 4: Generic Upholstered Furniture Fire Growth Model Prediction

Time* (s)	Time* (min)	Generic Upholstered Model HRR (kW)
0.0	0.0	0.0
105.6	1.8	1115.5
211.2	3.5	0.0

*Note: the time has not been shifted by the incubation time. Mattress one will be shifted by 60 s and mattress two by 300 s.

B.5 t-Squared HRR Model

The equations used to calculate the t-squared HRR are shown below.

$$\dot{Q} = \alpha(t - t_o)^2 \quad (\text{B.4})$$

where:

$$\dot{Q} = \text{HRR [kW]}$$

α = Fire Growth Coefficient

$$= .00293 \frac{\text{kW}}{\text{s}^2} \text{ for a "slow" fire}$$

$$= .01172 \frac{\text{kW}}{\text{s}^2} \text{ for a "medium" fire}$$

$$= .0469 \frac{\text{kW}}{\text{s}^2} \text{ for a "fast" fire}$$

$$= .1876 \frac{\text{kW}}{\text{s}^2} \text{ for an "ultra-fast" fire}$$

t = Time [s]

t_o = Incubation Time [s].

Sample calculations for the t-squared HRR model are shown below. Incubation times of 60 s and 300 s were used for mattresses one and two respectively. The following calculation will be done for mattress one at a time of 100 s for a fast t-squared fire.

$$\dot{Q} = .0469 \frac{\text{kW}}{\text{s}^2} (100\text{s} - 60\text{s})^2$$

$$\boxed{\dot{Q} = 75.04\text{kW}}$$

B.6 Fuel/Ventilation-Controlled Fire

The equations used to calculate the transition from fuel to ventilation controlled fire behaviour for the Edmonton II enclosure are shown below.

$$\begin{aligned}\dot{Q}_{vc} &= 3000 \cdot \dot{m}_a \quad [\text{kW}] \\ \dot{m}_a &= 0.5A_oH_o^{1/2} \quad [\text{kg/s}]\end{aligned}\tag{B.5}$$

where:

$$\begin{aligned}\dot{Q}_{vc} &= \text{HRR Required for Onset of Ventilation-Controlled Fire [kW]} \\ \dot{m}_a &= \text{Mass Flowrate of Air [kg/s]} \\ A_o &= \text{Area of Openings [m}^2\text{]} \\ H_o &= \text{Height of Openings [m].}\end{aligned}$$

Calculation of the HRR required for onset of a ventilation-controlled fire follows. The area of the opening (door), A_o , was found to be 1.568 m^2 and the height of the opening (door), H_o , was 2.057 m .

$$\begin{aligned}\dot{m}_a &= 0.5(1.568\text{m}^2)(2.057\text{m})^{1/2} \\ \dot{m}_a &= 1.124 \frac{\text{kg}}{\text{s}}\end{aligned}$$

$$\dot{Q}_{vc} = 3000 \cdot 1.124 \frac{\text{kg}}{\text{s}}$$

$$\boxed{\dot{Q}_{vc} = 3373\text{kW}}$$

B.7 McCaffrey Prediction of Flashover

The equations used to calculate the HRR required for flashover by the McCaffrey equation for the Edmonton II enclosure are shown below.

$$\dot{Q}_{FO} = 610(h_k A_T A_o H_o^{1/2})^{1/2} \quad (\text{B.6})$$

where:

- \dot{Q}_{FO} = HRR Required for Flashover [kW]
- h_k = Enclosure Conductance (defined below) [kW/m²/K]
- A_T = Internal Enclosure Area Excluding Openings [m²]
- A_o = Area of Ventilation Openings [m²]
- H_o = Height of Ventilation Opening [m].

The enclosure conductance is calculated as follows:

$$h_k = \left\{ \begin{array}{ll} \left(\frac{k_{thermal} \rho C}{t} \right)^{1/2} & t \leq t_p \\ k_{thermal} / \delta & t_p \leq t \end{array} \right\} \quad (\text{B.7})$$

$$t_p = \frac{\rho C}{k_{thermal}} \left(\frac{\delta}{2} \right)^2$$

where:

- $k_{thermal}$ = Thermal conductivity [kW/m · K]
- ρ = Density [kg/m³]
- c = Thermal capacity [kJ/kg · K]
- t = Time [s]
- t_p = Thermal penetration time [s]
- δ = Wall thickness [m].

Calculation of the HRR required for flashover by the McCaffrey equation follows. The area of the opening (door), A_o , was found to be 1.568 m² and the height of the opening

(door), H_o , was 2.057 m. The total internal enclosure area excluding openings, A_T , was found to be 71.06m^2 . The material properties for drywall, taken from [29] are listed below.

$$k_{thermal} = 0.48 \times 10^{-3} \text{ kW} / \text{m} \cdot \text{K}$$

$$\rho = 1440 \text{ kg} / \text{m}^3$$

$$c = 0.84 \text{ kJ} / \text{kg} \cdot \text{K}$$

$$\delta = 0.016 \text{ m}$$

The thermal penetration time, t_p is calculated as follows:

$$t_p = \frac{\left(1440 \frac{\text{kg}}{\text{m}^3}\right) \left(0.84 \frac{\text{kJ}}{\text{kg} \cdot \text{K}}\right)}{0.48 \times 10^{-3} \frac{\text{kW}}{\text{m} \cdot \text{K}}} \left(\frac{0.016 \text{ m}}{2}\right)^2$$

$$t_p = 161.3 \text{ s}$$

Assume flashover will occur at a time greater than 161.3 s, and therefore, the enclosure conductance is calculated as follows.

$$h_k = \frac{k}{\delta}$$

$$h_k = \frac{0.48 \times 10^{-3} \frac{\text{kW}}{\text{m} \cdot \text{K}}}{0.016 \text{ m}}$$

$$h_k = 0.03 \frac{\text{kW}}{\text{m}^2 \cdot \text{K}}$$

The HRR required for flashover can then be calculated as follows.

$$\dot{Q}_{FO} = 610 \left\{ \left(0.03 \frac{kW}{m \cdot K} \right) (71.06 m^2) (1.568 m^2) (2.06 m^2)^{1/2} \right\}^{1/2}$$

$$\boxed{\dot{Q}_{FO} = 1341.2 kW}$$

B.8 NIST/CBHF Upholstered Furniture and Mattress Peak HRR

Correlation

The equations used to calculate the peak mattress HRR are shown below:

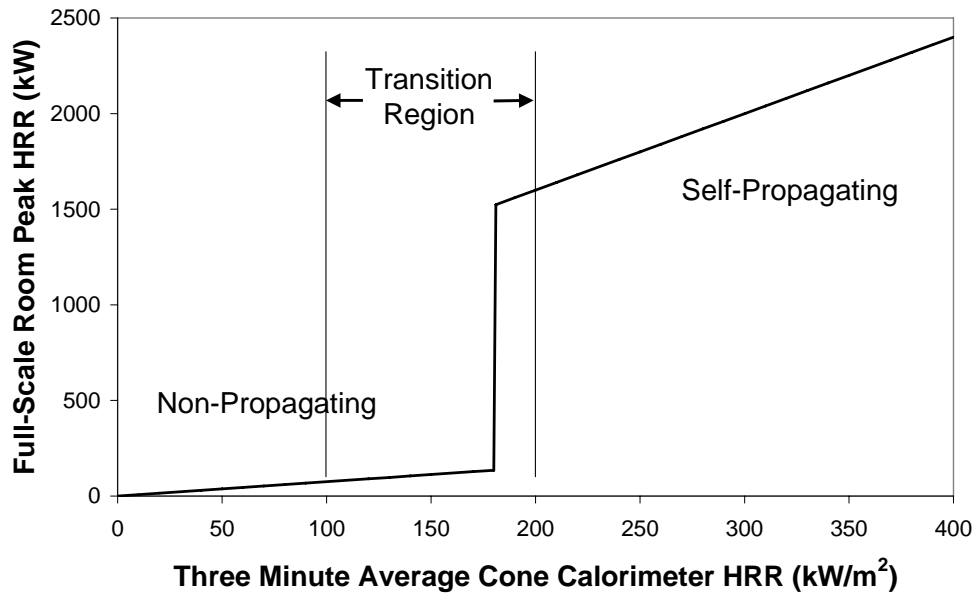


Figure B - 1: NIST/CBHF Upholstered Furniture and Mattress Correlation

The following equations accompany the above figure.

$$\dot{Q}_{FullScalePk} = \begin{cases} 0.75\dot{Q}_{3MinCone}'' & \text{Non-Propagating} \\ 4\dot{Q}_{3MinCone}'' + 800 & \text{Self-Propagating} \end{cases} \quad (B.8)$$

where:

$\dot{Q}_{FullScalePk}$ = Full-Scale Peak Heat Release Rate [kW]

$\dot{Q}_{3MinCone}''$ = 180 second Average Cone Calorimeter HRR [kW/m²].

Table B - 5, below, shows the cone calorimeter results used in the calculations.

Table B - 5: Average Cone Calorimeter Results for the Three Mattress Samples

Material	Cone Calorimeter Results		
	Peak HRR (kW/m ²)	180s Average (kW/m ²)	Total Heat Released at 180s (MJ/m ²)
Mattress 1	290.9	190.0	29.1
Mattress 2	225.7	126.4	23.2
Mattress 3	114.6	61.2	11.6

Calculation of the peak full scale HRR predicted using the NIST/CBHF correlation follows below. Mattress one will be used for the sample calculations. Considering that the 180 s average HRR for mattress one, seen in Table B - 5 was 190.0 kW/m², which falls in the transition region of the NIST/CBHF correlation, both the non-propagating and self-propagating peak HRR will be estimated using the correlations presented in Equation B.8.

$$\dot{Q}_{FullScalePk} = 0.75 \left(190.0 \frac{kW}{m^2} \right) \quad \text{Non-Propagating}$$

$$\dot{Q}_{FullScalePk} = 142.5kW \quad \text{Non-Propagating}$$

$$\dot{Q}_{FullScalePk} = 4 \left(190.0 \frac{kW}{m^2} \right) + 800 \quad \text{Self-Propagating}$$

$$\dot{Q}_{FullScalePk} = 1560.0kW \quad \text{Self-Propagating}$$

APPENDIX C: TEMPERATURE CALCULATIONS

The sample calculations for predicting temperature will be presented in this appendix.

Sample calculations of the Alpert ceiling temperature correlation and the average hot gas layer temperature correlation are presented.

C.1 Alpert Ceiling Temperature Correlation Predictions

The equations used to calculate the ceiling temperatures using the Alpert ceiling temperature correlations are presented below:

$$T_{\max} - T_{\infty} = \Delta T = \left\{ \begin{array}{ll} \frac{5.38(k\dot{Q}/r)^{2/3}}{H} & \text{if } r > 0.18H \\ \frac{16.9(k\dot{Q}^{2/3})}{H^{5/3}} & \text{if } r \leq 0.18H \end{array} \right\}$$

$k = 1$ if fire located in centre of room (C.1)

$k = 2$ if fire located against a flat wall

$k = 4$ if fire located in a 90° corner

where:

T = Temperature at Ceiling
 T_{∞} = Ambient Temperature
 ΔT = Temperature Rise Above Ambient
 $k = 1$ if Fire Located in Centre of Room
 $= 2$ if Fire Located Against a Flat Wall
 $= 4$ if Fire Located in a 90° Corner
 \dot{Q} = Fire HRR [kW]
 r = Radial Distance Between Fire Centre Axis and Point of Interest
 H = Distance from Base of Fire to Enclosure Ceiling.

A sample calculation for the ceiling temperature for a HRR of 75.0 kW, corresponding to a fast t-squared for mattress one at a time of 100 seconds follows below. The sample calculation will be done for Thermocouple Location 1 during the Edmonton II set of experiments, having a radial distance, r , of 1.1 m from the fire axis to the thermocouple as seen below in Figure C - 1 and Table C - 1, and assuming the fire is in the centre with a k value of 1. The distance from the base of the fire (i.e. top of the mattress) to the enclosure ceiling, H , was 2.3 m.

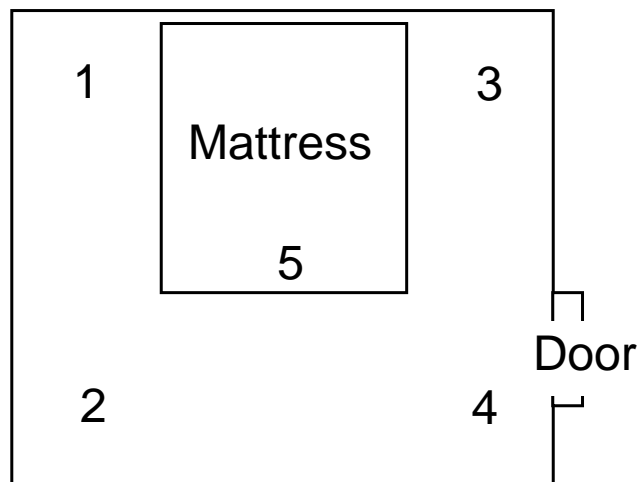


Figure C - 1: Schematic of Enclosure Showing Thermocouple Locations 1 to 5 Relative to Mattress

Table C - 1: Radial Distances for Edmonton II Thermocouple Locations

Thermocouple Location	Radial Distance*, r (m)
1	1.1
2	2.4
3	0.7
4	2.2
5	0.9

*Note: Radial distance is from centre of mattress to thermocouple location

The first temperature rise at the ceiling calculated using the Alpert ceiling temperature correlations follows.

$$0.18H = 0.18(2.3m)$$

$$0.18H = 0.4m$$

∴ for Thermocouple 1, $r > 0.18H$

$$\Delta T = \left\{ \frac{5.38 \left(\frac{75.0kW}{1.1m} \right)^{2/3}}{2.3m} \right\}$$

$$\boxed{\Delta T = 37.9^{\circ}C}$$

C.2 Average Hot Upper Gas Layer Temperature Correlation

The equations used to calculate the ceiling temperature using the average hot gas layer temperature correlation are presented below:

$$\Delta T_g = 6.85 \left(\frac{\dot{Q}^2}{A_o \sqrt{H_o} h_k A_t} \right)^{1/3} \quad (C.2)$$

where:

ΔT_g = Average Hot Gas Layer Temperature Rise Above Ambient

\dot{Q} = HRR [kW]

A_o = Area of Openings [m²]

H_o = Height of Openings [m]

h_k = Enclosure Conductance (defined below)[kW/m²/K]

A_t = Internal Enclosure Area Excluding Openings [m²].

The enclosure conductance is calculated as follows:

$$h_k = \begin{cases} \left(\frac{k_{thermal} \rho c}{t} \right)^{1/2} & t \leq t_p \\ k_{thermal} / \delta & t_p \leq t \end{cases} \quad (C.3)$$

$$t_p = \frac{\rho c}{k_{thermal}} \left(\frac{\delta}{2} \right)^2$$

where:

$k_{thermal}$ = Thermal conductivity [kW/m · K]

ρ = Density [kg/m³]

c = Thermal capacity [kJ/kg · K]

t = Time [s]

t_p = Thermal penetration time [s]

δ = Wall thickness [m].

Calculation of the average hot gas layer temperature follows. The area of the opening (door), A_o , was found to be 1.6 m^2 and the height of the opening (door), H_o , was 2.1 m. The total internal enclosure area excluding openings, A_T , was found to be 71.1 m^2 . The properties for drywall, taken from [5] are shown below.

$$k_{thermal} = 0.48 \times 10^{-3} \text{ kW} / \text{m} \cdot \text{K}$$

$$\rho = 1440 \text{ kg} / \text{m}^3$$

$$c = 0.84 \text{ kJ} / \text{kg} \cdot \text{K}$$

$$\delta = 0.016 \text{ m}$$

The thermal penetration time, t_p is calculated as follows:

$$t_p = \frac{\left(1440 \frac{\text{kg}}{\text{m}^3}\right) \left(0.84 \frac{\text{kJ}}{\text{kg} \cdot \text{K}}\right) \left(\frac{0.016 \text{ m}}{2}\right)^2}{0.48 \times 10^{-3} \frac{\text{kW}}{\text{m} \cdot \text{K}}}$$

$$t_p = 161.3 \text{ s}$$

At times less than the thermal penetration time, t_p , the enclosure conductance is calculated as follows. This sample calculation has been done for mattress one, and a time of 100 s, assuming a fast t-squared fire, giving a HRR of 75.04 kW.

$$h_k = \left(\frac{\left(0.48 \times 10^{-3} \frac{\text{kW}}{\text{m} \cdot \text{K}}\right) \left(1440 \frac{\text{kg}}{\text{m}^3}\right) \left(0.84 \frac{\text{kJ}}{\text{kg} \cdot \text{K}}\right)}{100 \text{ s}} \right)^{1/2}$$

$$h_k = 0.0762 \frac{\text{kW}}{\text{m}^2 \cdot \text{K}}$$

For test times greater than the thermal penetration time, the enclosure conductance is constant, and is calculated as follows:

$$h_k = \frac{0.48 \times 10^{-3} \frac{kW}{m \cdot K}}{0.016m}$$

$$\boxed{h_k = 0.03 \frac{kW}{m^2 \cdot K}}$$

The average hot gas layer temperature, corresponding to a fast t-squared fire at 100 s is then calculated as follows:

$$\Delta T_g = 6.85 \left\{ \frac{(75.0kW)^2}{(1.6m^2)\sqrt{2.1m} \left(0.0762 \frac{kW}{m^2 \cdot K} \right) (71.1m^2)} \right\}^{1/3}$$

$$\boxed{\Delta T_g = 53.0^\circ C}$$